First functional expression of lichen cytochrome P450 enzymes enabling *in vitro* biosynthesis of usnic acid

By

Huynh Ngoc Dieu Vu

A Thesis submitted to the Faculty of Graduate and Postdoctoral Studies

The University of Manitoba

In partial fulfilment of the requirement of the degree of

MASTER OF SCIENCE

Department of Chemistry

University of Manitoba

Winnipeg

April 2026

Abstract

Lichens are symbiotic associations between fungi and photosynthetic partners, typically algae or cyanobacteria (Ingólfsdóttir, 2002). These stable communities of microorganisms are well known for producing wide array of secondary metabolites with diverse biological activities. One such notable metabolite is usnic acid (UA), a dibenzofuran compound extracted from lichen *Cladonia uncialis,* exhibits antimicrobial, anti-inflammatory, anti-viral and anticancer properties (Azhamuthu et al., 2024; Ingólfsdóttir, 2002). Despite its therapeutic potential, large-scale production is limited due to the extremely slow growth of lichens. To address this challenge, this thesis aims to elucidate and reconstruct the biosynthetic pathway of UA using a heterologous expression. In this work, biosynthetic gene clusters associate with UA production in *C. uncialis* were identified, and a heterologous expression system was established in *Escherichia coli* for lichen-derived cytochrome P450 enzymes. The study focuses on methylphloroacetophenone oxidase (MPAO), a cytochrome P450 enzyme, and its redox partner, cytochrome P450 reductase (CPR357), both of which are derived from *C. uncialis*. MPAO is proposed to catalyze the oxidative dimerization of methylphloroacetophenone (MPA) to form UA, with electron transfer facilitated by CPR357 from NAD(P)H (Abdel-Hameed et al., 2016; Mittal N., 2023). Following heterologous expression, both enzymes were purified using His-Tag Affinity Chromatography to obtain pure catalytically active enzyme. *In vitro* bioconversion assays using purified MPAO and CPR357 successfully converted MPA to UA, as confirmed by liquid chromatography–mass spectrometry, demonstrating the feasibility of enzymatic UA biosynthesis.

In parallel, a comprehensive phylogenetic analysis of a lichen-derived cytochrome P450 associated with depsidone biosynthesis was conducted to investigate evolutionary relationships

and identification which allowed us to identify a putative enzyme that catalyzes in this transformation.

This work represents the first functional characterization of lichen-derived cytochrome P450 enzymes involved in usnic acid biosynthesis using purified enzymes. Additionally, the phylogenetic investigation offers insights into depsidone biosynthetic pathway. Together, these complementary approaches contribute to advancing the biotechnological potential of lichen-derived natural products.

Acknowledgements

This thesis work would not have been possible without the support, guidance, and encouragement of many remarkable individuals, and I am deeply grateful for the opportunity to acknowledge them here.

First and foremost, I extend my heartfelt thanks to my supervisor, Dr. John Sorensen, for his unwavering support, patience, and mentorship throughout my academic journey. His passion for science, thoughtful guidance, and genuine care profoundly shaped not only this research but also my personal and professional growth. I am truly grateful for the trust and encouragement he has shown me over the years.

I sincerely thank my committee members, Dr. David E. Herbert and Dr. Az (Ashley A.) Klymiuk, for their valuable insights, constructive feedback, and encouragement. Their expertise and thoughtful suggestions greatly strengthened this work and enriched my learning experience.

I am especially thankful for the mentorship and support of Dr. April Johnson, Dakshina and Dr. Harman Gill. Their guidance, kindness, and encouragement have been invaluable, and I am deeply appreciative of the time and care they invested in my development.

My deepest thanks go to my family, friends, and the Sorensen lab family, which has truly been a second home to me. This lab has been a place of learning, growth, and shared emotions, and I am grateful for the sense of belonging it provided. I am especially thankful to my friends April Didi, Dakshina, Sara, Harjasmin, Saeid, Maia, and to Hoi Chi Em: Ngoc Anh Nguyen, Minh Thu Le, Thi My Suong Hoan, Nguyen Hoang Long Duong, Ha Chi Nguyen, Lam Duong Dang, Yen Thu Nguyen, Uyen Rodgers, Thi Cam Ha Tran for their constant companionship, encouragement, and willingness to help whenever needed.

Above all, I owe an immeasurable debt of gratitude to my family. I am profoundly grateful to my parents, Thi Thuy Dung Huynh and Ngoc Minh Vu, whose unconditional love, sacrifice, and unwavering belief in me carried me through even the most challenging moments. Their support has been my greatest source of strength. I also thank my extended family for their constant encouragement, Huynh Ngoc Tan Vu, Thi Nhung Nguyen, Thi Nguyen Ho, Dieu Quang Vu, and Anh Khoi Ngo, whose love, presence, and support have been essential since the very beginning of my research journey. I am incredibly fortunate to have them in my life.

Dedication

I dedicate this thesis to my parents, Thi Thuy Dung Huynh and Ngoc Minh Vu

Their unconditional love, unwavering trust, and tireless hard work gave me the strength to never give up.

Contribution of Authors

Chapter 1: Prepared exclusively by the author.

Chapter 2: Prepared exclusively by the author.

Chapter 3: The work presented in this chapter builds upon research previously conducted and published by Dr. Navriti Mittal and Dr. Robert Bertrand. In this project, my contributions (Dieu Vu) focused on designed the expression plasmids, optimizing protein expression conditions, purifying recombinant enzymes, and performing the *in vitro* usnic acid bioconversion assays. Dr. Robert Bertrand identified the usnic acid biosynthetic gene cluster and its corresponding redox partner sequences, while Dr. Narvriti Mittal demonstrated that co-expression with the CPR357 redox partner enables successful usnic acid bioconversion.

Chapter 4: Prepared exclusively by the author.

Chapter 5: Prepared exclusively by the author.

Table of Contents

List of Tables

List of Schema

List of Figures

List of Supporting Informations

Figure list:

List of Supplementary Tables:

List of Abbreviations

Abbreviation	Meaning
ACP	Acyl carrier protein
AT	Acyltransferase (selects and loads starter/extender units)
BGCs	Biosynthetic gene clusters
CMet	C-methyltransferase
CYP	Cytochrome P450 monooxygenases
CLC	Claisen cyclase domain
EIC	Extracted ion chromatogram
ER	Enoylreductase
EtOAc	Ethyl acetate
HPLC	High-Performance Liquid Chromatography
hr-PKS	Highly reducing polyketide synthases
iPKS	Iterative polyketide synthase
KR	Ketoreductase
KS	Ketosynthase (forms C–C bonds)
LC-MS	Liquid Chromatography-Mass Spectrometry
MPA	Methyl Phloroacetophenone
mPKS	Modular polyketide synthase
NADH	Nicotinamide adenine dinucleotide
NADPH	Nicotinamide adenine dinucleotide phosphate
NMR	Nuclear Magnetic Resonance
nr-PKS	Non-reducing polyketide synthases
NRPSs	Non-ribosomal peptide synthetases
pr-PKS	Partially reducing polyketide synthases
PT	Product template
SAM	S-adenosyl methionine
SM / SMs	Secondary metabolites

TE	Thioesterase (catalyzes chain termination)
TIC	Total ion chromatogram
TMD	Transmembrane domain
UA	Usnic acid

Chapter 1

Introduction to lichens and their secondary metabolites

1.1 Lichenized fungi

Historically, lichens have been defined as slow-growing, assemblages of two symbiotic organisms, namely a thallus-forming fungal species mycobiont and photosynthetic algae and/or cyanobacteria (photobiont) (Lutzoni & Miadlikowska, 2009) **(Figure 1)**. This symbiotic relationship of lichens was first discovered by Schwendener in 1867. Lichen assemblages are taxonomically identified on the basis of the dominant mycobiont refers to the whole structure of the lichen. For instance, *Cladonia uncialis* can describe the lichenized fungus alone or in its natural symbiotic relationship with the photobiont algae (Lutzoni et al., 2009). Recent studies have shown that lichens are miniature ecosystems, with lichen thallus and its surface harbouring a multiple microbial species, including bacteria, yeast and so-called lichenicolous fungi (Morillas et al., 2022; Spribille et al., 2016a). Building on this view, more recent review has demonstrated that basidiomycetous yeasts are frequent associates in lichen cortex and, together with extracellular polymeric substances (EPS) they secrete, form part of a hydrated EPS matrix that provides mechanical cohesion and helps define the three-dimensional architecture of the thallus, leading to the interpretation of many lichen cortices as biofilms (Spribille et al., 2016b, 2020, 2022) .These associated microorganisms can either support the symbiosis by nutrition acquisition and stress tolerance (Grube et al., 2009, 2015; Sigurbjörnsdóttir & Vilhelmsson, 2016) or behave as lichen pathogens (Merinero & Gauslaa, 2018).

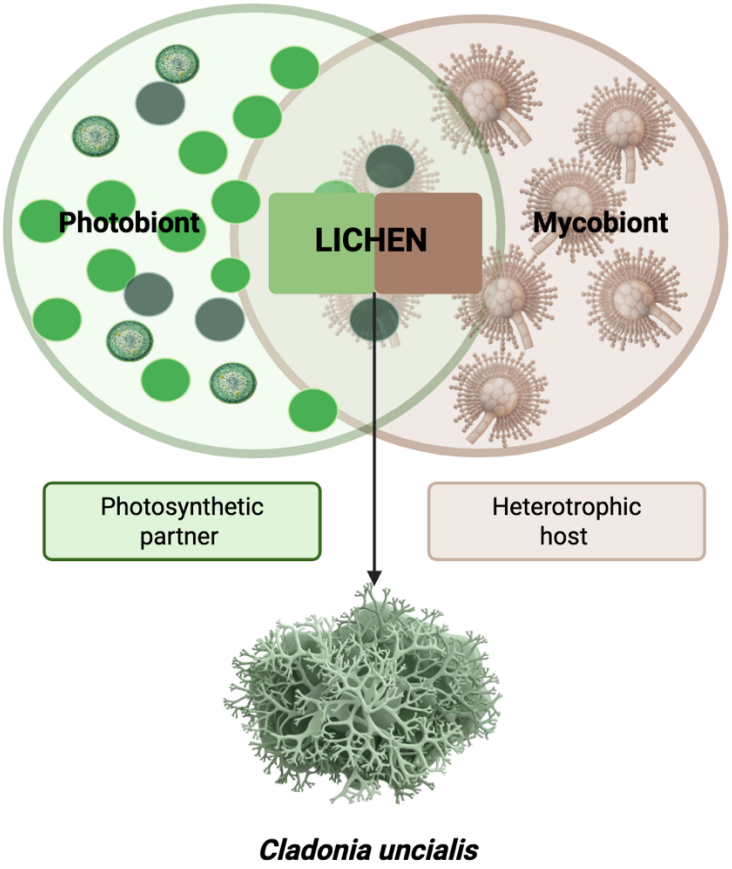

Figure 1. A simplified illustration of symbiotic relationship between a photosynthetic partner (algae and/or cyanobacteria) and a heterotrophic host-fungal partner (mycobiont) forming a lichen.

Lichens can be found in nearly all terrestrial habitats on Earth, from the mildest conditions like gardens, and parks to the extreme environments found in deserts or the Artic tundra. They can grow on or inside rocks, on the bark of woody plants as epiphytes, on wood, soil, mosses, leaves of vascular plants (especially in the tropics), on other lichens, as well as on human-made materials such as concrete, glass, metals and plastics (Lücking & Spribille, 2024) **(Figure 2)**. In a European Space Agency experiment, lichens were exposed to the full ultraviolet light spectrum, gamma radiation and vacuum conditions of low earth orbit. It was observed that the lichen survived these harsh conditions with 70% to 90% remaining viable (Lücking & Spribille, 2024) (**Figure 2**). Average lichen growth varies between 0.5 and 8 mm per year, depending on the species and

environmental factors (Hale, 1973). Due to their slow growth and the challenges of recreating the symbiotic relationship in controlled conditions, lichens are difficult to cultivate in the laboratory, and our understanding of how these communities are established and sustained in various habitats remains limited.

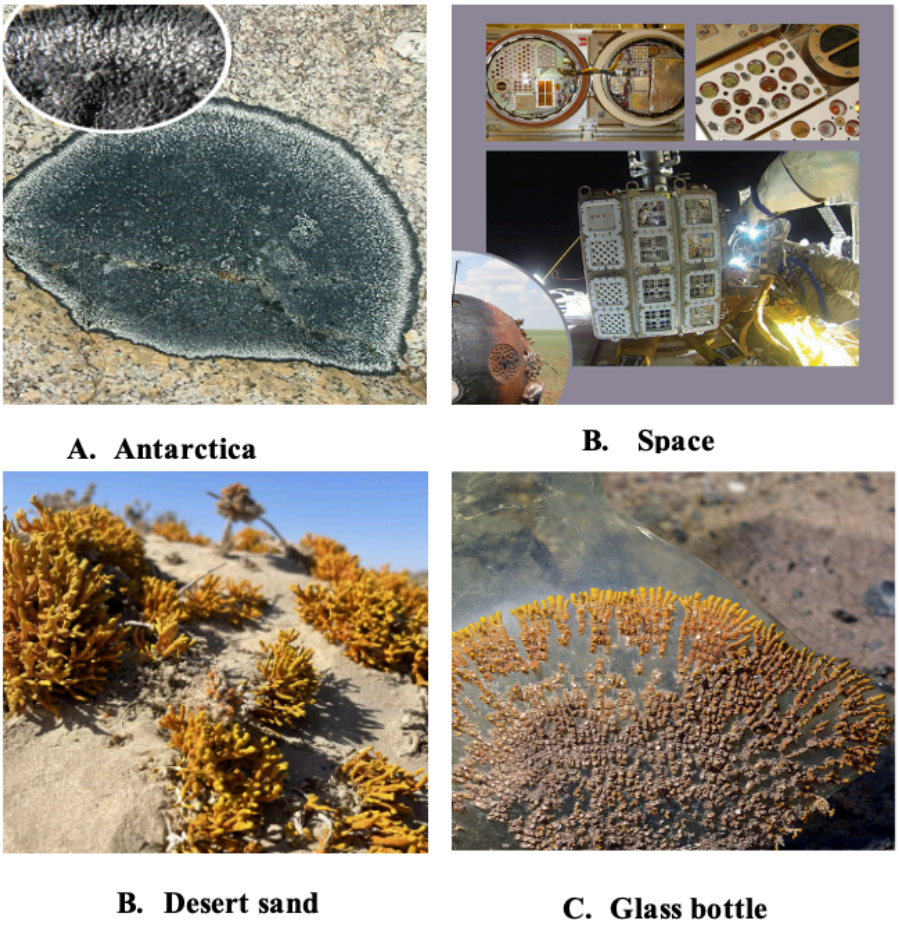

Figure 2. Adaptive lichen species in diverse habitats.

A) *Buellia frigida*, Antarctica.

B) *Xanthoria elegans,* exposed to space.

C) *Dufourea flamme*, Namib Desert.

D) *Xanthoparmelia mougeotina,* on glass bottle.

Reproduced from Smith, J. (2024).

1.2 Secondary metabolites from lichen mycobionts

Lichen produce a wide variety of low-molecular-weight aliphatic and aromatic compounds derived from both primary and secondary metabolism. Primary metabolites encompass intracellular molecules such as amino acids, nucleotides, carbohydrates, and lipids which are crucial for an organism's survival, growth, reproduction, and overall biological functions (Nayaka & Haridas, 2020). Unlike primary metabolites, secondary metabolites (SMs) are molecules that are not directly involved in fundamental biochemical processes, but rather provide defense and competitive advantages for surviving and proliferating within an ecosystem (N. K. Singh et al., 2023). These compounds are synthesized through specific biochemical pathways, where the simpler structures of primary metabolites undergo a series of enzymatic transformations, forming more intricate and specialized secondary metabolites (Nayaka & Haridas, 2020). These secondary metabolites comprise between 5-20 % of the dry weight of lichens (Molnár & Farkas, 2010). Lichen secondary metabolites (SM) belong to various groups, including dibenzofuran, depside, steroid, chromone, terpene, and anthraquinone **(Figure 3)**. Their specific roles within the symbiosis and the broader ecosystem are still not fully understood and continue to be an area of ongoing research in Sorensen lab.

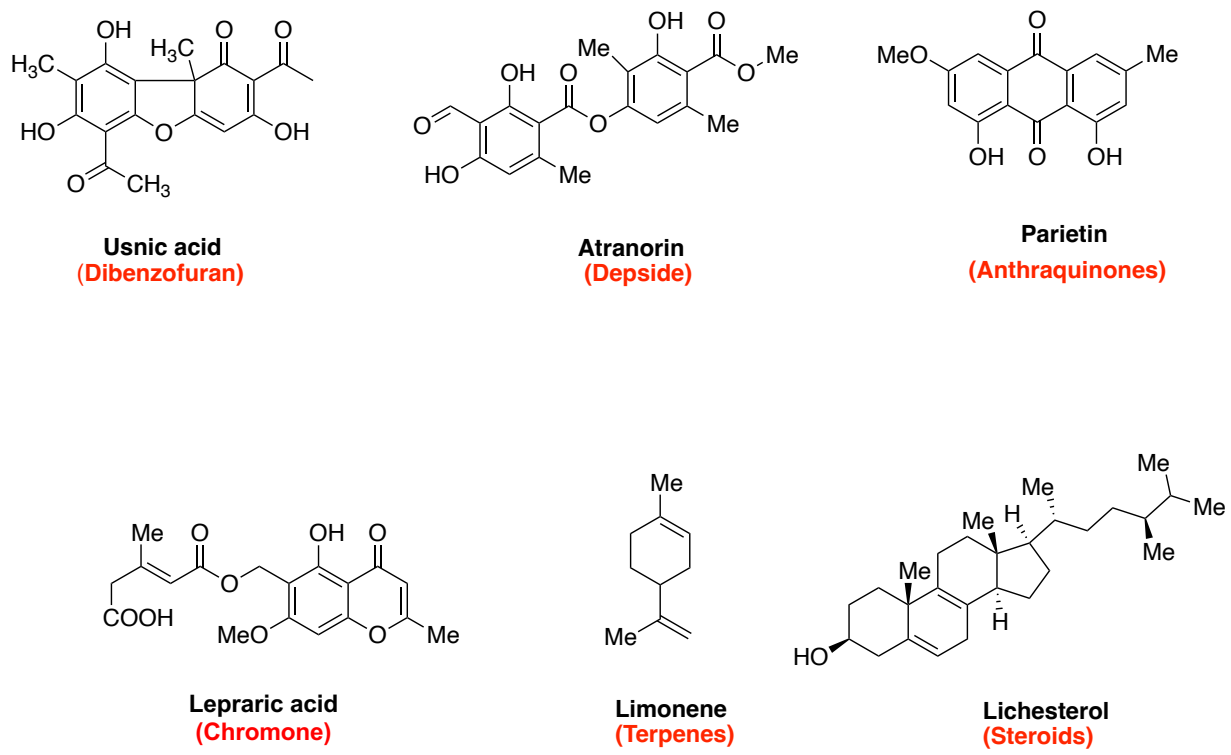

Figure 3. The major structural classes of secondary metabolites produced by lichen fungi.

1.3 Structural organization of lichen thallus

The structure of the lichen thallus is highly organized, with each symbiotic partner exhibiting complementary functions **(Figure 4).** The mycobiont forms a dense cortical layer composed of fungal hyphae that offers mechanical support and protection to the photobiont (Honegger, 1997). Located in the medulla layer, the photobiont contributes by producing carbon nutrients through photosynthesis, which are then shared with other symbiotic partners (Honegger, 1997). In some lichens, cyanobacteria are responsible for nitrogen fixation (Seneviratne & Indrasena, 2006). Moreover, the lichen microbiome exhibits spatial heterogeneity, with differences between the center and edges of the lichen thallus (Mushegian et al., 2011), as well as vertically between the surface and substrate (Noh et al., 2020). Secondary metabolites produced by the mycobiont or

lichenicolous fungi also show specific localization patterns that is likely related to their biological functions (Gill et al., 2023).

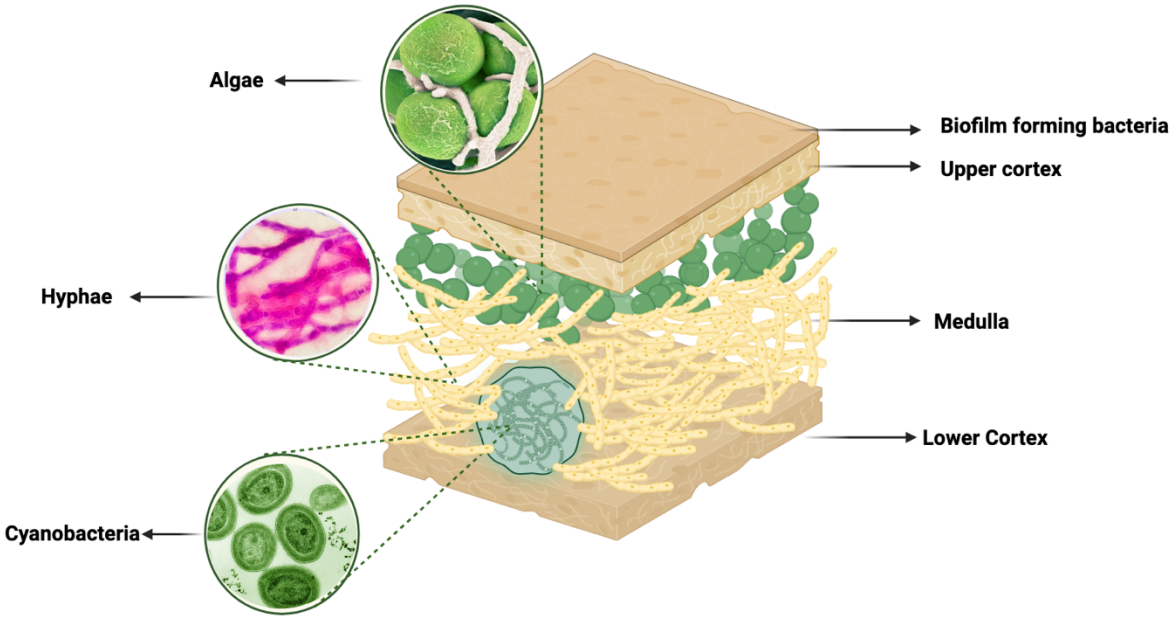

Figure 4. Complex organization of the lichen thallus. The algal and/or cyanobacterial photobionts are surrounded by fungal hyphae of the mycobiont. Illustration was created by author using BioRender®.

1.4 Biological activities of lichen secondary metabolites

Lichen produce a remarkably diverse array of secondary metabolites (SMs), with more than 1,000 unique compounds identified from lichenized fungi (Goga et al., 2018). These metabolites exhibit a wide range of biological activities, making lichen promising sources for pharmaceutical and other applications (Shrestha & St. Clair, 2013; Zambare & Christopher, 2012). Many of SMs are exclusively found in lichen (Shrestha & St. Clair, 2013); for instance, usnic acid appears to be only observed in lichen (Ingólfsdóttir, 2002). Metabolomic analyses indicated that lichenized fungi within the *Cladoniaceae* (Lecanoromycetes, Ascomycota) possess a distinct chemical profile compared to non-lichenized fungal class (Robey et al., 2021). Lichen SMs have been extensively

screened for bioactivity **(Figure 5)**, for example, antimicrobial (fumarprotocetraric acid), antioxidant (usnic acid), antifungal (lecanoric acid), and anti-inflammatory (diffractaic acid) activities were observed. In addition, physodic acid, norlobaric acid, salazinic acid, parellic acid, and virensic acid have been identified as inhibitors of HIV-1 integrase (Neamati et al., 1997); while pannarin, 10-chloropannarin, and sphaerophorin exhibit cytotoxic activity against rat lymphocytes (Correche et al., 2002). These examples highlight the broad potential of lichen metabolites in various applications.

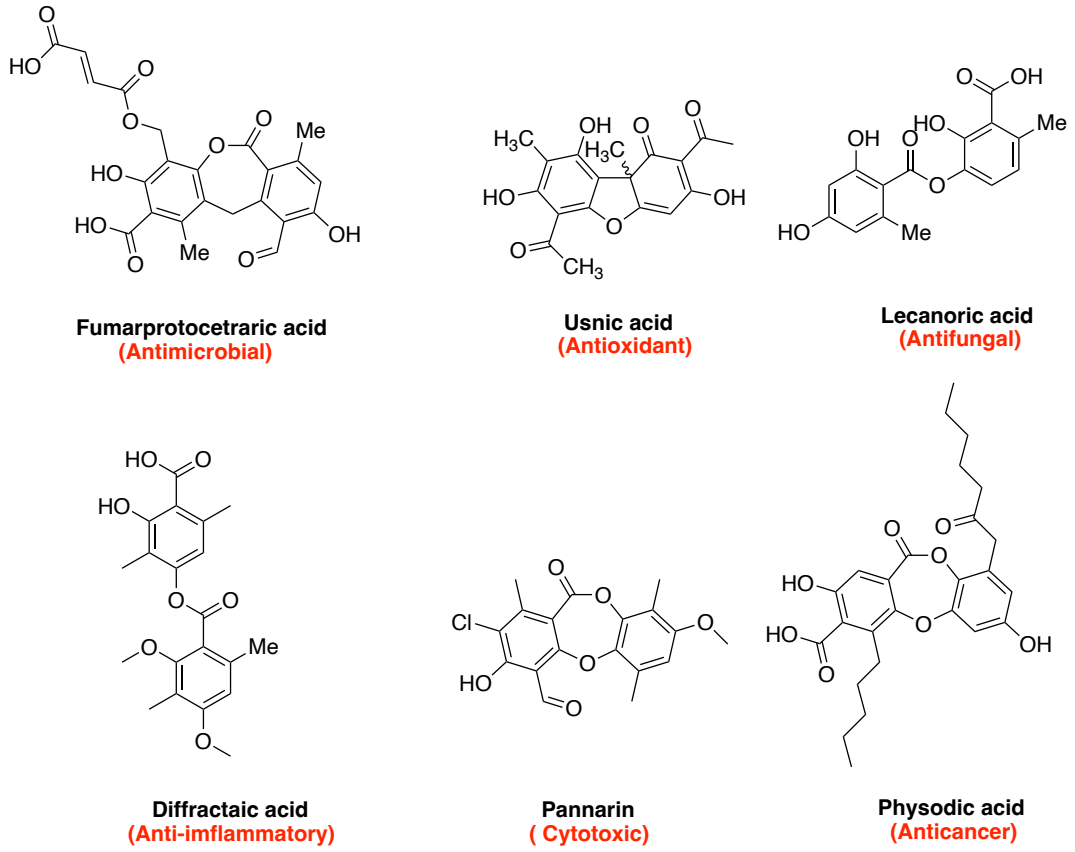

Figure 5. Examples of lichen secondary metabolites and reported bioactivities (Goga et al., 2018).

1.5 Biosynthetic pathways of SMs production by lichen mycobionts

In lichens, the algal or cyanobacterial photobiont serves as the primary carbon source to produce carbohydrates through photosynthesis. These carbohydrates, classified as primary metabolites, are then transferred to the fungal partner (mycobiont). However, recent studies have raised questions about this long-standing view, indicating that the supporting evidence remains limited and that alternative models of carbon exchange within the lichen symbiosis require further investigation (Spribille et al., 2022). Within the mycobiont, primary metabolites undergo conversion into secondary metabolites, a metabolic process outlined by Mosbach (1969). The term "biosynthesis" refers to the enzymatically-catalyzed production of structurally diverse secondary metabolites, governed by specific genes within a microorganism's genome. A sequence of biochemical reactions leading to the formation of an SM is known as a biosynthetic pathway (Morrison, 1969). Biosynthetic pathways leading to the production of lichen SMs are differentiated into three types **(Figure 6)**, based on various starter units: acetyl-CoA and malonyl-CoA for the polyketide pathway; isopentyl and dimethyl allyl pyrophosphates for the terpene pathway; erythrose-4-phosphate and phosphoenolpyruvate for the shikimate pathway (Mosbach, 1969).

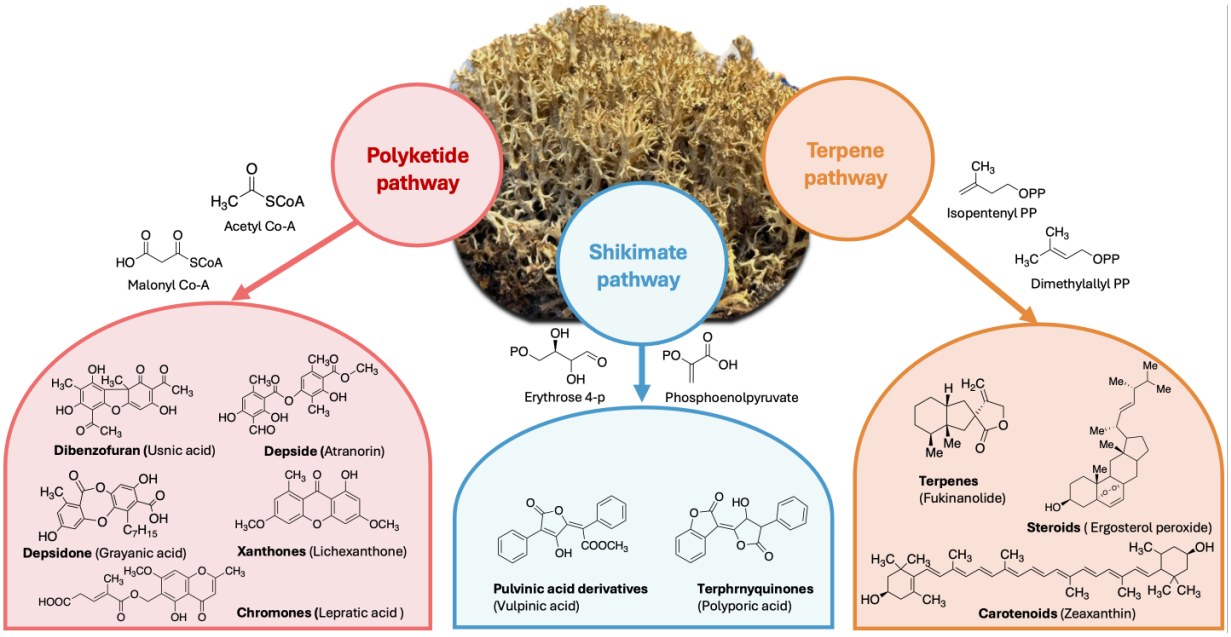

Figure 6. Illustration of three biosynthetic pathways of lichen secondary metabolites: polyketides, terpene, and shikimate (Gill et al., 2023).

1.6 Domain architecture and polyketide synthases (PKSs) pathway

Polyketides are polymers of acyl units assembled to form phenolic or aliphatic structures (Weissman, 2009). They represent a structurally and functionally diverse family of bioactive natural products that can be found in bacteria, fungi, and plants (Hertweck, 2009). These structurally diverse lichen metabolites include depsides, depsidones, dibenzofurans, xanthones, and chromones. Polyketides biosynthesis is catalyzed by polyketide synthases (PKSs), which are large and complex multidomain enzymes, with each domain serving a specific catalytic function (Weissman, 2009). The basic process of polyketide assembly by PKSs involves several catalytic modules: loading, extension, reducing, and terminal modules, each comprising various domains necessary for polyketide biosynthesis (Keating & Walsh, 1999). The core catalytic domains include ketosynthase (KS), which forms carbon-carbon bonds; acyltransferase (AT), which selects

and loads the starter unit that initiate the polyketide chain and extender units (malonyl- or methylmalonyl- derived building blocks); and the acyl carrier protein (ACP), which transfers the growing intermediates using a flexible phosphopantetheine "arm" (Dewick, 2009; H. Park et al., 2014). Many PKSs also contain tailoring domains that modify the growing polyketide chain during assembly. These include C-methyltransferases (cMeT), which transfer methyl groups from S-adenosylmethionine to the α-carbon (Skiba et al., 2016), and product template (PT) or Claisen cyclase (CLC) domains, which mediate folding and cyclization in non-reducing polyketide synthases (nr-PKSs) (Crawford et al., 2009; Udwary et al., 2002). Chain termination is typically catalyzed by thioesterase (TE) domains that hydrolyze the final product, although reductase domains or CLC domains may also be involved (Du & Lou, 2010). The use of alternative starter (e.g., propionyl-CoA, hexanoyl-CoA) and extender (e.g., methylmalonyl-CoA) units further contributes to polyketide structural diversity (Chan et al., 2009; Ma et al., 2008). Due to their complex structures and broad biological activities, polyketides are among the most extensively studied natural products, with notable pharmaceutical applications including lovastatin (a cholesterol-lowering agent), erythromycin (an antibiotic for bacterial infections), and rifamycin (antibiotic used in the treatment of tuberculosis) (Campbell & Vederas, 2010; Qi et al., 2018; H. Zhang et al., 2010). Based on domain organization and catalytic mechanisms, PKSs are classified into three major types: Type I, II and III (Staunton & Weissman, 2001; Weissman, 2009) **(Figure 7).** Type I PKSs are further subdivided into two types: iterative PKSs (iPKs) found in fungi, and modular PKSs (mPKSs), found in bacteria **(Figure 7)**. Iterative PKSs reuse the same functional domains multiple times, while mPKSs similar to an assembly line employing multiple catalytic modules (Cox et al., 2018; Staunton & Weissman, 2001; Weissman, 2009). Based on the domain architecture of type I iterative PKSs, they are grouped into three categories depending on the

degree of reduction of poly- β ketone chain: non-reducing (nr-PKS), partially reducing (pr-PKS), and highly-reducing (hr-PKS) (Dewick, 2009) (**Figure 8**). Hr-PKSs can reduce all poly-β ketone intermediates to saturated carbon-carbon bonds, facilitated by the presence of ketoreductase (KR), dehydratase (DH), and enoyl-reductase (ER) domains which catalyze the biosynthesis of both free-living and lichen fungal linear polyketides. pr-PKSs contain a KR and/or DH domain and generate polyketides harboring hydroxyl groups through the reduction of specific β-ketone groups, thereby catalyzing both linear and aromatic fungal and lichen fungal polyketides. Nr-PKSs lack KRs, DHs and ERs domains, resulting in the synthesis of extended poly-β-ketone intermediates that undergo cyclization to yield heterocyclic aromatic compounds. Type II PKSs are confined to bacteria, and consist of separate monofunctional proteins acting in complexes; Type II PKSs are therefore not relevant to lichen systems (Hertweck et al., 2007). Type III PKSs are small homodimeric enzymes that lack ACP domains and use CoA-linked starter units such as cinnamoyl-CoA to produce flavonoids and stilbenes, and are found in plants, bacteria, and fungi (Austin & Noel, 2003; Funa et al., 1999; Rubin-Pitel et al., 2008).

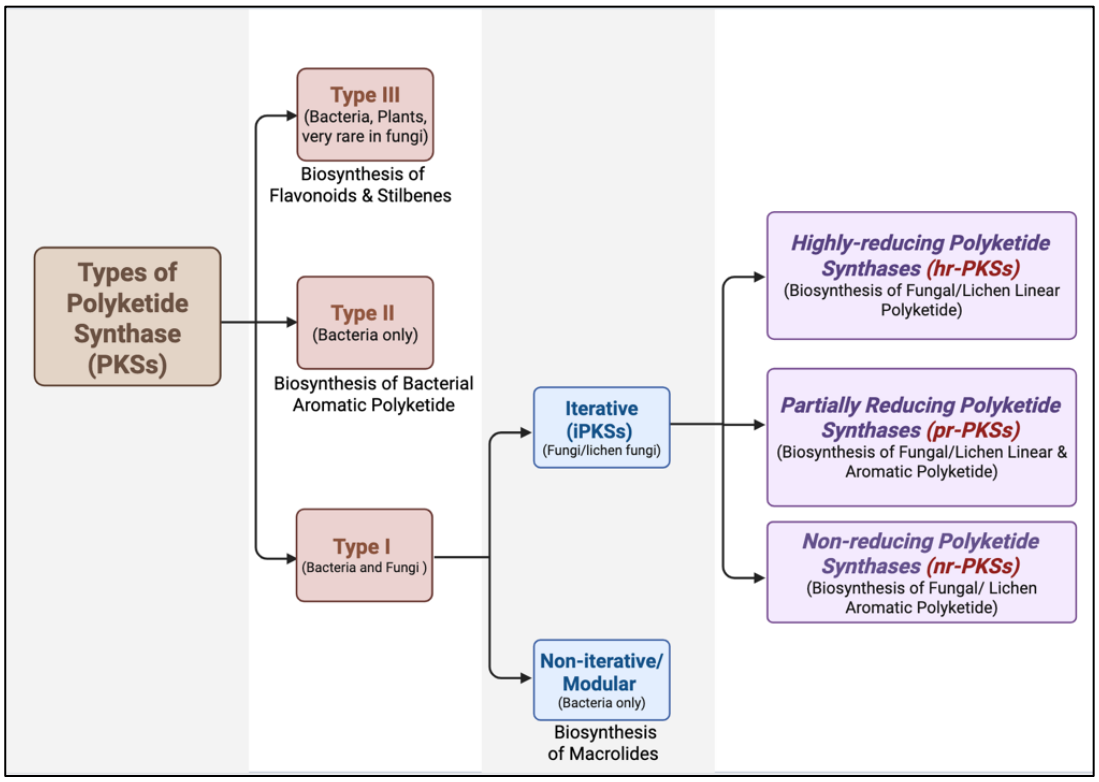

Figure 7. Type of polyketide synthases (Staunton & Weissman, 2001)

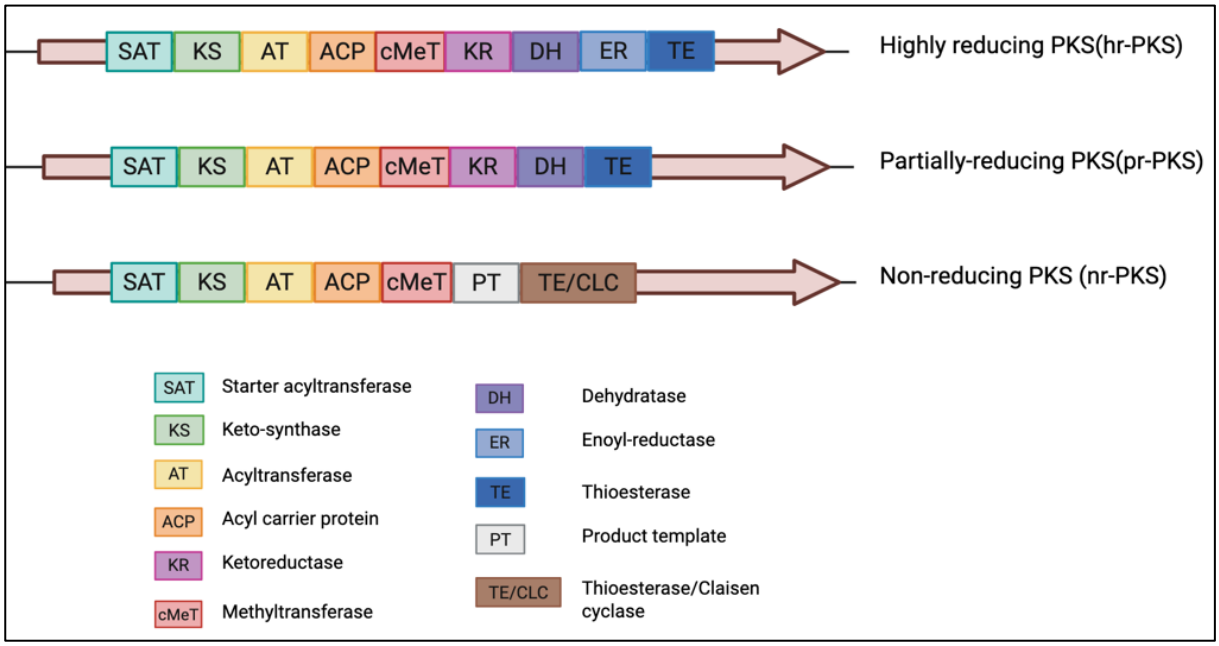

Figure 8. Classification of PKS type I iPKSs based on its domain architecture (Dewick, 2009; Staunton & Weissman, 2001)

1.7 Genomic insights into lichenized fungi

Although many secondary metabolites have been isolated from lichens and extensively studied for their biological properties and potential uses, our understanding of the connection between their chemical structures and their biosynthetic gene clusters that produce SMs is still limited. This gap is largely due to the difficulty of cultivating lichen symbioses or the corresponding mycobiont in the laboratory. These limitations hinder functional studies, such as using gene deletion to examine how specific genes influence SMs production. The advances in next-generation sequencing have greatly improved our ability to investigate SM biosynthesis in lichen-forming fungi. Whole lichen genomes have now been sequenced, and freely accessible online tools such as antiSMASH (Blin et al., 2021) enable efficient annotation of SM biosynthetic gene clusters (BGCs).

In lichen-forming fungi, the genes responsible for the biosynthesis of secondary metabolites are typically arranged as biosynthetic gene clusters within the genome (Medema et al., 2015). These clusters commonly consist of one or more core biosynthetic genes encoding carbon backbone enzymes, such as polyketide synthases or non-ribosomal peptide synthetases (NPRSs), which are responsible for constructing the fundamental scaffold of the metabolites **(Figure 9).** These backbone genes are often surrounded by accessory genes encoding tailoring enzymes such as methyltransferases, cytochrome P450s, transcription factors, transporter genes and some with hypothetical functions **(Figure 9).** Tailoring enzymes are critical in secondary metabolite biosynthesis because they introduce diverse modifications the core biosynthetic scaffolds, thereby generating most of the structural and functional diversity observed in natural product families.

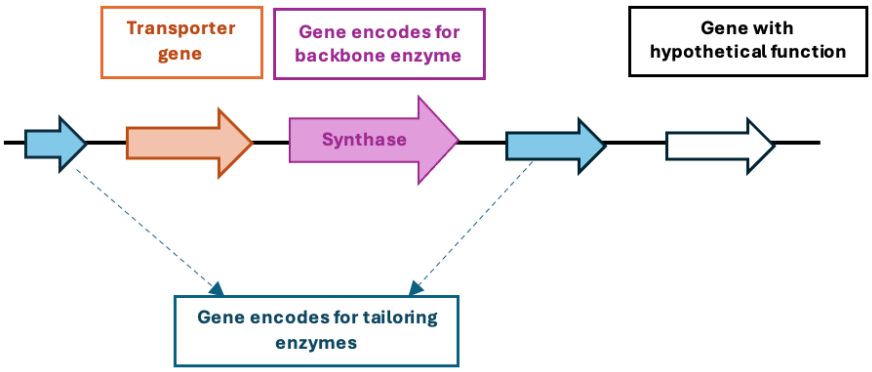

Figure 9. Illustration of a biosynthetic gene cluster. The cluster includes a synthase gene (pink), tailoring genes (blue), transporter gene (orange), and a gene with a hypothetical function (white).

1.8 Post-polyketide synthase/ Tailoring enzymes in lichen BGCs

Polyketide synthase gene clusters in lichens consist not only of the core PKS gene but also include a range of accessory genes. These genes are responsible for modifying the polyketide backbone, ultimately producing the final bioactive compounds. For instance, the transformation of methylphloroacetophenone (MPA) into usnic acid is mediated by post-PKS enzymes cytochrome P450 (Abdel-Hameed et al., 2016; Taguchi et al., 1966). These tailoring enzymes are encoded by genes that are commonly located either upstream or downstream of the PKS gene within the biosynthetic gene cluster **(Figure 10A)**. Tailoring enzymes introduce specific chemical modifications to the polyketide core, such as oxidation, methylation, reduction, and halogenation. Examples of these enzymes include cytochrome P450 monooxygenases, which catalyze oxidation reactions; O-methyltransferases, which add methyl groups; halogenases, which incorporate halogen atoms; and various oxidoreductases involved in redox processes **(Figure 10A).** This thesis focuses specifically on the functional characterization of a lichen-derived cytochrome P450

enzyme involved in usnic acid biosynthesis, aiming to elucidate its catalytic role in the post-PKS modification of MPA (**Figure 10B**).

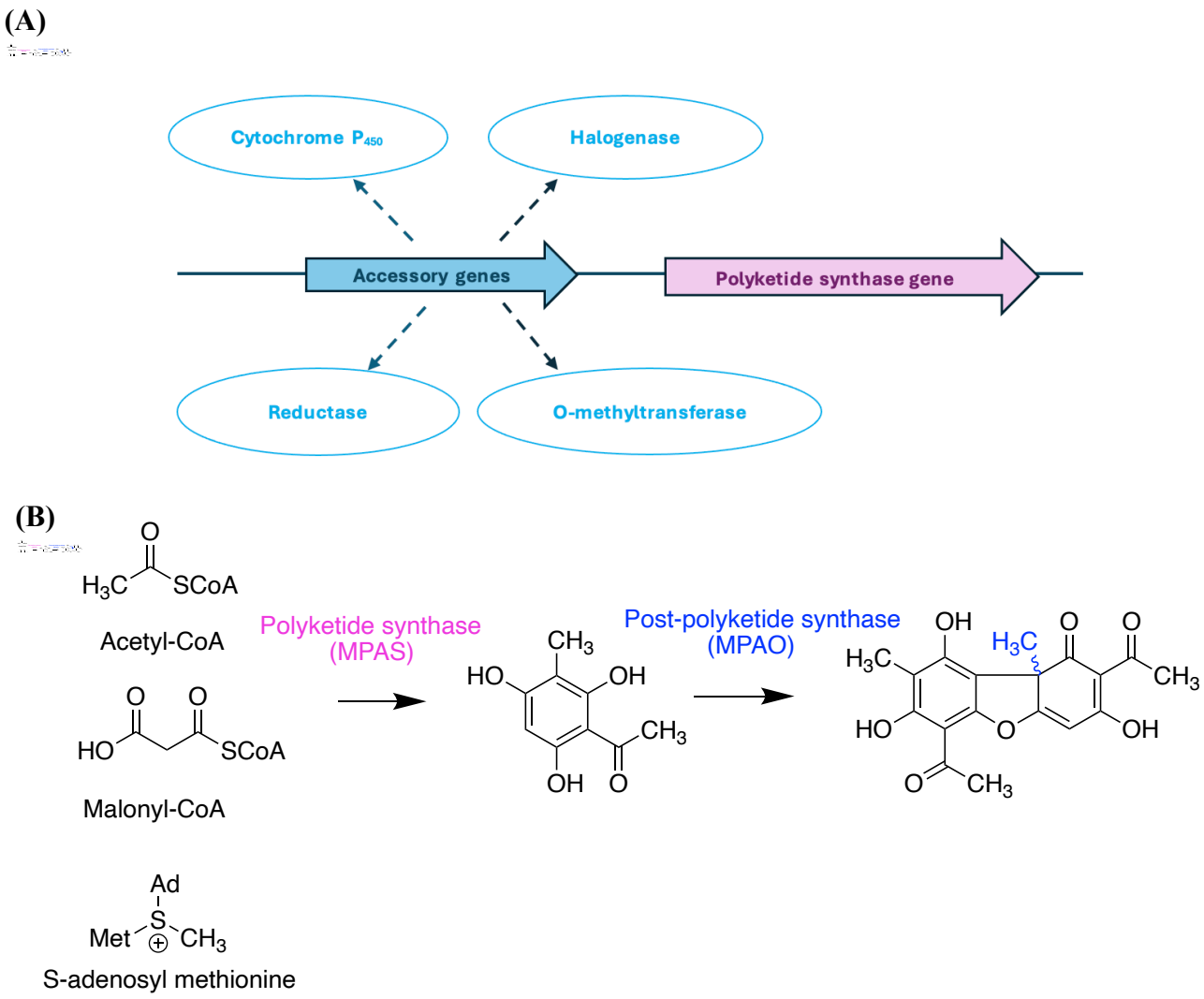

Figure 10. (A) Example of accessory genes (upstream) in biosynthetic gene cluster. (B) The transformation of methylphloroacetophenone (MPA) into usnic acid is mediated by post-PKS enzymes cytochrome P450

1.9 Cytochrome P450s enzymes and their role in polyketide modification

Cytochrome P450s (CYPs) are heme-containing enzymes that represent one of the most ancient and evolutionarily conserved gene superfamilies, playing critical roles in numerous biochemical pathways and physiological processes across all domains of life (Degtyarenko & Archakov, 1993). Cytochrome P450 was initially discovered in rat liver in 1958 as a protein that

facilitates the oxidative transformation of hydrophobic molecules, increasing their hydrophilicity (Klingenberg, 1958). The term "cytochrome P450" was formally introduced by Omura and Sato in 1964. They determined it as a terminal oxidase, belonging to a class of proteins characterized by carbon monoxide binding in the reduced state, an absorption peak at 450 nm, and the presence of a heme prosthetic group (Omura & Sato, 1964). The cytochrome P450 gene family has been observed in all organisms, ranging from noncellular viruses to prokaryotes (archaea and bacteria) and eukaryotes (plants, animals, and fungi) (Omura, 1999; Lamb et al., 2019; Teng et al., 2019; Ngcobo et al., 2023; Dadras et al., 2025; Fang et al., 2024). The catalytic versatility of these enzymes is remarkable, facilitating reactions such as C–H bond hydroxylation, alkene epoxidation, heteroatom oxygenation, oxidative, and peroxidative (Dubey & Shaik, 2019; Lamb & Waterman, 2013; Winker et al., 2018). More than 300,000 CYP sequences have been identified across various organisms include viral genomes, aquatic organisms, plants, fungi, bacteria, and archaea(Ershov et al., 2019; Fang et al., 2024; Lamb et al., 2019; Nelson, 2018; Ngcobo et al., 2023). For example, the "Fungal Cytochrome P450 Database" maintained by Seoul National University catalogs more than 21,568 fungal CYP sequences from 190 species (J. Park et al., 2020). Despite their abundance and importance, the structural complexity of most cytochrome P450s presents substantial challenges for biochemical characterization. The majority of these enzymes are membrane-bound, particularly those from eukaryotic sources, which complicates their expression and purification.

In lichen secondary metabolism, cytochrome P450 monooxygenases are of the particular interest because they catalyze oxidative tailoring reactions that are essential for the biosynthesis of structurally complex and biologically active compounds such as usnic acid. Cytochrome P450 monooxygenases are heme b containing enzyme, incorporate one oxygen atom from molecular O_2 into substrate, while the other oxygen is incorporated into H_2O, using two electrons from

NAD(P)H via their redox partner proteins **(Figure 11).** Other cytochrome P450 functional classes include also include cytochrome P450 peroxygenases, which employs H_2O_2 as both oxygen donor and reductant for fatty acid hydroxylation, independent of NAD(P)H-driven redox partner systems (Munro et al., 2018).

Importantly, the central focus of this study is the functional characterization of a cytochrome P450 involved in the biosynthesis of usnic acid, a dibenzofuran compound and biologically active secondary metabolite from lichen polyketides. CYP acts as a key tailoring enzyme, performing oxidative dimerization that is essential in the formation of usnic acid. This research aims to achieve the functional *in vitro* expression of a lichen-derived CYP MPAO and its redox partner cytochrome P450 reductase (CPR357) for the first time **(Figure 12).**

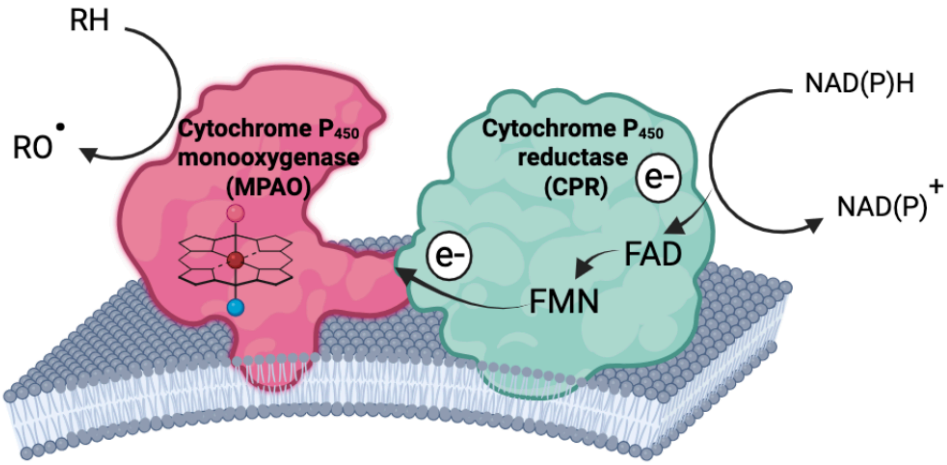

Figure 11. Cytochrome P450 monooxygenase and its redox partner – cytochrome P450 reductase (CPR357).

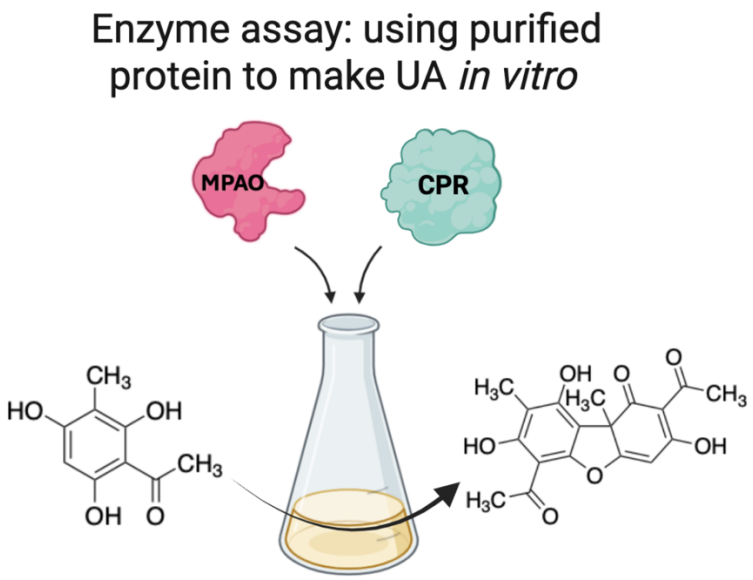

Figure 12. Enzyme assay using purified proteins MPAO and CPR357 to make UA *in vitro*.

1.10 Prosthetic group of cytochromes P450

The defining characteristic of cytochrome P450 enzymes is the presence of a heme prosthetic group, which plays the important roles in both substrate binding and catalytic activity. The term 'heme' (American English) or 'haem' (British English) refers to a coordination complex (metalloporphyrin) consisting of a central iron ion which is coordinated to a porphyrin moiety as tetradentate ligand. This iron centre also coordinate of one or two ligands above or below the plane of the porphyrin **(Figure 13A)** (Cvjetan & Walde, 2023; Moss et al., 1995). The general term porphyrin is used for the unsubstituted parent structure of all porphyrins (**Figure 13B**). All porphyrins consist of a cyclic tetrapyrrole unit in which four pyrrole rings are linked through methine bridge (-CH=) at their α-positions (Moss, 1988), forming a planar, aromatic macrocycle of 18 delocalized π-electrons **(Figure 13B).** This delocalized π-electron system is responsible for the characteristic absorption of porphyrins in the near-ultraviolet and visible regions of the electromagnetic spectrum (Gouterman, 1961). In **Figure 13C** shows the chemical structure of one of the four possible tautomer of the base form of protoporphyrin IX (= H_2PPIX). The difference between this and the parent structure shown on **Figure 13B** is the presence of a methyl group at C2, C7, C12 and C18, a vinyl group at C3 and C8, and a propionic acid group at C13 and C17. To specify the four pyrrole rings, they are designated A, B, C, and D, as indicated. Upon the metalation with Fe(II) or Fe(III), the two protons connected to the two nitrogen atoms in H_2PPIX are released and the corresponding metalloporphyrin heme *b* is formed, (PPIX)Fe^{II} or $[(PPIX)Fe^{III}]^+$ (Cvjetan & Walde, 2023).

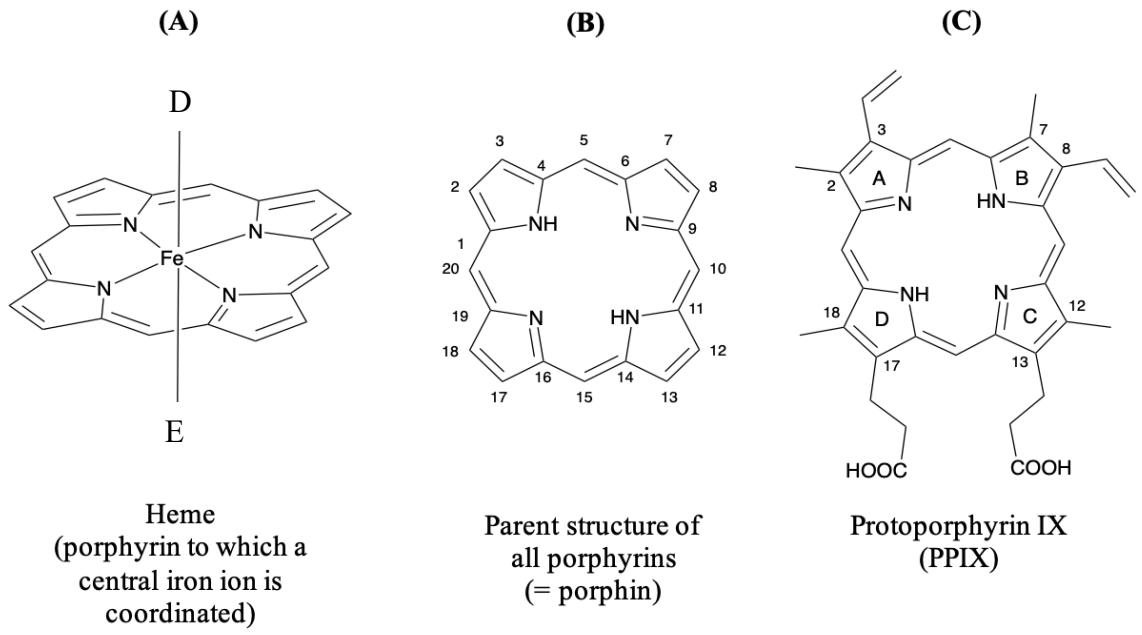

Figure 13. (A) Chemical structure of heme consisting of an iron which is coordinated to the four nitrogen atoms of a planar macrocyclic porphyrin ring, D and E are the two axial ligands at the 5th and 6th coordination sites, respectively. **(B)** Using the '1-24' atom numbering system for parent structure, often called 'porphin'. **(C)** Chemical structure of one of the four possible tautomer of the base form of protoporphyrin IX (Moss,1988).

1.11 Heme *b* in cytochrome P450 monooxygenases

Heme groups occur in several distinct types, each defined by specific modifications to the porphyrin ring or attached side chain. The catalytic center of cytochrome P450 monooxygenase enzymes, which is the focus of this thesis, is composed of a heme-iron complex, specifically heme *b* **(Figure 14).** Heme *b* is the most prevalent form of heme in biological systems, also found in hemoglobin and myoglobin (Yuan et al., 2016). There are known biosynthetic routes that lead to heme *b*, with δ- aminolevulinic acid (5-ALA) **(Figure 14)** (Kořený et al., 2022; Layer, 2021). In any case, heme *b* is present as a prosthetic group in the active site of many different types of heme

proteins, heme consists of a protoporphyrin IX macrocyclic ring system in which a central iron atom, is coordinated to the four nitrogen atoms of the tetrapyrrole ring, forming a rigid planar environment that constitutes the core of the enzyme's active site **(Figure 14).**

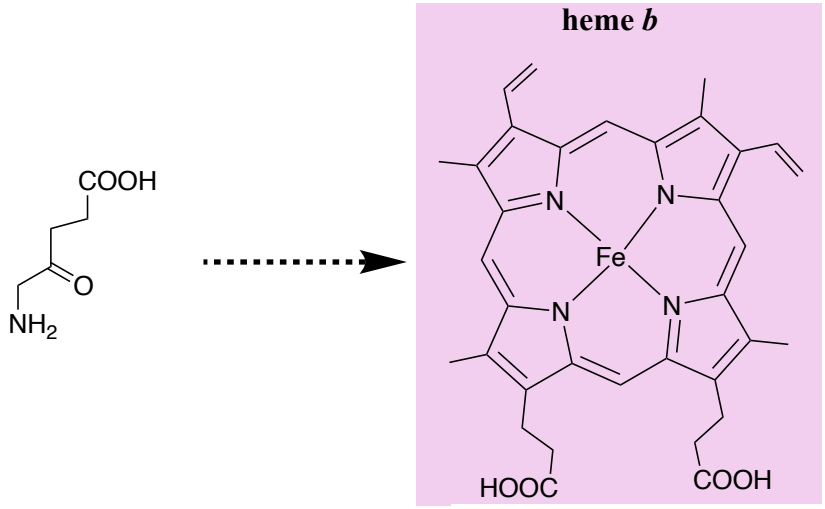

δ-Aminolevulinic acid **Fe (III)-Ferric heme *b***

Figure 14. The chemical structures of δ-aminolevulinic acid (precursor), heme *b* (iron protoporphyrin IX) in heme biosynthetic pathway (Cvjetan & Walde, 2023).

1.12 Molecular Oxygen Activation CYP

The catalytic cycle of cytochrome P450 enzymes is illustrated in Part **A** of **Scheme 1**. In its resting state, when a ligand (such as water) occupies the axial position, the ferric iron (Fe^{3+}) exists in a nearly planar, low-spin configuration (**6.1**); the parallelogram represents the heme's porphyrin ring, with each corner denoting a pyrrole nitrogen. The heme is bounded to the protein via Cysteine-357, which coordinates the bottom axial position of the iron through its sulfur atom, serving the fifth ligand (Silverman, 2002). Upon substrate (R–H) binding, the substrate displaces the axial water ligand, resulting in the formation of a five-coordinate high-spin ferric iron in which the iron is displaced out of the porphyrin plane (**6.2**). This transition from low-spin to high-spin is a key step in activating the catalytic cycle.

The completion of the catalytic cycle requires the sequential transfer of two electrons, typically derived from cellular cofactors such as nicotinamide adenine dinucleotide (NADH) or nicotinamide adenine dinucleotide phosphate (NADPH). These electrons are delivered to the cytochrome P450 enzymes by redox partner proteins that contain flavin adenine dinucleotide (FAD) and flavin mononucleotide (FMN). The first electron reduces the enzyme-substrate complex, increasing the redox potential of the heme prosthetic group and converting the iron from the ferric (Fe^{3+}) to the ferrous (Fe^{2+}) state (**6.3**).

Subsequently, molecular oxygen binds to the reduced ferrous iron centre, leading to electron transfer from the iron to the oxygen, forming a low-spin ferric superoxide complex, also referred to as the ferric-peroxy radical (**6.4**). A second electron transfer event produces a low-spin iron-peroxy anion (**6.5),** which upon protonation generates a heme peroxide (**6.6**). A second proton is transferred to the distal oxygen which induces cleavage of the O–O bond, releasing a water molecule and forming the highly reactive oxo-ferryl heme **(6.7)**. Research from Loew et al. support **6.7b** as the active oxygen (Cleland, 1990). The reactions have been shown to be catalyzed by π-radical cationic form of **6.7b** via hydrogen abstraction from a substrate R–H bond (formally a proton-coupled one electron oxidation of the substrate yielding **6.8** and a substrate radical (**Scheme 1B**). This is followed a hydroxyl radical rebound from the heme to the substrate, resulting in the release of a hydroxylated product. This reaction is both thermodynamically and kinetically favored. The enzyme returns to the default ferric resting state restarting the catalytic cycle (**Scheme 1B**) (Silverman, 2002).

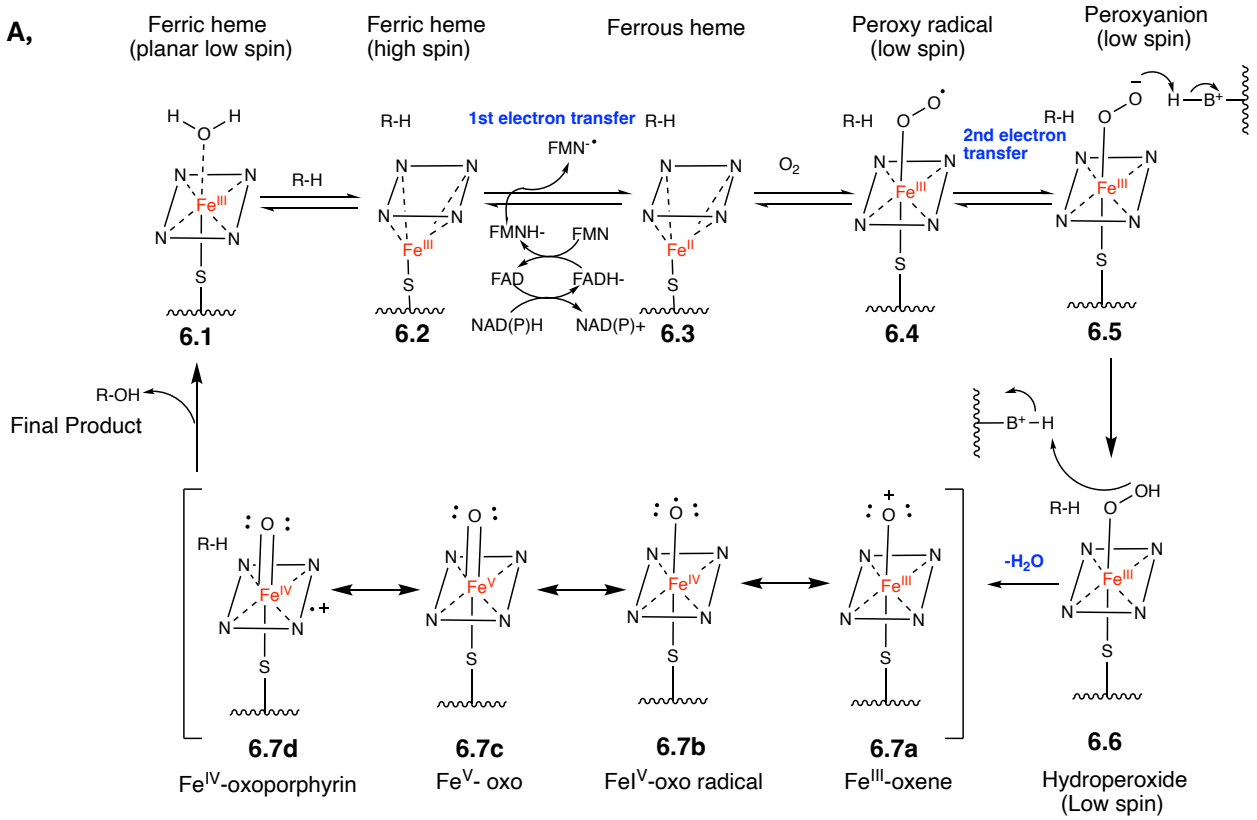

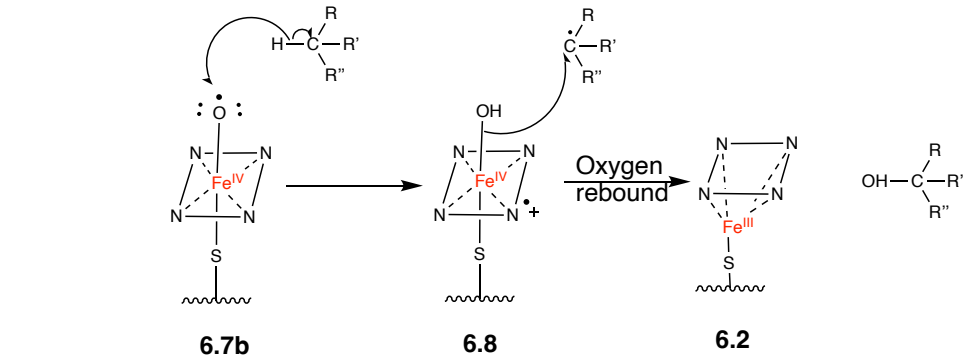

Scheme 1. A) The catalytic cycle of cytochrome P450 enzymes, illustrating the activation of molecular oxygen by heme-dependent monooxygenases, **B)** Two-step radical mechanism with oxygen rebound for alkane oxygenase by heme-dependent monooxygenase (Silverman, 2002).

1.13 Proposed Radical-Radical Cytochrome P450 Mechanism in Usnic Acid Biosynthesis

The usnic acid (UA) biosynthetic gene cluster was identified based on the genome sequencing of *Cladonia uncialis* (Abdel-Hameed et al., 2016). Within this cluster, the key oxidation step in UA biosynthesis is catalyzed by a cytochrome P450 monooxygenase, referred to as methylphloroacetophenone oxidase (MPAO). This enzyme, encoded by an accessory gene in the UA gene cluster, mediates the oxidative dimerization of two molecules of methylphloroacetophenone (MPA) to form UA **(Scheme 2).** The first mechanism involves a typical CYP catalytic cycle step **(Scheme 2-I)**, where hydrogen abstraction from the phenolic –OH group of MPA is initiated by the Fe(IV)-oxoporphyrin π-radical cation intermediate **(6.7b).** This step generates an MPA radical with electron density localized primarily on the oxygen atom and simultaneously converts **(6.7d)** FeIV-oxoporphyrin π-radical into the Fe(IV)-hydroxo species. The MPA radical is resonance stabilized, with its unpaired electron predominantly localized on the tertiary carbon in the major contributing structure **(A).** Subsequent hydrogen abstraction from a second MPA molecule by the Fe(IV)-hydroxo species leads to the formation of a second resonance-stabilized radical **(B) (Scheme 2-I).**

Radicals A and B are stabilized by resonance delocalization of the unpaired electron, primarily through the tertiary structures that benefit from hyperconjugation with adjacent alkyl groups. We then propose that radical coupling between these two stabilized radicals (A and B) **(Scheme 2-II)**, followed by Michael addition and condensation steps, leads to the formation of the structure of UA. In addition, cyclic voltammetry suggests that MPA undergoes a multi-step electro-oxidation initiated by a two-electron, two-proton loss, forming a quinone-like intermediate. This intermediate is then attacked by water, yielding a benzyl alcohol species. A third electron is

rapidly removed to generate a resonance-stabilized radical centered on the tertiary carbon adjacent to the benzylic position. This radical is proposed to dimerize, consistent with the formation of higher-order products and the absence of a corresponding cathodic peak. The final oxidation may also occur at one of the phenolic hydroxyl groups (C2, C4, or C6), further diversifying the product profile. The observation of a single anodic peak in Cyclic Voltammetry (CV) indicates that these redox steps occur at nearly the same potential (Mendes Hacke et al., 2025).

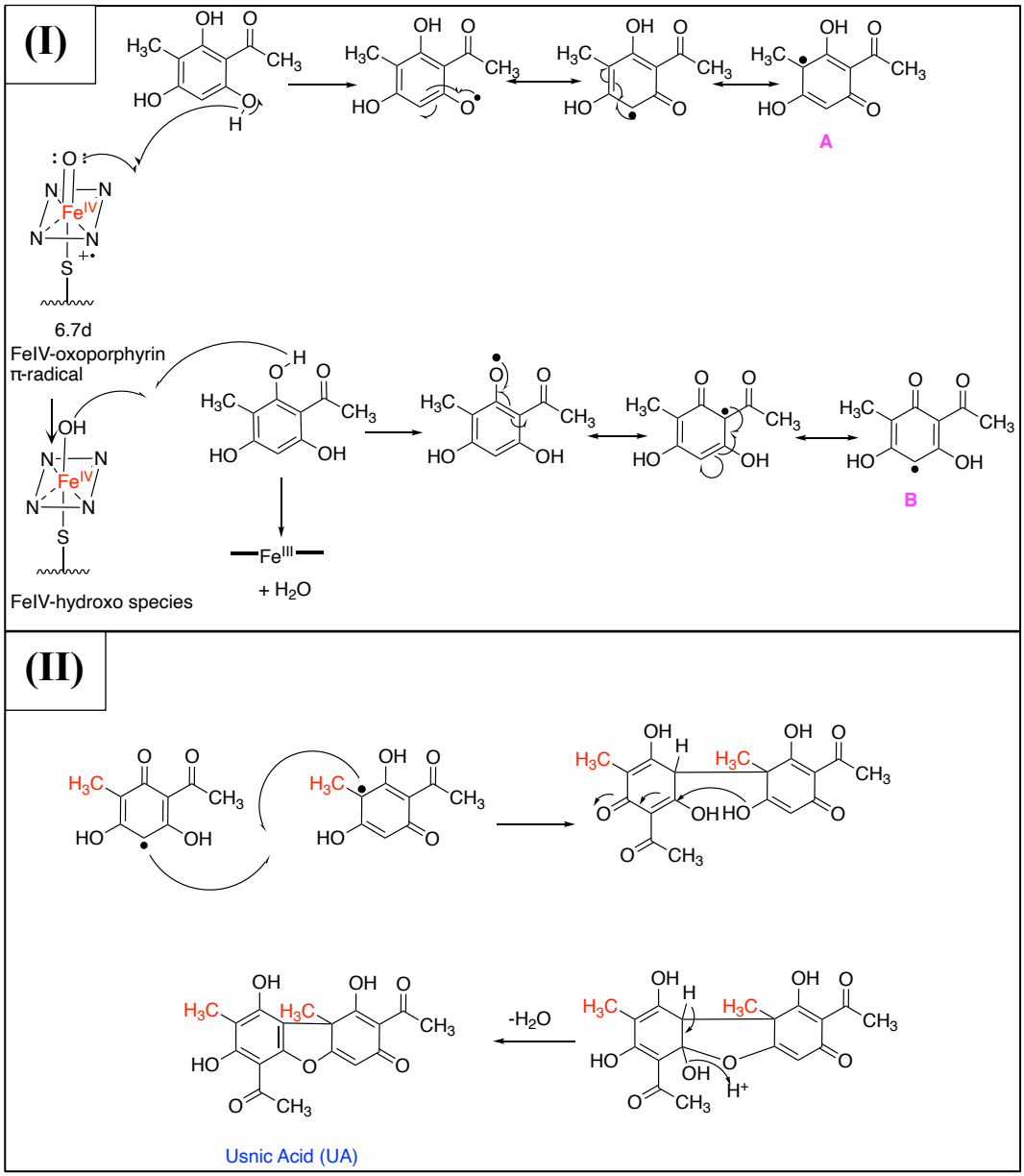

Scheme 2. (I) The cytochrome P450 enzyme (MPAO) involved in UA biosynthesis catalyzes two consecutive hydrogen abstraction reactions from two MPA substrate molecules, generating two resonance-stabilized MPA radicals, designated as A and B. **(II)** Radical-radical C-C oxidative coupling of two MPA radicals leading to formation of UA (Mittal, 2023).

1.14 The importance of redox partners (RPs)

In addition to the detailed catalytic mechanism of cytochrome P450 enzymes already described in **Section 1.11**, the CYPP450 catalytic cycle also requires the sequential input of two electrons. To facilitate the transfer of these two electrons, CYPP450s utilize diverse redox chains composed of various redox partners, including ferredoxins (**Fdx**: iron-sulfur proteins), ferredoxin reductase (**FdR**), cytochrome P450 reductase (**CPR**), cytochrome b5 (**CB5**), and cytochrome b5 reductase (**CB5R**) (Durairaj et al., 2016).

In prokaryotes, the typical redox partners are Fdx and FdR, whereas CPR, CB5, and CB5R are more commonly found in eukaryotes (Chiliza et al., 2020; Wayne et al., 2013; W. Zhang et al., 2018). Like CYP, cytochrome P450 reductase is a membrane-bound protein that contains the prosthetic cofactors flavin adenine dinucleotide (FAD) and flavin mononucleotide (FMN). These cofactors mediate the sequential transfer of two electrons from NAD(P)H to the heme moiety of CYPs located in the endoplasmic reticulum. Electron transfer proceeds from NAD(P)H to FAD, then to FMN, and subsequently to the CYPs **(Figure 15A).** Alternatively, CPR can transfer one electron directly to CYP and the second to CB5, which in turn donates it to the CYP **(Figure 15B)**. In rare cases, certain CYPs (e.g., CYP5150A2: a fungal cytochrome P450 monooxygenase from the white-rot basidiomycete *Phanerochaete chrysosporium*) can be directly activated by CB5 and

NADH-dependent CB5R in the absence of CPR (Hatakeyama et al., 2016; Ichinose et al., 2004) **(Figure 15C).**

There is experimental evidence of electrostatic interactions between negatively charged amino acids of the FMN domain of CPR protein and positively charged amino acids of CYP protein (Campelo et al., 2018; Esteves et al., 2020). As the number of functionally eukaryotic CYPs continues to grow, the selection of an optimal redox partner is crucial. The type and ratio of partners affect catalytic efficiency, since the second electron transfer is often rate-limiting. Furthermore, recent studies also show that the redox partners can change substrate preference and product outcomes (Durairaj et al., 2016; Durairaj & Li, 2022). As a result of the CYP functioning-regulating role of redox partners, it has become extremely important to choose the right redox partner for a specific CYP. Since CPR is a key redox partner for CYPs and considering the potential involvement of CB5 and CB5R in some cases the separate expression of these redox partners alongside CYPs is essential to ensure optimal catalytic activity and efficient bioconversion.

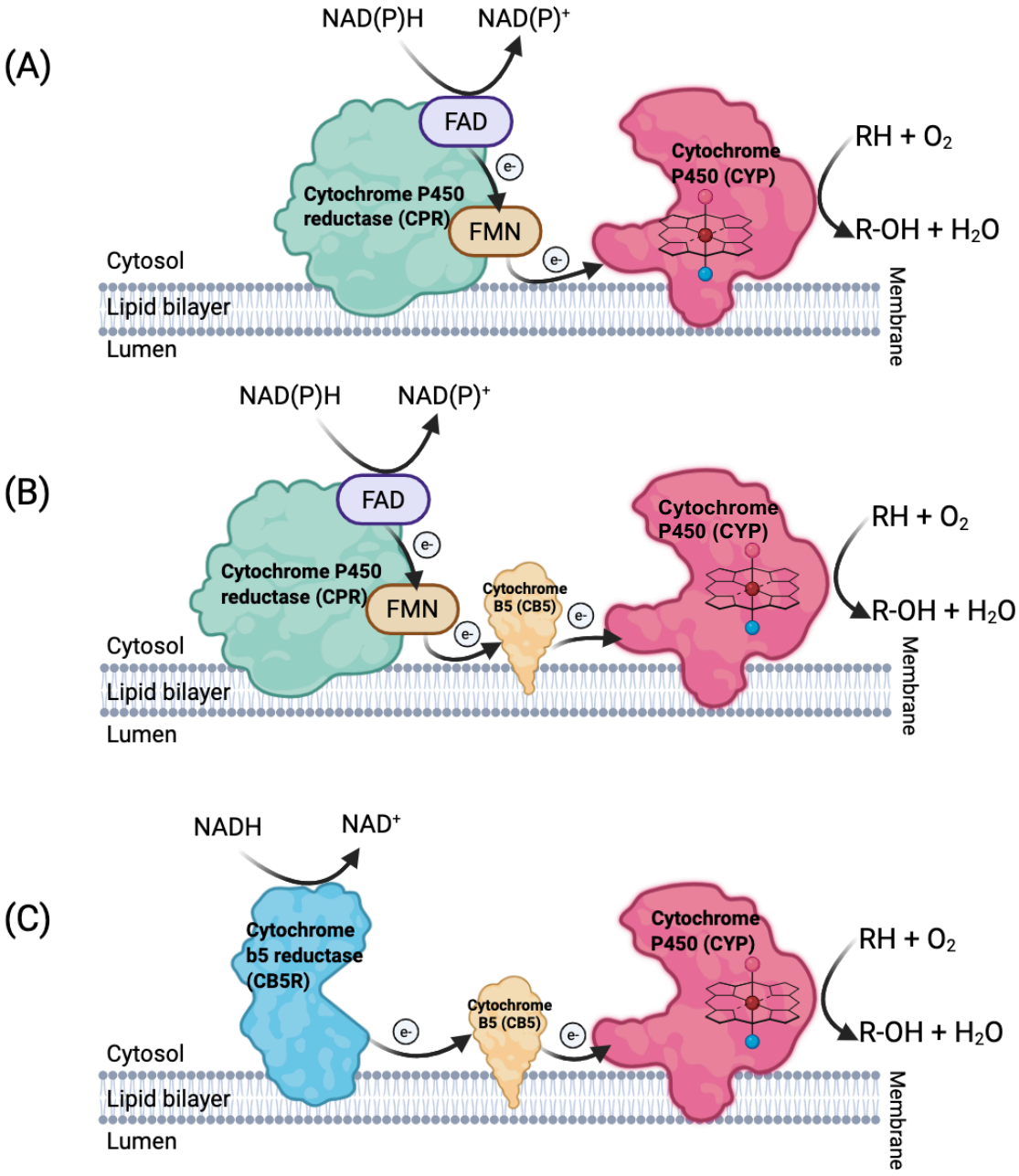

Figure 15. Three different pathways by which CYP enzymes get electrons from their partners. **(A)** From NAD(P)H through CPR to CYP. **(B)** From NAD(P)H through CPR and then cytochrome B5 (CB5) to CYP. **(C)** From NADH through cytochrome b5 reductase (CB5) then cytochrome B5 to CYP (Durairaj et al., 2016).

1.15 The cytochrome P450 redox partner selection

Although fungal CYPs are large and diverse, most fungi possess only one or two CPRs exception include four putative CPRs found in *Fusarium oxysporum* (Durairaj, P. et al., 2016; Durairaj, P. et al., 2015). For recombinant expression eukaryotic CYPs are typically reconstituted with redox partners from one of three sources: (1) endogenous CPR (eukaryotic expression host's native CPR), (2) homologous CPR (from the same source as CYP), (3) heterologous CPR (from other fungal or yeast species). However, studies have shown that homologous CYP-CPR combinations often yield higher electron transfer efficiency and coupling (Braun et al., 2012; Durairaj et al., 2015; Durairaj & Li, 2022; Jennewein et al., 2005). Importantly, the source of the reductase can significantly influence the substrate specificity of fungal CYPs. Former students of the Sorensen lab used Augustus software to identify three genes in the *Cladonia uncialis* genome (Bertrand, n.d., 2016; Mittal, n.d., 2023) that are highly homologous to known fungal CPRs: cytochrome P450 reductase (CPRs), cytochrome b5s (CB5s), and cytochrome b5 reductases (CB5Rs). These genes were named **cu-cpr357, cu-cb5-247,** and **cu-cb5r-347** based on the lichen species, gene function, and contig number in the genome, and they encode the proteins CPR357, CB5247, and CB5R347, respectively. Since CPR alone typically transfers both electrons from NAD(P)H to CYP, our initial goal was to perform heterologous expression of **cu-cpr357** (CPR357) in *E. coli* alongside with MPAO to enable *in vitro* bioconversion of MPA to usnic acid. Additionally, experimental evidence supports that electrostatic interactions between negatively charged residues of CPR's FMN domain and positively charged residues on CYPs mediate complex formation and effective electron transfer (Campelo et al., 2018; Esteves et al., 2020). The gene encoding **cu-cb5-247** and **cu-cb5r-347** were retained as alternative options if **cu-cpr357** alone was insufficient to complete the electron transfer cycle.

1.16 Usnic acid

Building on the functional of MPAO and CPR357 system described in **Section 1.11**, this section introduces usnic acid as the bioactive product generated through this enzymatic system. Usnic acid is biosynthesized through a polyketide pathway **(Section 1.6)** and has gained significant attention due to its diverse biological activities. UA is a naturally occurring lichen-derived SMs characterized by the presence of a single chiral center at the C-9b position, resulting in two enantiomeric forms: (+)-usnic acid and (-)-usnic acid (Xu et al., 2022) **(Figure 16A).** Both enantiomers occur in nature, and their distribution is species specific. (+)-usnic acid has been reported as the predominant enantiomer in *Usnea* Dill. ex. Adans. species (*Parmeliaceae*), whereas the genus *Alectoria* Ach. (*Parmeliaceae*) seems to mainly produce (-)-usnic acid (Galanty et al., 2019; Guo et al., 2008; Xu et al., 2016) **(Figure 16B)**. Both the (+) and (-) UA enantiomers are effective against a large variety of Gram-positive (G^+) bacterial strains for example, by inhibiting the growth of multi-resistant strains of *Streptococcus aureus*, enterococci, and mycobacteria. The (+)-UA enantiomer shows selectivity against *Streptococcus mutans* without inducing perturbing side effects on human oral saprophytic flora (Cocchietto et al., 2002). On the other hand, the (-)-UA enantiomer acts as a selective natural herbicide due to its blocking action on specific key plant enzymes (Cocchietto et al., 2002). In addition, its ultraviolet absorption and preserving properties are why it is explored as a protective agent in pharmaceutical and cosmetic applications (Aslan Engin, 2025).

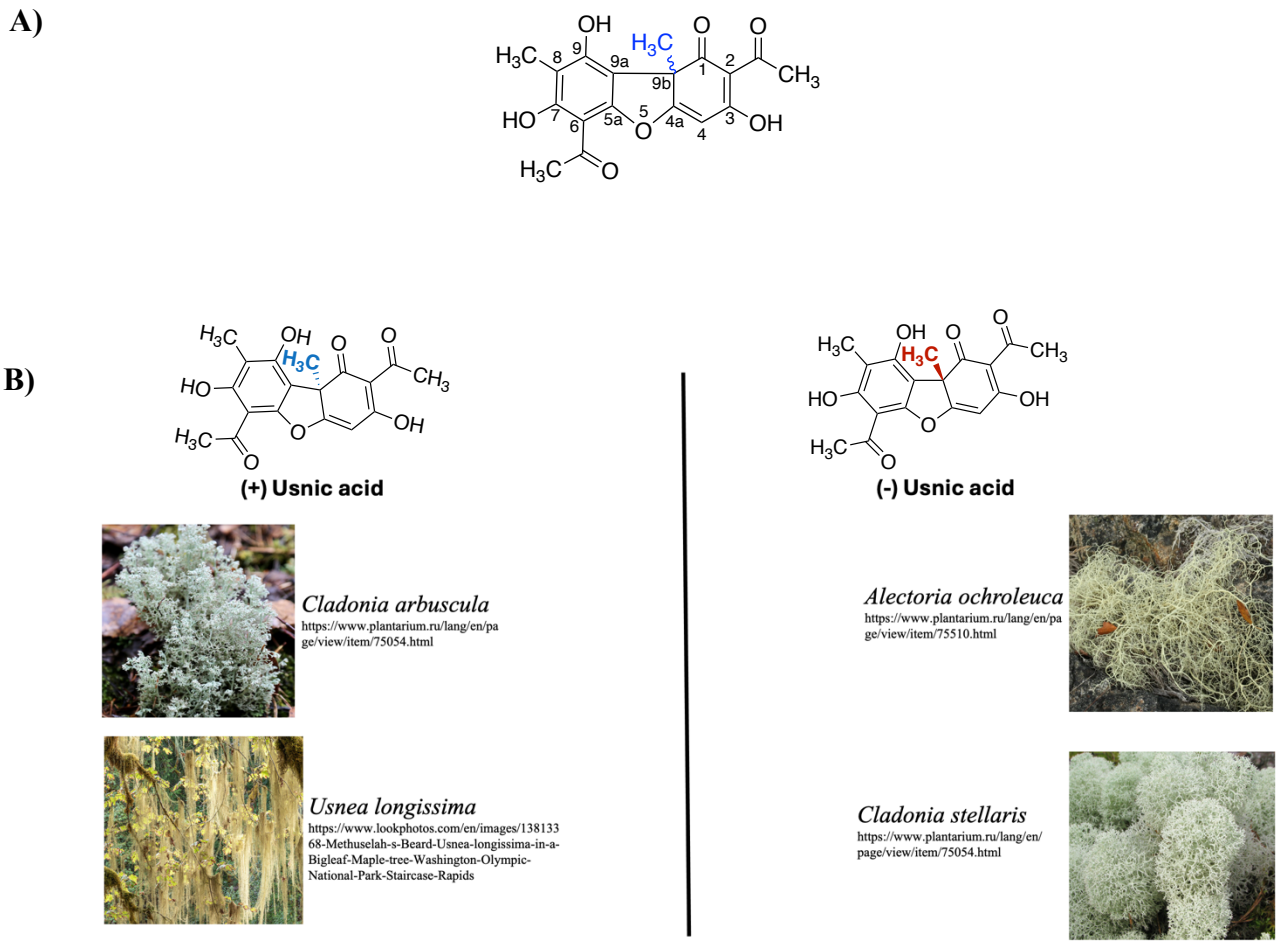

Figure 16. **(A)** Usnic acid chemical structure; **(B)** Usnic acid enantiomers variation depends on lichen species.

To date, most research has focused on the bioactivity of (+)-usnic acid, possibly due to its historical use in traditional medicine and commercial products. Lichens containing (+)-usnic acid, such as *Usnea barbata* and *Evernia prunastri*, have been traditionally used in herbal remedies and perfumery (Ahad et al., 1991; Guo et al., 2008; Huneck, S., Yoshimura, I., n.d.). This enantiomer has also been formulated into various European consumer products, including ointments, foot creams, and cosmetics (Guo et al., 2008), primarily due to its antibacterial properties, especially

against Gram-positive bacteria and *Mycobacterium* species (Ingólfsdóttir et al., 1998; Lauterwein et al., 1995). However, oral overdose of (+)-usnic acid has been associated with hepatotoxicity, primarily due to disruption of mitochondrial function in liver cells (Joseph et al., 2009; Moreira et al., 2013; Sonko et al., 2011, Xu et al., 2022). It also interferes with cellular signaling pathways involved in apoptosis and autophagy (Chen et al., 2014). Novel delivery systems, such as nanoencapsulation, have shown potential to mitigate these toxic effects (Macedo et al., 2021).

Fewer studies have examined both enantiomers in parallel. One comparative study isolated (+)- and (-)-usnic acid from *Cladonia arbuscula* and *Cladonia stellaris*, reporting that (-)-usnic acid was approximately twice as genotoxic as the (+)-form in assays using human peripheral blood lymphocytes (Prokopiev et al., 2017). Similarly, (-)-usnic acid exhibited greater cytotoxicity against multiple murine and human cancer cell lines compared to its enantiomer (Bazin et al., 2008), although the lichen sources were not specified. In contrast, another study using (+)-usnic acid from *Cladonia arbuscula* and (-)-usnic acid *Alectoria ochroleuca* found no significant enantiomeric difference in cytotoxicity toward human breast cancer cells (Einarsdóttir et al., 2010).

Although comparative data on antitumor activity are limited, some studies suggest that the (-)-UA exhibited higher cytotoxic potency (Bazin et al., 2008). Nonetheless, the intrinsic antitumor activities of both enantiomers are relatively modest, and few patents exist based on the cytotoxic properties of usnic acid itself (Galanty et al., 2019; Siedlarczyk et al., 2025). In addition, there was a study of both enantiomers which revealed time-dependent enantiomer preference in their anticancer activity. While (-)-UA demonstrated twice the potency of (+)-UA at 24 hours, but this preference reversed dramatically at 48 and 72 hours, with (+)- UA demonstrating nearly ten-fold greater activity than (-)-UA, particularly at lower concentrations (2.9 and 29 μM). (Cavalloro et al., 2025). Given these findings, more systematic studies are needed to investigate the distribution,

concentration, and biological activities of usnic acid enantiomers across different lichen species. Also, validated chiral chromatographic techniques will be essential for accurately distinguishing and quantifying enantiomers.

1.17 Research Objectives

To explore the molecular basis of the stereo and regioselective formation of usnic acid in lichens, we aimed to functionally express cytochrome P450 enzymes predicted to be involved in its post-polyketide modification steps. Given the limitation of studying the biosynthesis directly with lichens, our approach focused on expressing the target genes in a heterologous system. By cloning and introducing these genes into a fast-growing host, *Escherichia coli*, we can achieve continuous and reproducible enzyme production. A critical component of this study was to express and purify these enzymes, enabling us to conduct *in vitro* bioconversion assays. This would allow us to directly test enzyme activity using defined substrates, and also to functionally characterize the enzymes involved in the biosynthetic pathway of usnic acid. This can be summarized as three main objectives:

Objective 1. Heterologous expression of candidate cytochrome P450 genes, MPAO and CPR357, from *Cladonia uncialis* into *Escherichia coli*

Objective 2: Achieve purification of the recombinant cytochrome P450 enzyme and its redox partner CPR357.

Objective 3: Use the purified enzymes to perform *in vitro* bioconversion assays to determine if MPA can be converted into UA by this P450.

Chapter 2

Material and Methods

2.1 Material and methods related to Chapter 1

Not applicable

2.2 Materials and methods related to Chapter 2

Not applicable

2.3 Materials and methods related to Chapter 3

2.3.1 Chemical synthesis and characterization of Methylphloroacetophenone

The synthesis of MPA was described by Hawranik (2009) and was later modified by Mittal (2023) to improve the overall yield. To 1mmol (186 mg) of trihydroxyacetophenone monohydrate, 2.5 equivalents potassium carbonate (K_2CO_3) (345 mg) and 4 mL of acetone were added, and mixture was brought to 0 °C with stirring. Next, 3 equivalent iodomethane (CH_3I) (186 µL) were added dropwise over 3 hours: the 1st equivalent at the start of the reaction, the 2nd after 1 hour and the 3rd after 2h, while maintain the reaction at 0 °C with stirring. The reaction was quenched with 10 mL 1M HCl, followed by extraction with ethyl acetate (EtOAc) (2 X 30 mL), and the organic layer was dried (Na_2SO_4) and evaporated to dryness using a rotatory evaporator. The crude extract (200 mg) was fractionated using a pre-packed normal-phase spherical silica (10 g, 60 µm particle) flash chromatography column (Biotage ® Sfär Silica) with a Biotage Isolera Prime 3.3.0 apparatus. The flow rate was maintained at 1 mL min^{-1}, and detection was performed at 264 and 245 nm. A gradient was employed, beginning with 100% Hexane and progressing to Hexane: EtOAc (6:4). Fractions were collected in 20 mL test tubes and analyzed by using Nuclear Magnetic Resonance (NMR) and HPLC. Test tubes containing similar compounds were pooled together. The reaction

resulted in many O-methylated side products along with the synthesis of MPA (**Scheme 3**). The isolated yield of methylphloroacetophenone (MPA) was 48%.The NMR spectra were collected on Bruker Avance-400 and Avance-500 consoles and were reference to solvent Methanol-d4 (3.1 ppm in ^{1}H). Waters HPLC Separations Module 2695 system equipped with a PDA Detector Model 2996 by injecting 20 µL of the supernatant using an autosampler. The column was a µBondapak® Waters C18 (3.9 X 300 mm) with a particle diameter of 15-20 µm with 125 Å pores. A gradient of Milli-Q water and methanol was used as the mobile phase (solvent A was Milli-Q water with 0.1% formic acid, and solvent B was methanol) at a flow rate of 1 ml/min. The UV signal was monitored at 250 nm, and spectra were collected from 200 to 600 nm. The complete NMR and HPLC characterization provided in **Figure S1-4 and Table S 2**.

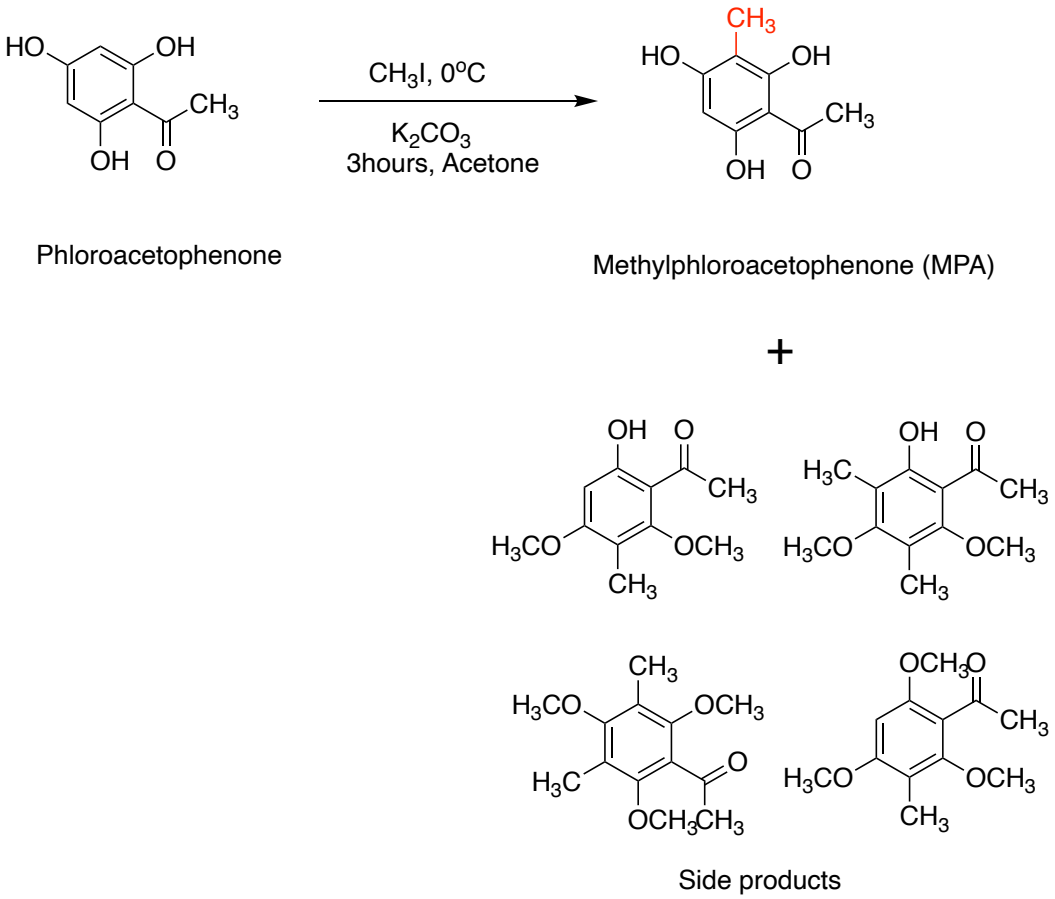

Scheme 3. The synthesis of Methylphloroacetophenone . CH_3I: Iodomethane, K_2CO_3: Potassium carbonate.

2.3.2 Test compounds for bioassays

Usnic Acid (UA) was purchased from ChromaDex® USA (>98% purity by HPLC) and used as received. Methylphloroacetohenone (MPA) was synthesized as described above and the characterization data given in supplementary section **(Figure S1-4)**.

2.3.3 Plasmid design C. uncialis cytochrome P450

2.3.3.1 Cytochrome P450 monooxygenase- MPAO plasmid design

This study was used codon optimized for *E. coli* and transmembrane domain (TMD) was truncated. This gene was named CO(Eco)_MPAO (C: codon O: optimized Eco: *E. coli*) (1456

bps).Previous research reported the functional sustainability of cytochrome P450s even after the removal of TMD (Hausjell et al., 2018). The CO(Eco)_MPAO gene was provided by Professor Ikuro Abe at the University of Tokyo (Tokyo). To facilitate heterologous expression, the MPAO gene sequence (w/o TMD, codon optimized for *E.coli*) into the pET28a(+) expression vector, and the plasmid commercially synthesized by Twist Bioscience, which included N-terminal 6xHis-tag, which facilitates downstream purification using Ni-NTA His-tag affinity chromatography (***Figure S 5***). Kanamycin was chosen as the antibiotic selection marker. The MPAO plasmid was received form Twist with 1453 ng/μL concentration and was resuspended according to the manufacturer's DNA resuspension guidelines (Twist Bioscience, 2023).

2.3.3.2 Cytochrome P450s reductase – CPR357 plasmid design

Cytochrome P450 enzymes require the sequential input of two electrons to complete their catalytic cycle. Cytochrome P450 reductase facilitates electron transfers from NAD(P)H to cytochrome P450 and therefore an essential component of the P450 redox cycle. As described in **Section 1.12**, a CPR357 gene was identified in the *Cladonia uncialis* genome, showing high sequence homology to previous characterized fungal CPRs. To perform heterologous expression, the CPR357 gene sequence (without intron) was customized into the pET28a(+) expression vector, and the plasmid commercially synthesized by Twist Bioscience, which included N-terminal 6xHis-tag, which facilitates downstream purification using Ni-NTA His-tag affinity chromatography. Kanamycin was chosen as antibiotics selection marker for plasmid maintenance (***Figure S 6***). The CPR357 plasmid was received from Twist with a concentration at 1819 ng/μL and was resuspended according to the manufacturer's DNA resuspension guidelines (Twist Bioscience, 2023).

2.3.4 Transformation of MPAO plasmid (w/o TMD, codon optimized) into E.coli BL21(DE3)pLySs

To prepare plasmids, MPAO plasmids containing the synthesized MPAO gene (1453 ng/uL) were resuspended in nucleases-free Tris-EDTA (TE) buffer (pH 8.0) to final concnetration10 ng/uL **(Section 2.3.3.1).** LB plates containing kanamycin for plasmid selection, include 34 µg/mL chloramphenicol as recommended by the manufacturer for BL21(DE3)pLysS cells.

For transformation: MPAO plasmid was transformed into *E.coli* BL21(DE3)pLysS (Thermo Scientific*)* cells separately using the manufacturer's recommended heat-shock method. Colonies were selected on the agar plate with the respective antibiotics. The colonies were resuspended in 5mL of LB media with kanamycin (30 µg/mL) and was cultured overnight at 37°C. The overnight bacterial culture was aliquoted into multiple microcentrifuge tubes (each with 500 µL of sample) and 500 µL of 40% glycerol was added to each of the tubes to make the final 1mL of stock solution and stored at -80 °C. The plasmid was purified using Monarch® Plasmid Miniprep Kit, and full plasmid sequencing by Genewiz confirmed the presence of the correct construct.

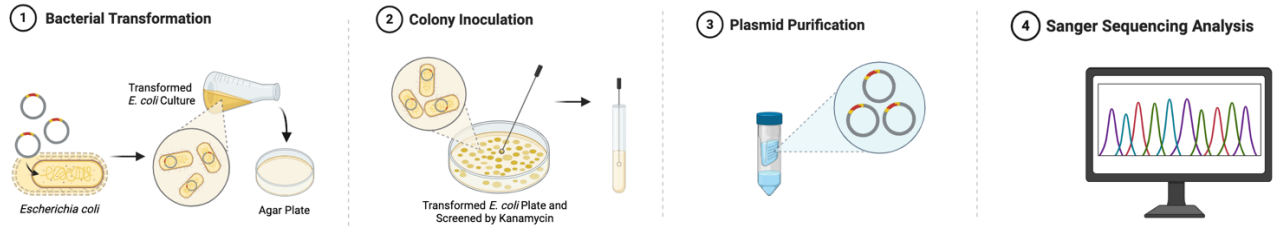

Figure 17. Plasmid transformation in *E.coli* workflow. Created by BioRender®.

2.3.5 Heterologous expression of the MPAO in E.coli

To prepare the overnight culture, 5 mL of Luria Broth (LB) containing 30 µg/mL kanamycin was inoculated with 100µL of stock solution (thawed on ice) and incubates at 37°C with shaking at 250 rpm (revolutions per minute). The overnight culture was transferred to 1L (OD_{600} 0.02-0.04) of LB with 30 µg/mL kanamycin, 40 mM 5-aminolevulinic acid (5-ALA), and incubated at 37 °C with shaking at 250 rpm for 3 hours, until the OD_{600} reached an absorbance range of 0.4 - 0.6 AU. The culture was the induced with 0.5mM isopropyl-β-D-thio-galactopyranoside (IPTG), and incubated was continued at 30 °C with shaking at 200 rpm for 24 hours.

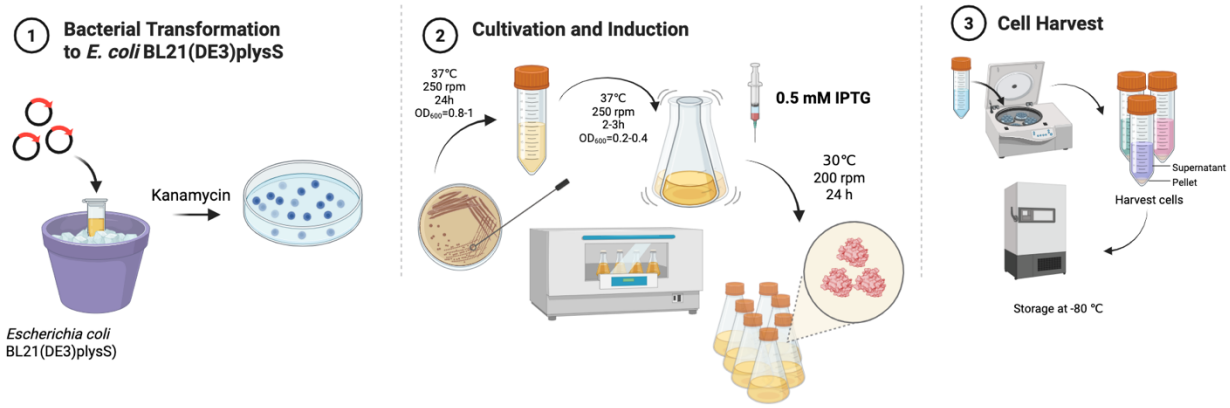

Figure 18. Heterologous expression of MPAO in *E.coli* workflow. Created by BioRender®.

2.3.6 Cell lysis and purification of MPAO enzyme

2.3.6.1 MPAO-Cell Lysis

The bacterial cells were collected by centrifugation at 5,000 × g (Thermo Scientific Sorvall™) for 15 min at 4°C. For SDS-PAGE analysis, the obtained cell pellet was resuspended in 50 µL of 4× SDS-PAGE loading buffer (**Table S 1**) and stored at –20 °C. Protein expression was evaluated by running the samples on a 10% SDS-PAGE gel.

For preparation of protein purification, the supernatant was discarded, and pellet was re-suspended in 5mL (1/20 to 1/50 lysis buffer of the volume of culture used) of cold lysis buffer **A1** (**Table 1**) on ice. Protease inhibitor cocktail (10 µL / 100 X) (Thermo Scientific) was added to 5 mL of the lysis buffer, which protects an intact, active cellular protein from degradation by endogenous proteases. The resuspended cells were placed on ice, and the cell membrane was lysed by sonication (40% amplitude, 4 pulses at 10s intervals and 1 min between each pulse) using an ultrasonic homogenizer (Branson model 150T) and 1% Triton (Thermo Scientific) was added to avoid aggregation of MPAO (Johnson, 2013). A second centrifugation step was performed at 30,000 × g (Thermo Scientific TM Sorvall TM) for 30 min at 4 ◦C. The cell debris was discarded, and the supernatant was filtered with a 0.22 µm filter before purification.

2.3.6.2 MPAO-Protein purification

For MPAO enzyme purification, all procedures were performed in a cold room at 4 °C. The protein was purified with an ÄKTApure® (GE Healthcare) using a HisTrap™ HP 1 mL column (GE Healthcare, Chicago, IL, USA). The supernatant was loaded onto the column, and stepwise elution was carried out at a flow rate of 1 mL/min using the following eluents **(Table 1).** The column was washed with 25 mL of eluent **A1** to remove unbound proteins, followed by 30 mL of eluents **B1** and **B1'** for further washing. His-tagged MPAO was then eluted with 25 mL of eluent **C1**. The fractions were analyzed via 10% SDS-PAGE electrophoresis to confirm protein purification. Protein concentration was determined using a Coomassie (Bradford) protein assay (Bradford, 1976).

Table 1. Buffer composition for MPAO purification

Buffer name	**Reagent**	**pH**
MPAO - Lysis Buffer **(A1)**	20 mM potassium phosphate, 300 mM NaCl	7.4
MPAO - Wash buffer with high salt **(B1)**	20 mM potassium phosphate, 500 mM NaCl	7.4
MPAO - Wash buffer with imidazole **(B1')**	20 mM potassium phosphate, 300 mM NaCl, 36 mM Imidazole	7.4
MPAO - Elution buffer **(C1)**	20 mM potassium phosphate, 300 mM NaCl, 300 mM Imidazole	7.4

2.3.7 Transformation of CPR357 into *E.coli* BL21(DE3)pLysS

Detailed as described in section 2.3.4

2.3.8 Heterologous expression of the CPR357 in *E.coli*

Detailed as described in Section 2.3.5

2.3.9 Cell lysis and purification of CPR357

2.3.9.1 CPR357-Cell Lysis

The CPR357 cell lysis procedure was similar to that described in **Section 2.3.6.1**, except that the A2 lysis buffer was used (**Table 2**), and sonication was performed at 40% amplitude, 8 pulses at 10s intervals and 30 seconds between each pulse) and no 1% Triton X-100 was used.

2.3.9.2 CPR357-Purification of Cytochrome P450

For CPR357 enzyme purification, all procedures were performed in a cold room at 4 °C. The protein was purified with an AKTA pure (GE Healthcare) using a HisTrap HP 1 mL column (GE Healthcare, Chicago, IL, USA). The supernatant was loaded onto the column, and stepwise elution was carried out at a flow rate of 1 mL min–1 using the following eluents **(Table 2).** The column was washed with 25 mL of eluent **A2** to remove unbound proteins, followed by 20 mL of eluents **B2** for further washing. CPR357 was then eluted with 25 mL of eluent **C2**. The fractions were analyzed via 10% SDS-PAGE electrophoresis to confirm protein purification. Fractions containing pure MPAO were pooled and concentrated using an Amicon® concentrator (Amicon® Ultra 30K Device), achieving a final protein concentration of 6 mg/mL.

Table 2. Buffer composition for CPR357 purification

Buffer name	**Reagent**	**pH**
CPR357-Lysis buffer **(A2)**	20 mM Tris-HCl, 150 mM NaCl	7.4
CPR357-Wash buffer (B2)	20 mM Tris-HCl, 21 mM NaCl	7.4
CPR357- Elution buffer(C2)	20 mM Tris-HCl, 300 mM NaCl, 300 mM Imidazole	7.4

2.3.10 Size Exchange Chromatography (SEC)

SEC was performed using an Enrich SEC 650 (10 × 300 mm) column (Bio-Rad), which was equilibrated with 100mM Phosphate buffer, 12.5 mM Glucose (pH 7.4). The protein fractions obtained from the His-tag purification column was concentrated using an Amicon® device before loading onto the SEC column. Chromatography was carried out using an FPLC system (Bio-Rad)

at a constant flow rate of 0.2 mL/min, and 0.5 mL fractions were collected. Aliquots of each fraction were analyzed by SDS-PAGE to assess protein purity and distribution.

2.3.11 SDS-PAGE procedure

A stacking gel was prepared within Mini-Protean System Glass Plates (BioRad®) to a final acrylamide concentration of 7.5% or 10% (Resolving layer, per 20mL: 4.68 mL or 6.24 mL of 40% 29/1 acrylamide/bisacrylamide, 7.50 mL of 1M Tris (pH 8.8, 0.20mL of 10% ammonium persulfate, 0.02 mL of TEMED, 7.86 or 9.42 mL of water; stacking layer, per 10 mL: 0.93 mL or 1.24 mL of 40% 29/1 acrylamide/ bisacrylamide, 3.76 mL of 1M Tris (pH 6.8); 0.10 mL of 10% ammonium persulfate, 0.01 mL of TEMED, 5.20 mL or 5.51 mL of water). Protein samples were mixed in a 3:1 ratio with 4x loading buffer 2 mL of 1 M Tris (pH 6.8), 0.8 g of sodium dodecyl sulfate, 4 mL of glycerol, 0.4 mL of 14.7 M β-mercaptoethanol, 1 mL of 0.5 M EDTA, 0.008 g of bromophenol blue, water to 10 mL). Proteins were denatured by incubation at 95°C for 5 min. Molecular weight standards used were 2 uL of PageRuler Pre-Stained Protein Ladder (ThermoScientific®). Electrophoreiss was performed using Mini-Protean Tetra System (BioRad®) and a PowerPack (VWR®) set to 230 mM and 200V. Sample were electrophoresed under constant current 1 hour.

2.3.12 *In vitro* bioconversion condition for usnic acid production using purified MPAO and CPR357 enzymes.

The reaction mixture included 3.6 mg of 0.05 mM MPA in DMSO and 0.07 mM NADH in sterile water, 0.6mg/ml of purified MPAO, 0.6mg/mL of purified CPR357 were added to 1ml of the 100mM potassium phosphate buffer with 12.5 mM glucose. The reaction mixtures were incubated with the substrate and the electron donor for 4h at 4 °C in the cold room. Reaction was quenched with 500 µL methanol and a drop of concentrate HCl. Samples were vortexed a few

seconds and then centrifuged at 16000 x g for 2 min. The bioconversion samples were extracted with ethyl acetate (3 x10.0 ml). The organic extracts were dried with anhydrous Na_2SO_4, filtered, and concentrated under rotatory evaporator. The dried residue obtained from the rotovap was re-dissolved and diluted to a final concentration of 1mg/mL in HPLC-grade methanol for HPLC analysis, and 0.5 mg/ml in acetonitrile for LC-MS/MS analysis. Each solution was filtered through a 0.2μm filter.

2.3.13 HPLC method

Analysis of the enzyme assay was carried out on a Waters HPLC Separations Module 2695 system equipped with a PDA Detector Model 2996 by injecting 30 μL of the supernatant using an autosampler. The column was a μBondapak® Waters C18 (3.9 X 300 mm) with a particle diameter of 15-20 μm with 125 Å pores. A gradient of Milli-Q water and methanol was used as the mobile phase (solvent A was distilled water with 0.1% formic acid, and solvent B was methanol) at a flow rate of 1 ml/min. The elution was done at 20 % methanol and 80 % water containing 0.075 % aqueous trifluoracetic acid for 10 min, following which a linear gradient was applied to 80 % methanol and held at that composition for 20 min, followed by application of a linear gradient back to 20 % methanol for 10 min and held there for 10 min. The total run time was 60 min The UV signal was monitored at 250 nm, and spectra were collected from 200 to 400 nm.

2.3.14 Liquid Chromatography - Mass Spectroscopy (LC-MS)

2.3.14.1 Triple Quadrupole LC-MS

An Applied Biosystems® liquid chromatograph triple quadrupole mass spectrometer was used to conducted LC-MS. Samples were filtered using Frogga Bio Scientific Solutions® PES Syringe Filter (0.2 μm pore size) and injected (10uL) onto a C18 LC column. Chromatographic separation was performed at a flow rate of 0.2 ml/min using gradient elution program, starting from 80% of A (Water with 0.1 % formic acid (v/v)) and gradually changing to 5% A and back over 40 minutes. Exact gradient parameters: 80% of A / 20% B (100% acetonitrile acidified with 0.1% formic acid (v/v)) for 5 min, gradually changing to 5%A / 95%B over 23 min, held at 5%A / 95% for 5mins, and returned to 80% A / 20% B over 7 min.

Samples were introducing into MS via electrospray ionisation using the following conditions: sheath gas flow rate, 30 (arbitrary units); auxiliary gas, 5 (arbitrary units); ESI voltage, 4.0 (kV), capillary voltage, -35 (V); capillary temperature, 275 (°C); and tube lenses voltage, -100 (V). The Total Ion Chromatogram (TIC) collected spectra were scanned of 155-600 atomic mass units. And the Electrospray Ionization (ESI) collected spectra were scanned of 342-344 atomic mass units. MS spectra were generated by collision energy 10eV.

2.3.13.2 LC–MS/MS QTOF

Analyses were performed on a Bruker® system coupled to a Bruker compact QTOF mass spectrometer. Chromatographic separations were performed on an Synergi Polar-RP Column (50 × 2.00 mm, 4 μm) column. The mobile phase comprised H_2O **(A)** and acetonitile **(B)**, both of which were acidified with 0.1% formic acid. The column temperature and sample organizer were maintained at 40°C and 15 °C, respectively. A stepwise gradient method at constant flow rate of 0.25 mL/min was used to elute the column with the following conditions: 40-95-40% B (0–25min),

followed by a 30 min run of acetonitrile for washing and 5 min of reconditioning. Analyses of the samples (3.0 μL injected) were performed in negative ion mode consisting of a full MS survey scan in the m/z 50–1200 Da range (scan time: 100 ms). Samples were introducing into MS via electrospray ionisation using the following conditions: dry gas flow rate, 4 L h^{-1}; auxiliary gas; ESI voltage, 5.0 kV; Capillary voltage, 3500 V; Nebulizer temperature, 200 °C. The Total Ion Chromatogram (TIC) collected spectra were scanned in the range m/z 155-600 atomic mass units. And the Electrospray Ionization (ESI) collected spectra were scanned over m/z 342-344 atomic mass units. MS spectra were generated by collision energy 10 eV. All data analysis was through the Bruker® Data Analysis program.

2.4 Materials and methods related to Chapter 4

2.4.1 BLAST search, multiple sequence alignment and phylogenetic for depsidone formation

Genes of interest in *C. uncialis* were analyzed using protein BLAST (pBLAST)(Altschul, S. F. et al., 1990). The 29 most genetically similar sequences were retrieved from GenBank and compiled for phylogenetic analysis, using selecting hit ≥ 60% query coverage and ≥ 20% amino acid identity. A single outgroup was selected from ascomycotan fungus *Ovatospora sp*., which more distantly related to the in-group sequences but retained comparable functional characteristics. Amino acid sequences were aligned using the MUSCLE algorithm (Edgar, R. C., 2004) as implemented in MEGA12 (Kumar, S. et al., 2018). The resulting multiple sequence alignments were exported in MEGA-format and used for phylogenetic tree reconstruction. Phylogenetic analyses were performed using the Maximum-Likelihood (ML) method (Whelan, S. & Goldman, N., 2001) was applied in selected analyses to validate tree topology. Node support was evaluated by bootstrap analysis with 1,000 replicates (Felsenstein, J., 1985). Evolutionary distances were estimated using the Poisson substitution model (Zuckerkandl, E. & Pauling, L., 1965), with

uniform substitution rate variation across sites. Gaps and missing data were treated using partial deletion with a site coverage cutoff of 95%. All analyses were performed using 7 computational threads, and resulting phylogenetic trees were saved as PDF files.

The phylogenetic dataset included 29 unique cytochrome P450 sequences, comprising: **(1)** 25 sequences from cytochrome P450s from *Cladonia uncialis*; **(2)** one sequence from *Cladonia grayi* (ADM79460.1), representing a lineage associated in depsidone-grayanic acid biosynthesis; (3) MollD (QPI71217.1) from *Ovatospora*, a CYP involved in mollicellin biosynthesis, and (4) CYP682BG2 from *Pseudevernia furfuracea*, representing a lineage specialized in depsidone-physodic acid production.

Chapter 3

Usnic acid biosynthesis pathways and functional heterologous expression of lichen monooxygenase MPAO and its redox partner CPR357

3.1 Usnic acid

Usnic acid (UA) [2,6-diacetyl-7,9-dihydroxy-8,9b-dimethyl-1,3(2H,9bH)-dibenzo-furandione; $C_{18}H_{16}O_7$], is a naturally occurring yellow colored dibenzofuran derivative predominantly found in various lichen genera, including *Cladonia*, *Usnea*, and *Lecanora*. As previously described in **Section 1.15**, usnic acid is well known as an antibiotic and exhibits a wide range of biological activities, including antibacterial, antitumor, antiviral, anti-inflammatory, antiprotozoal, antimicrobial, antiproliferative, analgesic and antipyretic activities (**Figure *19***) (Ingólfsdóttir, 2002; Ranković & Kosanić, 2021). More interestingly, UA can exist in two different enantiomers: (+)-usnic acid and (-)-usnic acid. X-ray crystallographic analysis has already established the configuration at C-9b of usnic acid (**Figure *19***) (Huneck et al., 1981). Each enantiomer of UA exhibits unique biological activities, and the relative distribution of these enantiomers varies among lichen species as described in **Section 1.15**.

In this study, *Cladonia uncialis* (**Figure *19***) was selected as the model organism to investigate the biosynthesis of usnic acid. This lichen species used in Sorensen lab is naturally found in Manitoba, Canada, with UA as one of its principal chemical constituents (**Figure *20***). *C. uncialis* is classified within the order *Lecanorales* and the family *Cladoniaceae* (Shishido et al., 2021). The thallus of this lichen typically exhibits a yellow-green or greenish hue, often transitioning to brownish tones toward the pointed apices. *C. uncialis* is commonly found growing on soil among mosses in well-lit, generally dry environments. It is prevalent in coniferous forests, heathlands, and sand dunes across Europe, North America, and Asia (Purvis et al., 1992) .

Despite its biological and pharmaceutical significance, the biosynthesis of UA remains a major challenge due to the absence of a fully elucidated pathway and the slow growth rate of these lichen. In particular, the enzymatic pathways underlying the stereochemical outcome of UA biosynthesis, resulting in either (+) or (-) usnic acid has not yet been identified. Accordingly, the primary objective of this study is to establish a methodology for the functional heterologous expression of a lichen-derived cytochrome P450 enzyme and its redox partner-cytochrome P450 reductase (CPR357) in bacteria host. By enabling *in vitro* usnic acid biosynthesis using purified enzymes, this characterization provides the foundation for future studies on the enantioselective biosynthesis of usnic acid in lichens.

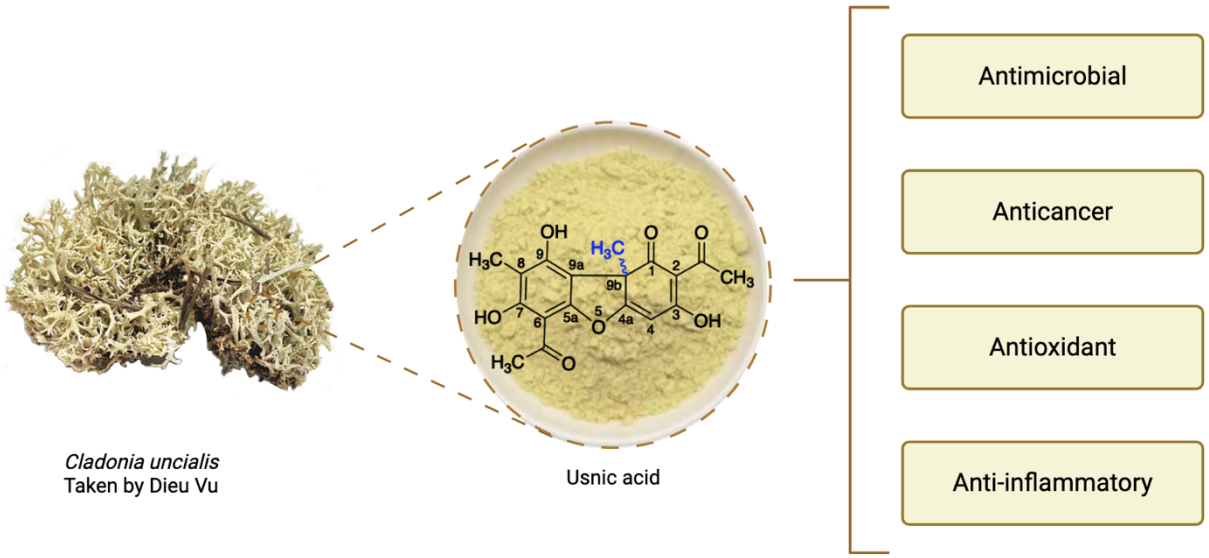

Figure 19. Usnic acid chemical structure and its reported biological properties

Figure 20. Lichen *Cladonia uncialis* found on McGillivray Trail, Manitoba, Canada

3.2 History of UA biosynthesis

The history of usnic acid biosynthesis dates back to 1844, when the German scientist W. Knop first isolated from lichen metabolites (Knop, 1844). Its precise chemical structure was elucidated throughout the 1930s by Frank H. Curd and Alexander Robertson (Curd & Robertson, 1933). The biosynthetic pathway scheme of usnic acid was proposed by H. Taguchi et al. in 1969 based on isotope-labeling studies conducted using whole lichen thalli, which revealed that its complex dibenzofuran skeleton is derived from the polyketide pathway **(Figure *21*)**. When lichens are fed with isotope-labeled acetate, the resulting enrichment pattern supports a polyketide biosynthetic origin **(Figure *21*Figure *21*A)**. Incorporation of labeled methylphloroacetophenone leads to the enriched re-isolation of labeled usnic acid, indicating that usnic acid is a dimer formed from two molecules of methylphloroacetophenone (MPA) **((Figure *21*B)**. In contrast, feeding labeled phloroacetophenone does not yield labeled usnic acid, confirming that the methyl group is introduced during the biosynthesis of MPA by the polyketide synthase **(Figure *21*C).** We now understand that this methylation is carried out by the C-methyltransferase (CMet) domain within the PKS, using S-adenosyl methionine (SAM) as the methyl donor. This work laid the foundation for the eventual classification of the UA-associated PKS as a nr-PKS, which introduce a methyl group prior to polyketide chain cyclization (Taguchi et al., 1969).

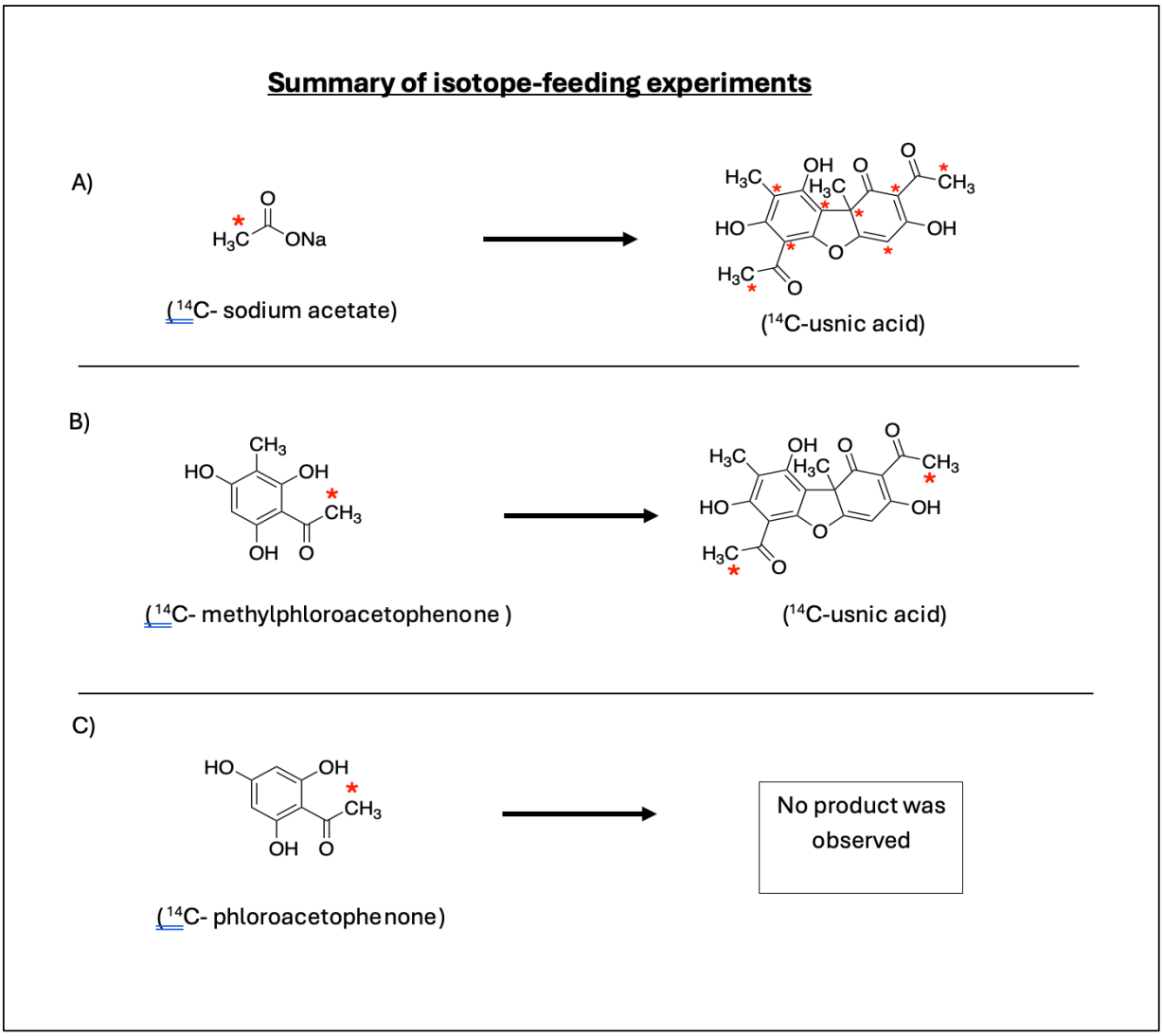

Figure 21. Summary of the isotope-feeding experiments on whole lichen thalli performed by Taguchi et al. (1969) to propose to biosynthesis pathway of usnic acid: **A)** Feeding lichens with isotope-labelled acetate results in an enrichment pattern consistent with polyketide biosynthesis (*=^{14}C). **B)** Isotope-labelled methylphloroacetophenone is fed to lichens, enriched usnic acid can be detected. **C)** Isotope-labelled phloroacetophenone is fed to lichens, enriched usnic acid cannot be detected.

3.3 Genome mining strategy for biosynthetic gene cluster identification in *Cladonia uncialis*

The annotation of biosynthetic genes in the genome of *Cladonia uncialis* was performed through a multi-step methodology, as originally described by Abdel-Hameed et al. (2016) **(Figure *22*)**. This workflow includes: **1)** generating sufficient fungal biomass for *de-novo* whole genome sequencing required collection and germination of spores of *C. uncialis* were first collected and germinated on water-agar media. Subsequently, germinated spores were transferred to nutrient rich malt yeast extract agar for one year. Lichens are a symbiotic system composed of a mycobiont (fungal partner) and photobiont (algae or cyanobacteria), where the mycobiont is responsible for the production of most lichen secondary metabolites (Ranković & Kosanić, 2021) **(Section 1.4)**. Therefore, it is critical to isolate and cultivate the fungal symbiont independently, under axenic (symbiont-free) laboratory conditions. Following the cultivation, **2)** The genomic DNA of *C. uncialis* was extracted from the axenic fungal culture and sequenced using the Illumina™ platform. The sequences were assembled with SPAdes assembler (Kearse et al., 2012), and then **3)** the resulting contigs were analyzed using Antibiotic and Secondary Metabolite Analysis Shell (AntiSMASH version 2.0) (Blin et al., 2013). In total, 48 putative biosynthetic gene clusters were found in the genome *C. uncialis*.

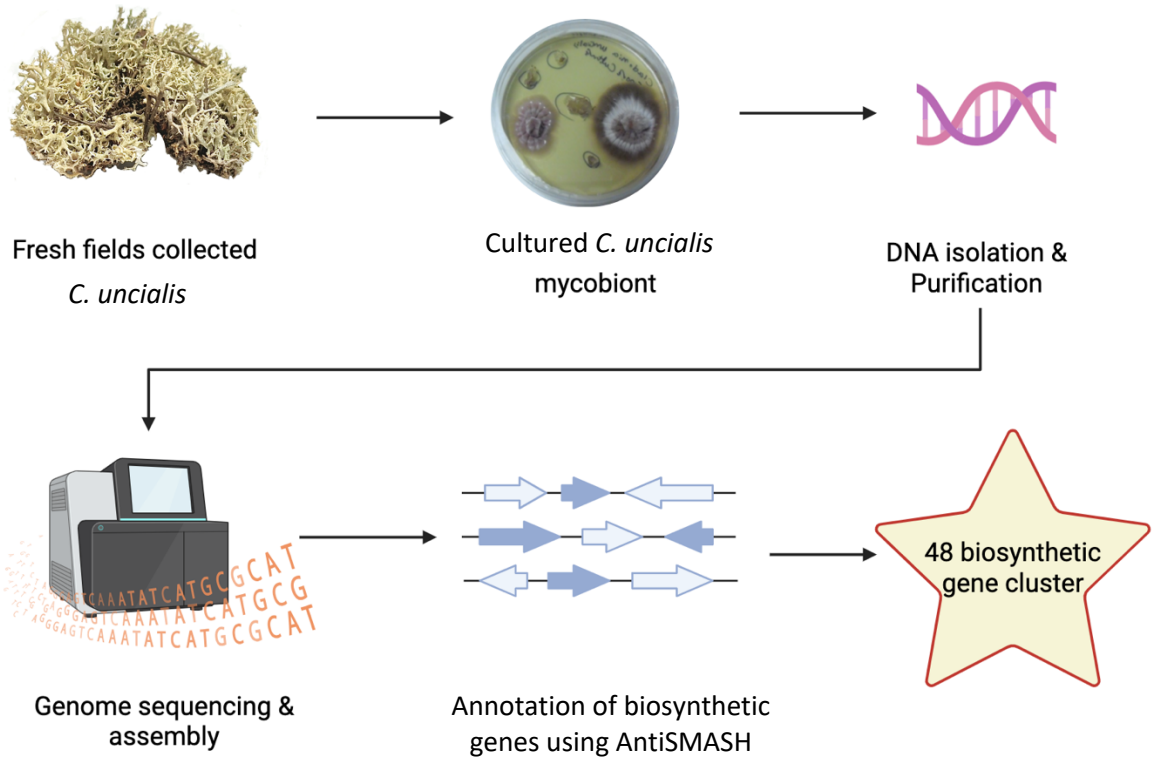

Figure 22. Illustration biosynthetic gene cluster identified in *Cladonia uncialis* by Abdel-Hameed (2016).

3.4 Identification of UA gene cluster

Within the assembled genomic contigs, 48 putative BGCs were annotated using AntiSMASH. Among these, 32 type I PKS genes were identified. Each identified gene sequence was further analyzed using the Basic Local Alignment Search Tool (BLAST) (Altschul et al., 1990). Functional predictions were inferred from sequence homology with previously characterized proteins in the GenBank database. Supporting evidence from earlier isotope-labelling studies of Taguchi in 1969 indicated that UA biosynthesis is produced by a non-reducing PKS (nr-PKS) **(Section 3.2)**. In addition, a single oxidative enzyme, most likely cytochrome P450 is expected to be encoded on the basis of closed proximity to the nr-PKS gene known as a post-PKS or tailoring

enzyme (Bernhardt, 2006; Chung et al., 2012; Guengerich & Munro, 2013). Domain analysis of the 32 type I PKS genes revealed that 14 were non-reducing while 18 encoded reducing PKS enzymes, based on the presence or absence of reducing domains (Abdel-Hameed et al., 2016). Among the 14 nr-PKS genes, only five possessed the requisite C-methyltransferase (cMeT) domain. Of these five candidates, just one gene exhibited the full domain architecture consistent with UA biosynthesis, including the presence of a Claisen cyclase (CLC) domain and a neighboring cytochrome P450 gene **(Figure *23*)**. The domain structure of this nr-PKS gene includes a starter unit: acyltransferase (SAT), ketoacyl synthase (KS), acetyltransferase (AT), acyl carrier protein (ACP), cMeT, product template (PT), and the CLC domains. The roles of these domains have been discussed in detail in **Section 1.6**. This nr-PKS gene was designated **mpas** (*methylphloroacetophenone synthase*) and encodes the MPAS enzyme. The adjacent cytochrome P450 gene, proposed to catalyze the oxidative tailoring step, was named **mpao** (*methylphloroacetophenone oxidase*), encoding the MPAO enzyme **(Figure *23*)** (Abdel-Hameed et al., 2016; Bertrand, n.d.).

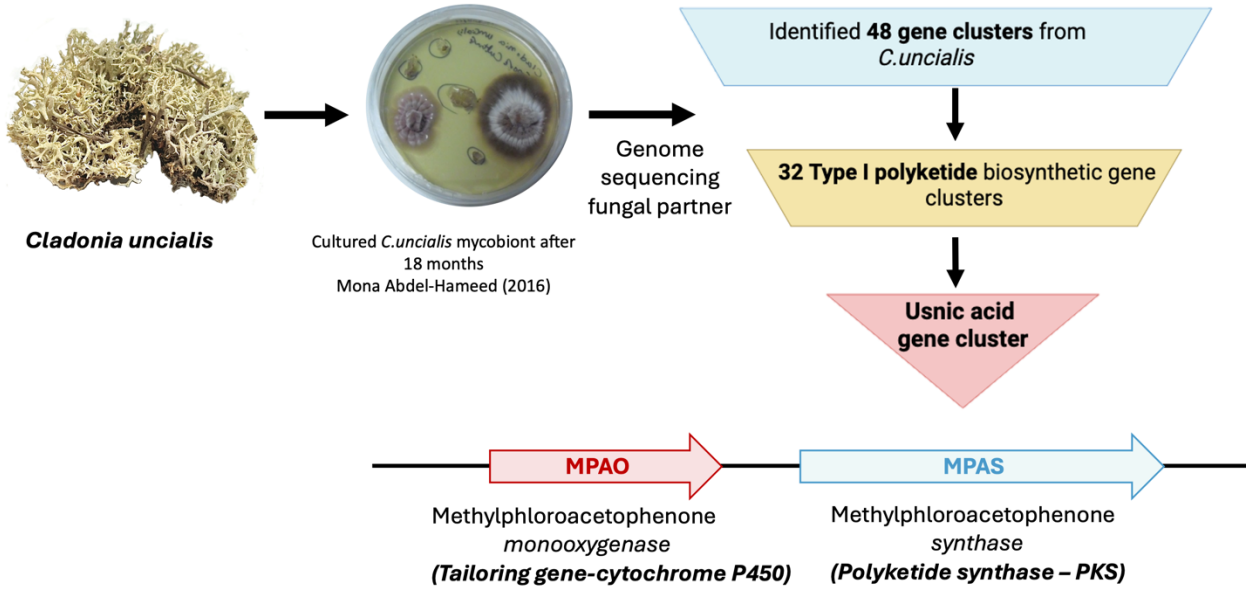

Figure 23. Illustration of the study identification of UA biosynthetic gene clusters of *C. uncialis*.

3.5 Biosynthesis of Usnic Acid (UA)

The biosynthesis of usnic acid (UA) has been demonstrated, with the process proceeding through the intermediate MPA **(Figure 24)** (Abdel-Hameed et al., 2016; Taguchi et al., 1969) **(Section 3.2).** This intermediate is synthesized from acetyl-CoA, malonyl-CoA, and S-adenosylmethionine (SAM) by the enzyme MPAS. Subsequently, MPA undergoes oxidative dimerization via action of MPAO enzyme to form UA.

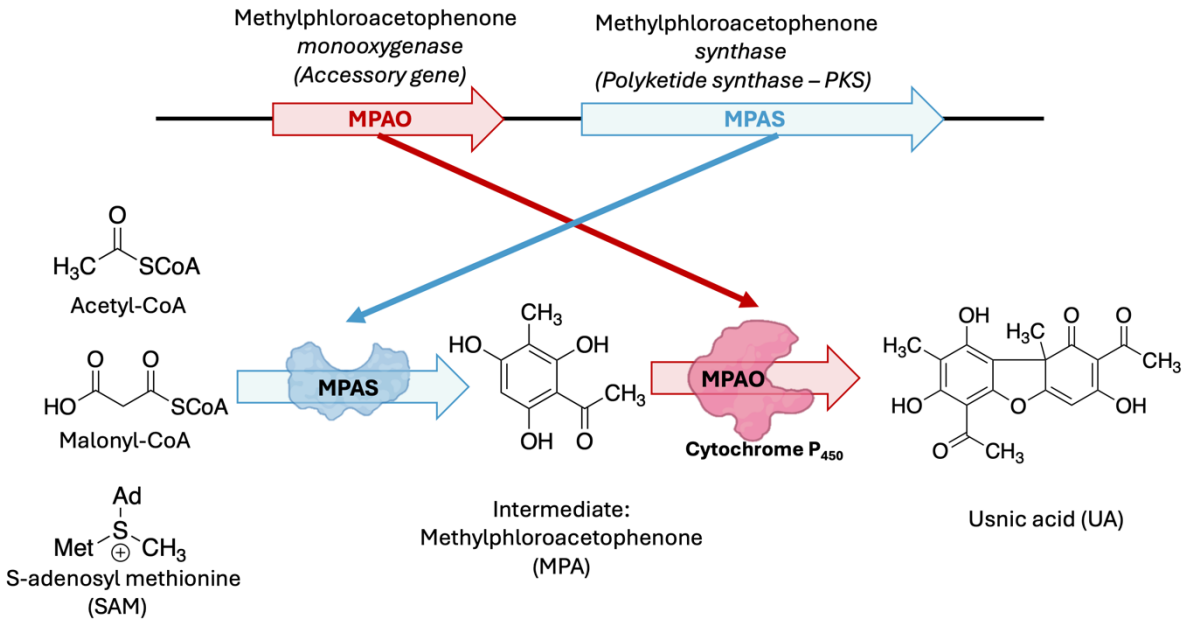

Figure 24. A general outline of biosynthesis of UA catalyzed MPAS and MPAO.

3.6 Experimental Approach

The experimental strategy employed in this study to achieve heterologous expression of *Cladonia uncialis* cytochrome P450 MPAO and its redox partner CPR357, and to enable the *in vitro* biosynthesis of usnic acid using purified enzymes, is summarized in **Figure 25** and described in detailed in **Section 2.3.**

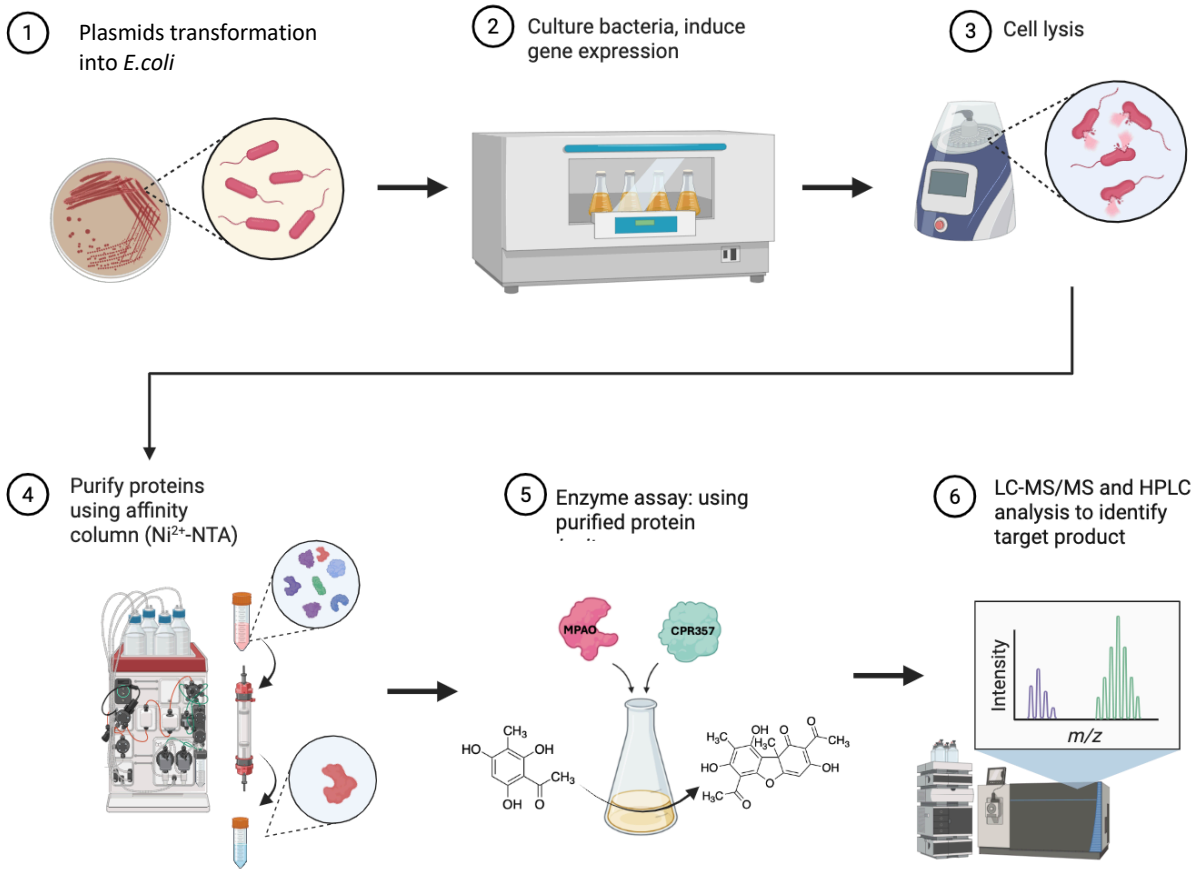

Figure 25. General experimental approach for the heterologous expression of the usnic acid *in vitro* bioconversion. Created with BioRender®.

3.6.1 **Plasmid transformation**

3.6.1.1 Transformation of MPAO (w/o TMD), codon-optimized for E.coli

The plasmid transformation into *E. coli* BL21(DE3)-pLysS cells was performed separately for the cytochrome P450 monooxygenase gene MPAO and its redox partner, cytochrome P450 reductase CPR357. The MPAO (w/o TMD, codon optimized for *E.coli*) was transformed into *E. coli* BL21(DE3)pLysS cells, as described in **Section 2.3.4**. After overnight incubation, the MPAO

transformation plates showed visible colonies formation, indication that the cells had successfully taken up the MPAO plasmids **(Figure 26)**.

3.6.1.2 Transformation of CPR357 (w/o intron), non-codon optimized

The CPR357 plasmid was transformed into *E.coli* BL21(DE3)pLysS was performed following the protocol described in **Section 2.3.4.** After overnight incubation, the visible colonies appeared on the transformation plate, indicating that the cells had successfully taken up the CPR357 plasmid **(Figure 26)**.

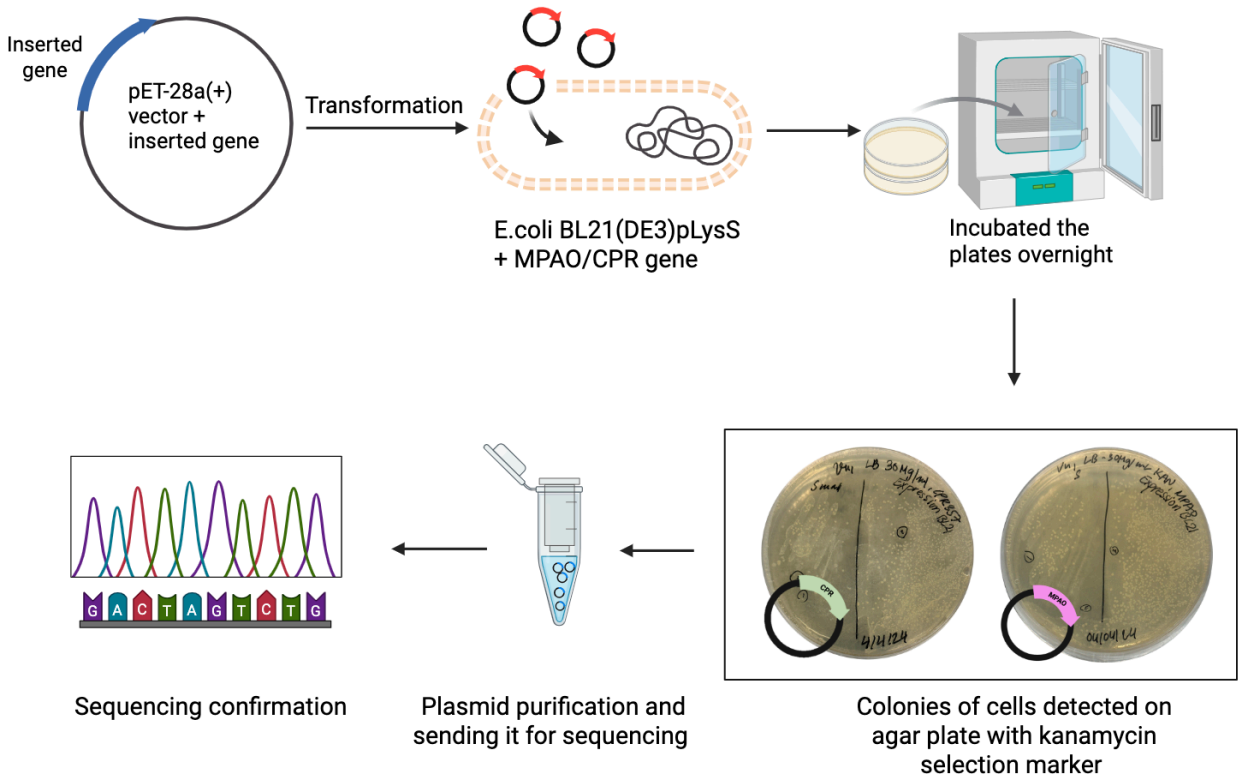

Figure 26. Illustration of the independent transformation of MPAO and CPR357 into the pET28(+) vector.

3.6.2 **Heterologous expression of MPAO and CPR357**

The successful heterologous expression of lichen cytochrome P450 enzymes in *E. coli* often requires careful optimization of multiple parameters to enhances protein solubility and functional yield. Factors such as temperature and media selection can significantly affect the folding efficiency, expression level, and overall quality of the recombinant protein. Based on the previous finding and literature, I evaluated several key variables to determine the optimal condition for expressing MPAO and its redox partner CPR357 in *E.coli*. The experiments included comparison of induction temperature (37°C, 30°C, and 28°C), and the use of different culture media (Luria Bertani [LB] vs. Terrific Broth [TB]). The use of TB did not result in a significant improvement in protein expression compared to LB media under the test conditions. As a result, LB was selected for subsequent experiments, and the detailed results from the TB cultures are provided in **Figure S 7.**

3.6.2.1 Heterologous expression under different temperature conditions

In this experiment, the heterologous expression of MPAO and CPR357 was compared at induction temperatures of 37°C, 30°C, and 28°C for 24 hours (**Figure 27, Gel A**). SDS-PAGE analysis indicated stronger visible expression of both MPAO and CPR357 at 30°C, and 28°C compared to 37°C. Based on these observations, subsequent experiments were performed at 30°C and 28°C to further assess protein yield and suitability for purification. However, during the downstream protein purification, only the protein expressed at 30°C yielded a detectable band on SDS-PAGE, whereas no corresponding was observed for protein at 28°C. Therefore, 30°C was selected as the induction temperature for all subsequence experiments. As showed in **Figure 27**, **Gel (B),** both MPAO and CPR357 showed prominent band in soluble fraction at 30°C.

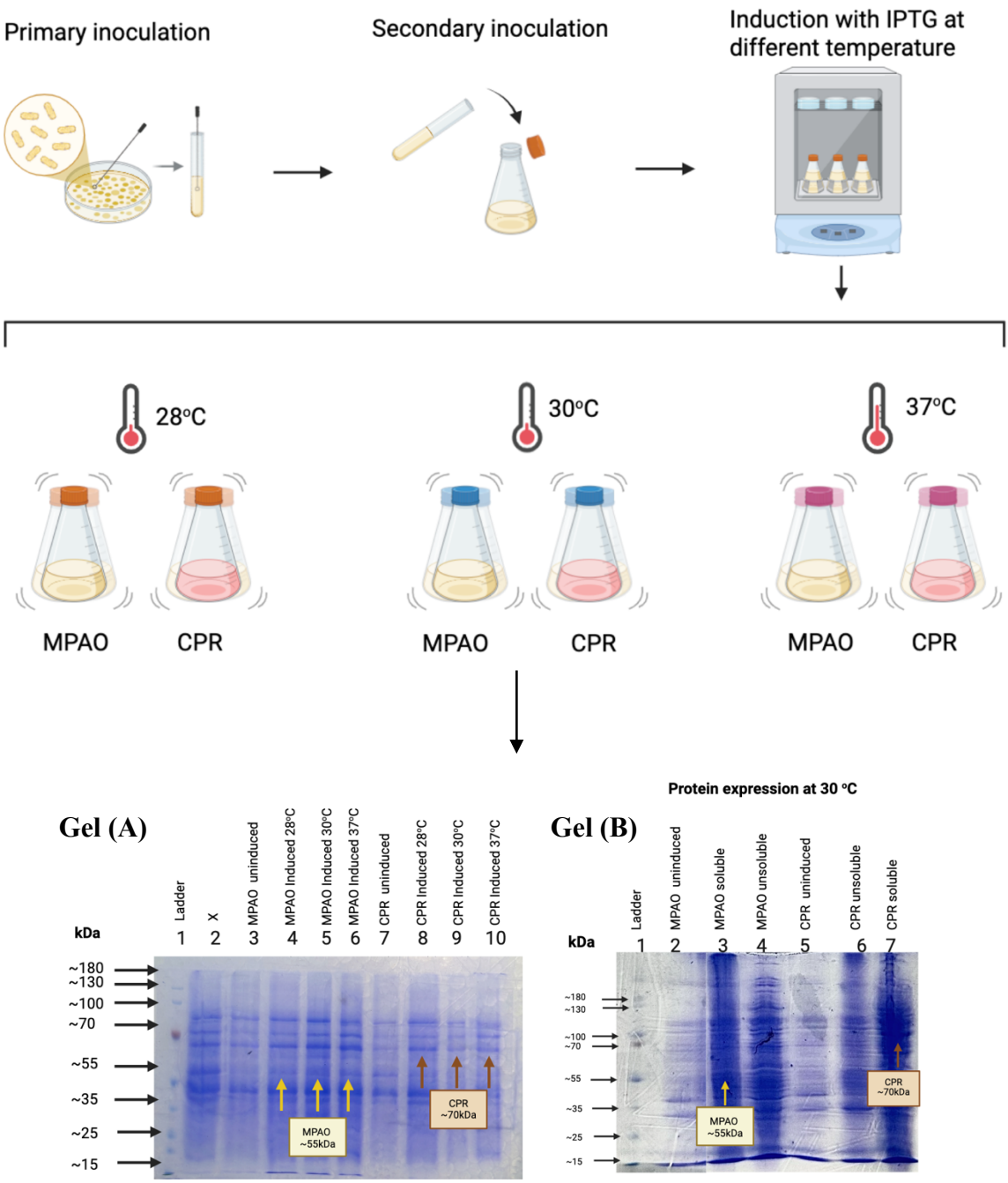

Figure 27. Illustration of the workflow for heterologous expression of cytochrome P450 enzymes at different temperatures. Gel **(A)**: MPAO and CPR357 expression was compared at induction temperatures of 37°C, 30°C, and 28°C for 24 hours. Gel **(B)**: both MPAO and CPR357 showed prominent band in soluble fraction at 30°C.

3.6.2.2 Heterologous expression of MPAO

Following successful transformation and heterologous expression trials **(Section 3.7.1.2)**, MPAO was expressed in *E. coli* BL21(DE3)pLysS. The cells were cultured in LB media supplemented with 5-aminolevulinic acid (5-ALA) to enhance heme biosynthesis and induced with IPTG for 24 hours at 30 °C **(Section 2.3.5)**. SDS-PAGE confirmed successful soluble expression **(Figure 28)**.

3.6.2.3 Heterologous expression of CPR357

Heterologous expression of cytochrome P450 reductase (CPR357) was performed following a protocol like that used for MPAO. The cells were cultured in LB media supplemented with 5-aminolevulinic acid (5-ALA) to enhance heme biosynthesis and induced with IPTG for 24 hours at 30 ˚C **(Section 2.3.4)**. SDS-PAGE analysis confirmed successful soluble expression **(Figure 28).**

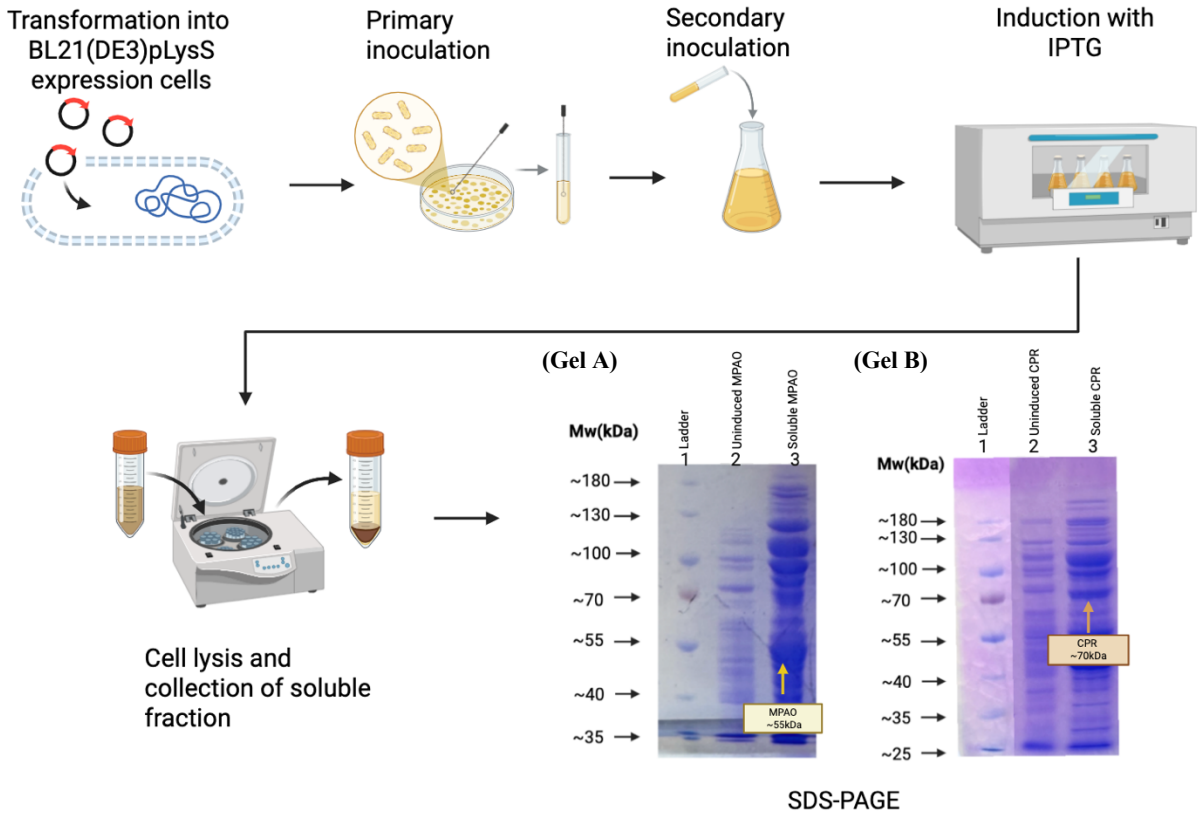

Figure 28. Illustration of workflow for heterologous expression of MPAO and CPR357. **Gel (A)** Lane **1**: Protein ladder, land **2**: uninduced MPAO, land **3**: induced-soluble MPAO with a thick size band at approximately 55 kDa of MPAO. **Gel (B)** Lane **1**: protein ladder, lane **2**: uninduced CPR357, lane **3**: induced-soluble CPR357 with size band 70 kDa.

3.6.3 **Protein purification**

Following expression in *E.coli*, the cells was lysed by sonication to generate cell lysate, which was then applied to an equilibrated HisTrap HP 1 mL column for protein purification as described in **Section 2.3.6**. After multiples trials, optimized buffer systems were established for MPAO and CPR357 **(Section 2.3.6.2 and 2.3.9.2),** providing the selectivity and purity for each protein. The eluted fractions were analyzed by SDS–PAGE to assess protein identity and purity. Purified MPAO consistently appeared as a single band at ~55 kDa, while purified CPR357 showed

a major band at ~70 kDa, confirming successful enrichment of each recombinant enzyme **(Figure 29).**

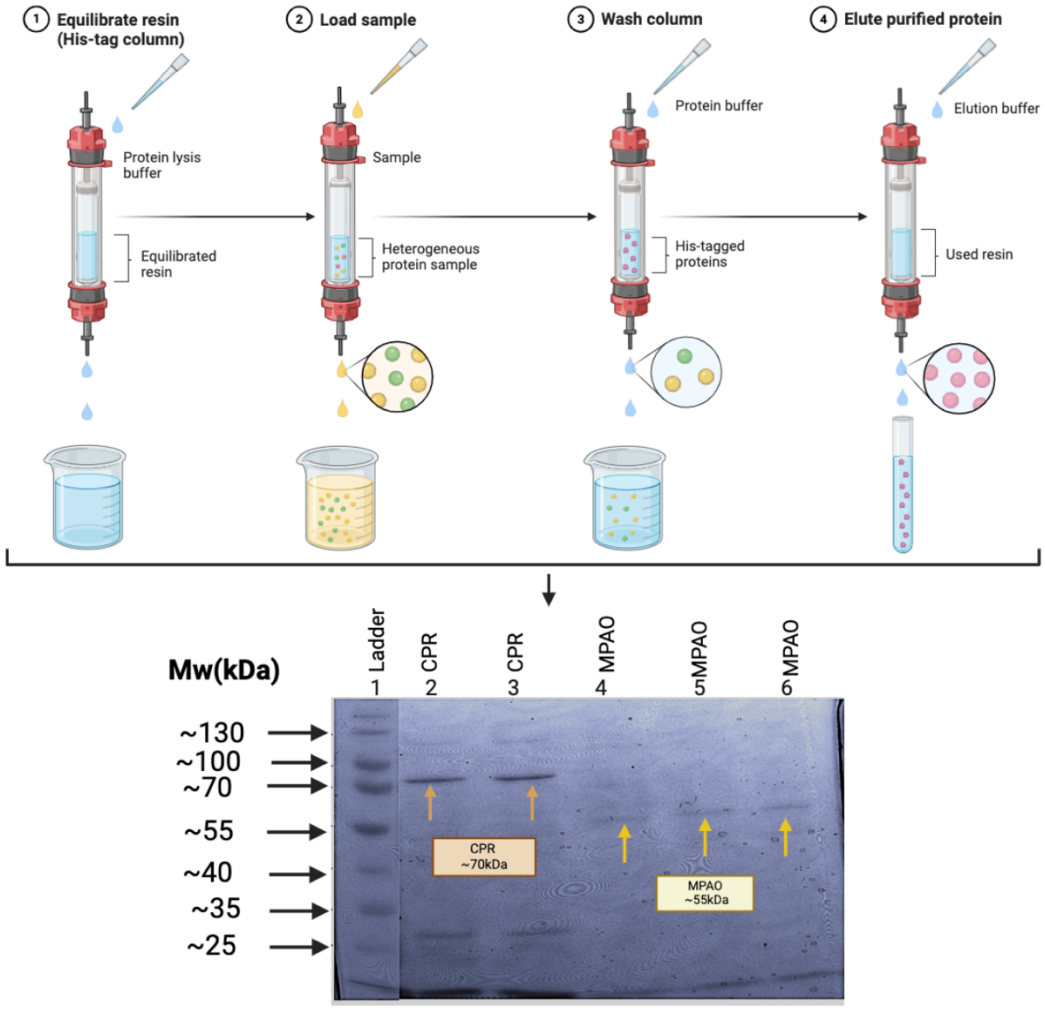

Figure 29. Illustration of protein purification of cytochrome P450 MPAO and its redox partner CPR357 using His-tag affinity column. **Lane 1:** protein ladder; **Lane 2 and 3**: purified CPR357**; Land 4,5 and 6:** purified MPAO.

3.7 *In vitro* Bioconversion using purified cytochrome P450 proteins

Bioconversion experiments converting MPA to UA were carried out under the conditions summarized in **Table 3**.

Table 3. Bioconversion conditions used for the conversion of MPA to UA

Condition No.	Buffer	MPA concentration	NADH Concentration	Proteins concentration	Time, Temperature
1	100mM Phosphate buffer (pH7.4),12.5 mM Glucose	0.05 mM in DMSO	0.07 mM in water	[MPAO]=0.06 mg/ml [CPR357] =0.06 mg/ml	4hrs, 4 °C
2	100mM Phosphate buffer (pH 7.8),12.5 mM Glucose, 750 µl H_2O_2	0.05 mM in DMSO	0.07 mM in water	[MPAO]=0.06 mg/ml [CPR357] =0.06 mg/ml	4hrs, 4 °C
3	100mM Phosphate buffer (pH 7.8),12.5 mM	0.05 mM in DMSO	0.07 mM in water	[MPAO]=0.06 mg/ml [CPR357] =0.06 mg/ml	4hrs, 4 °C

	Glucose, 750 µl H_2O_2				
4	100mM Phosphate buffer (pH 7.4),12.5 mM Glucose, 750 µl H_2O_2	0.05 mM in DMSO	0.07 mM in water	[MPAO]=0.06 mg/ml [CPR357] =0.06 mg/ml	4hrs, 4 °C

The expression and induction of MPAO and CPR357 were performed following the procedures outlined in **Section 2.3.5 and 2.3.8**. Then the proteins were purified were purified using affinity column as described in **Section 2.3.6**. The bioconversion experiment contains: 4 experimental conditions listed in **Table 3**, and four control samples, which included MPA only, NADH only, MPA + NADH + phosphate buffer pH (7.4); and MPA + NADH + phosphate buffer pH (7.8) **(Figure 30).**

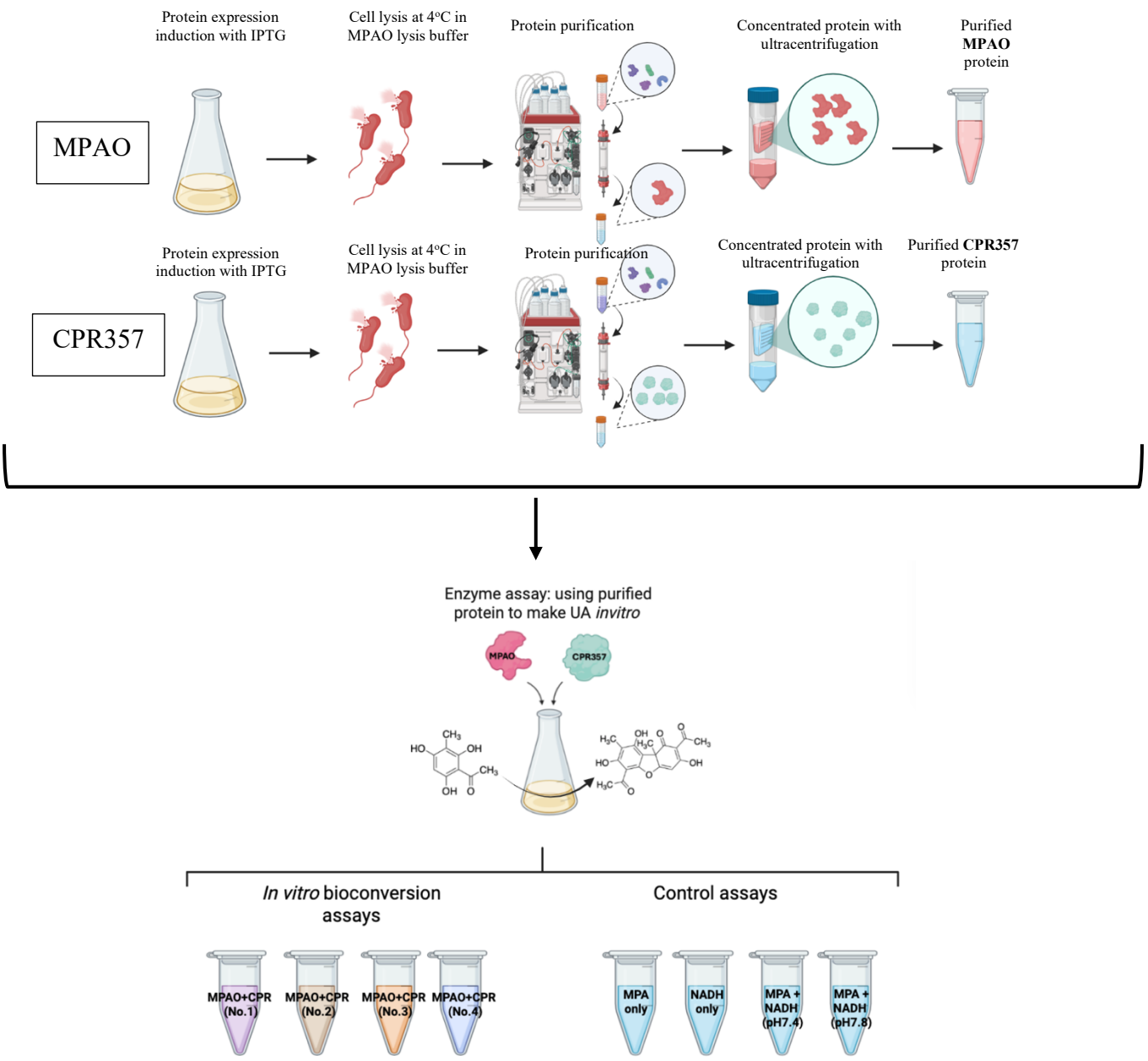

Figure 30. Illustration *in vitro* bioconversion assay using purified enzymes MPAO and CPR357 workflow.

3.8 HPLC and LC-MS/MS analysis of bioconversion assays using purified enzymes

HPLC analysis using our standard UA detection method did not reveal any detectable peaks that would correspond to usnic acid **Figure S 8-11,** suggesting that either UA was absent or present below the detection limit of the method. Therefore, to improve sensitivity and enable more definitive detection, LC-MS analysis was performed. Negative electrospray ionization mass spectrometry (ESI-MS) has been used routinely for analysis of UA, resulting in a characteristic peak at m/z 343.08 (Kutney et al., 1974; Mosbach, 1969). In this study, usnic acid was analyzed using a liquid chromatography-triple quadrupole mass spectrometer. As shown in **Figure 31A**, UA standard displayed a distinct peak in both the extracted ion chromatography (EIC) and total ion chromatogram (TIC) at a retention time (R_t) of 14.1 minute, with a peak at m/z 343.08 in negative ion mode.

In experimental samples, the EIC analysis revealed a clear peak at m/z 343.08 at Rt=14.1 min under condition **No.1 (Figure 31F)**, matching the UA standard. The control assays showed no detectable peak at this m/z and retention time **(Figure 31 C, D, E)**. However, in **Figure 31B**, the substrate MPA exhibited a peak at R_t 12.0 in TIC and there were two small peaks at R_t 14.0 and 14.6 min in EIC. These unexpected peaks prompted the re-analysis the sample using the Quadrupole Time-of-Flight (QTOF) LC-MS/MS system to accurately identify the compounds.

The conditions **No.2** and **No.4** also produced peaks at EIC m/z = 343.08, but their retention times differed from UA standard, appearing at Rt=14.0 min for **No.2** and Rt=14.0 min for **No.4 (Figure 31 H,I)**. Condition **No.3** yielded a peak at m/z 343.08 at Rt=14.1 min which match the UA standard, but the peak was less defined. Based on the LC-MS result, the condition **No.1** was selected for further investigation in bioconversion assays and LC-MS/MS analysis generated the most intense peak, providing the strongest evidence of UA formation in bioconversion. Therefore,

the experiment under condition **No.1** was repeated, and the samples was analyzed using LC-MS/MS qTOF to confirm the identity of the compound.

(A) TIC and EIC of UA standard

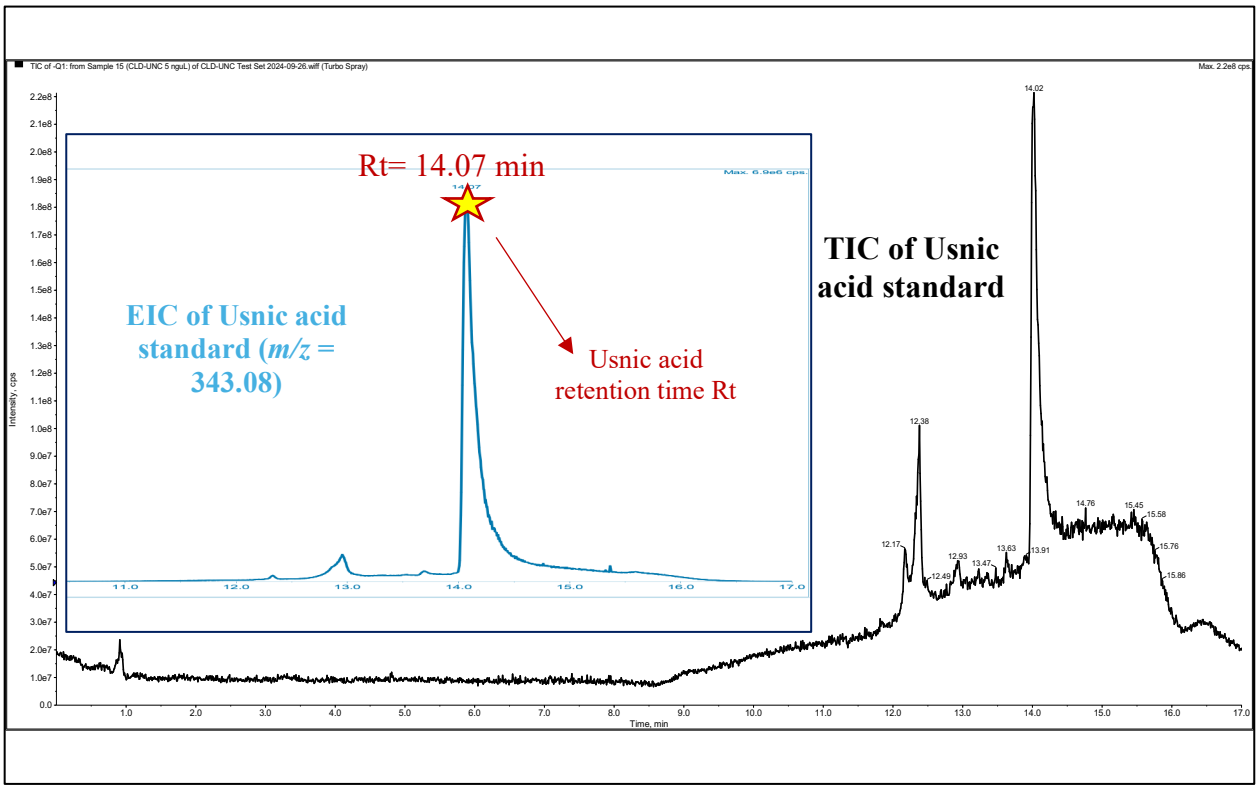

(B) TIC and EIC of MPA only (UA precursor)

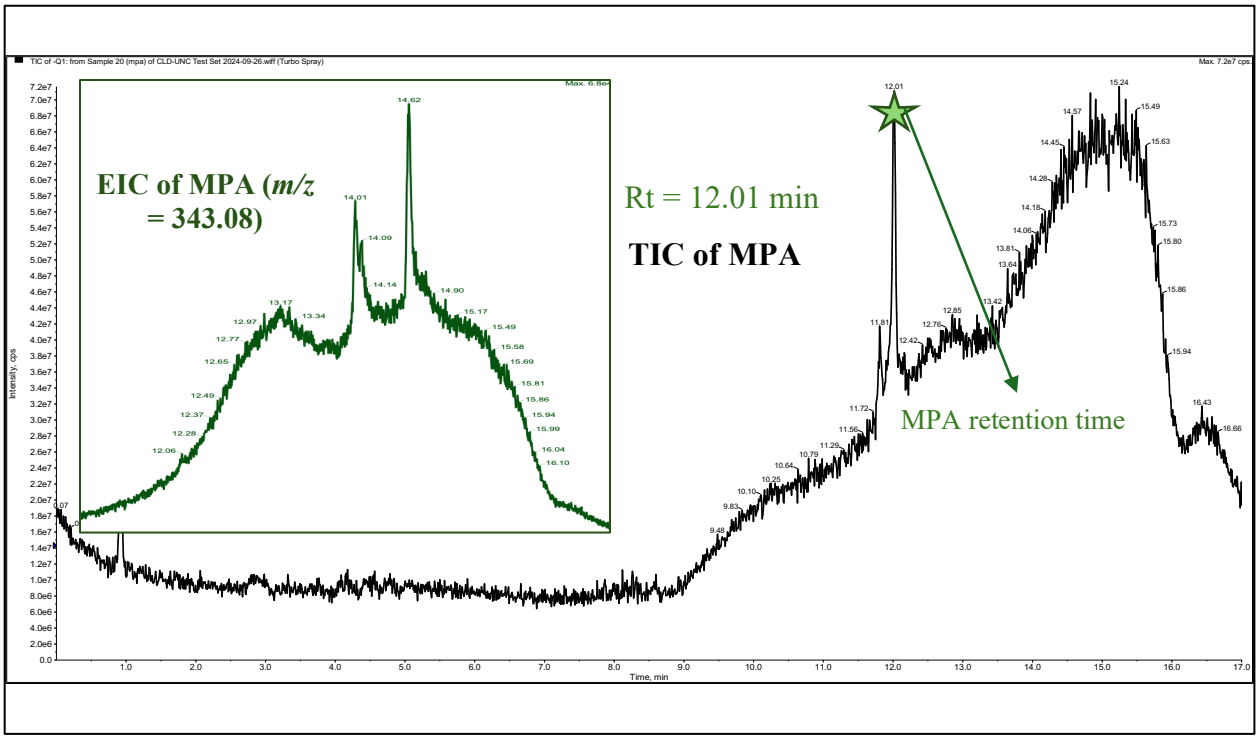

(C) TIC and EIC of NADH only

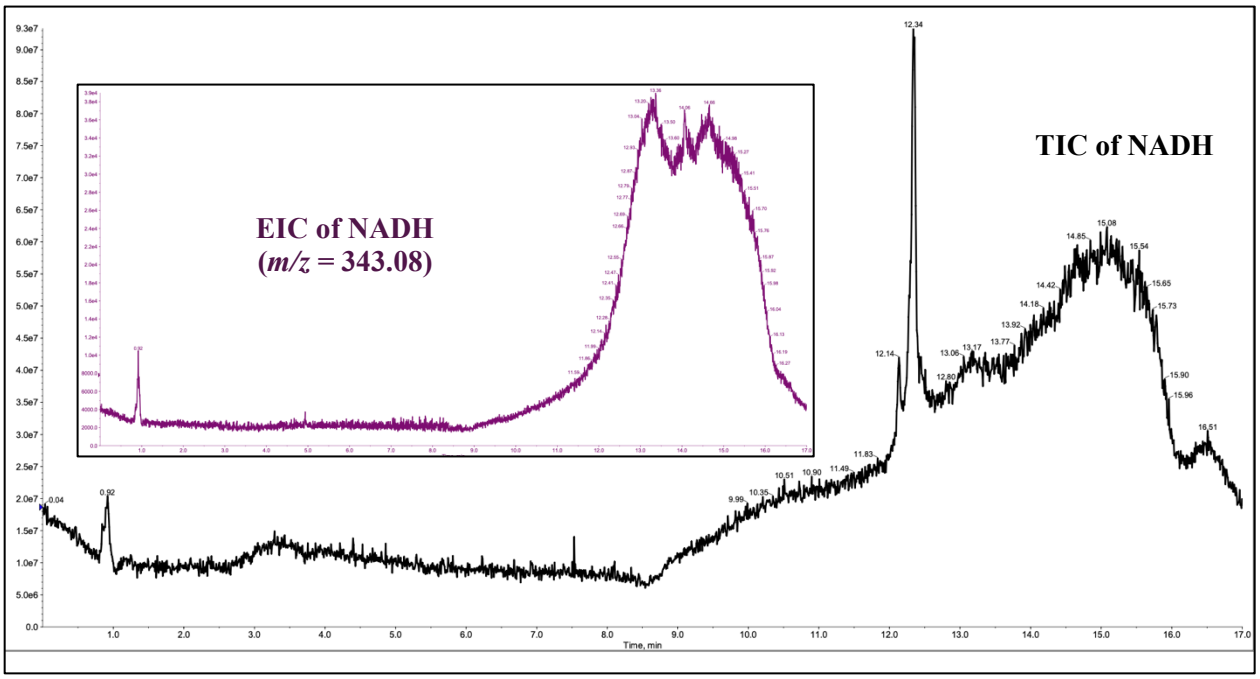

(D) TIC and EIC of NADH+MPA+ phosphate buffer (pH 7.4)

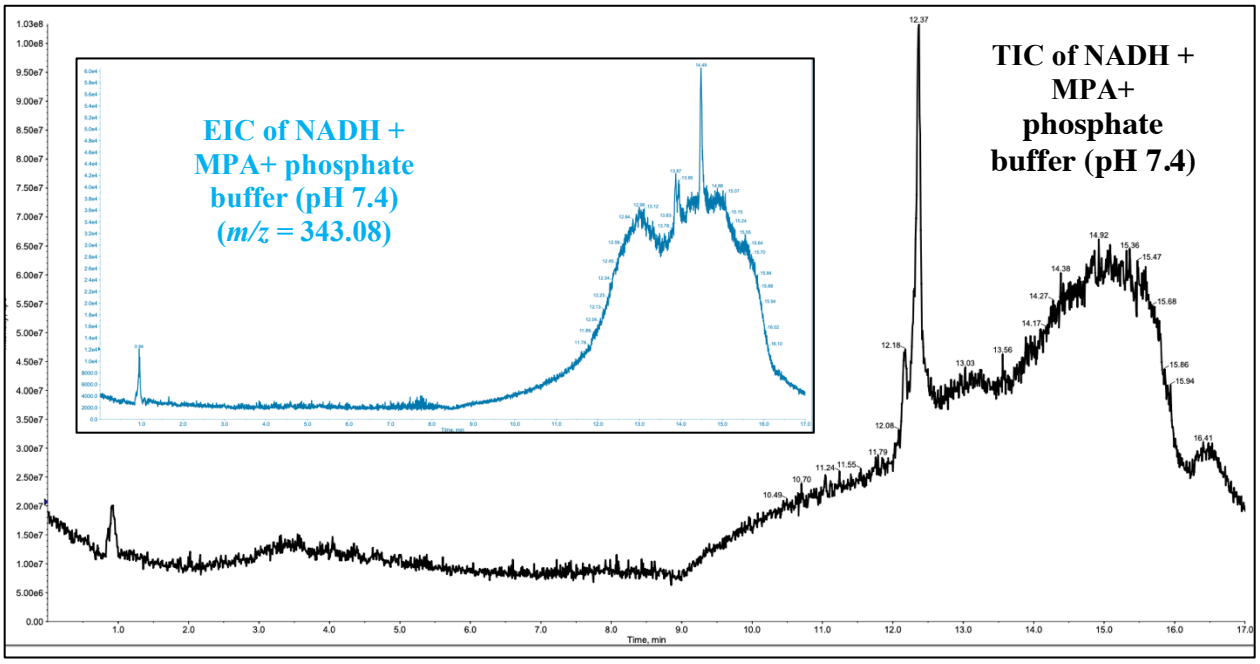

(E) TIC and EIC of NADH+MPA+ phosphate buffer, H_2O_2 (pH 7.8)

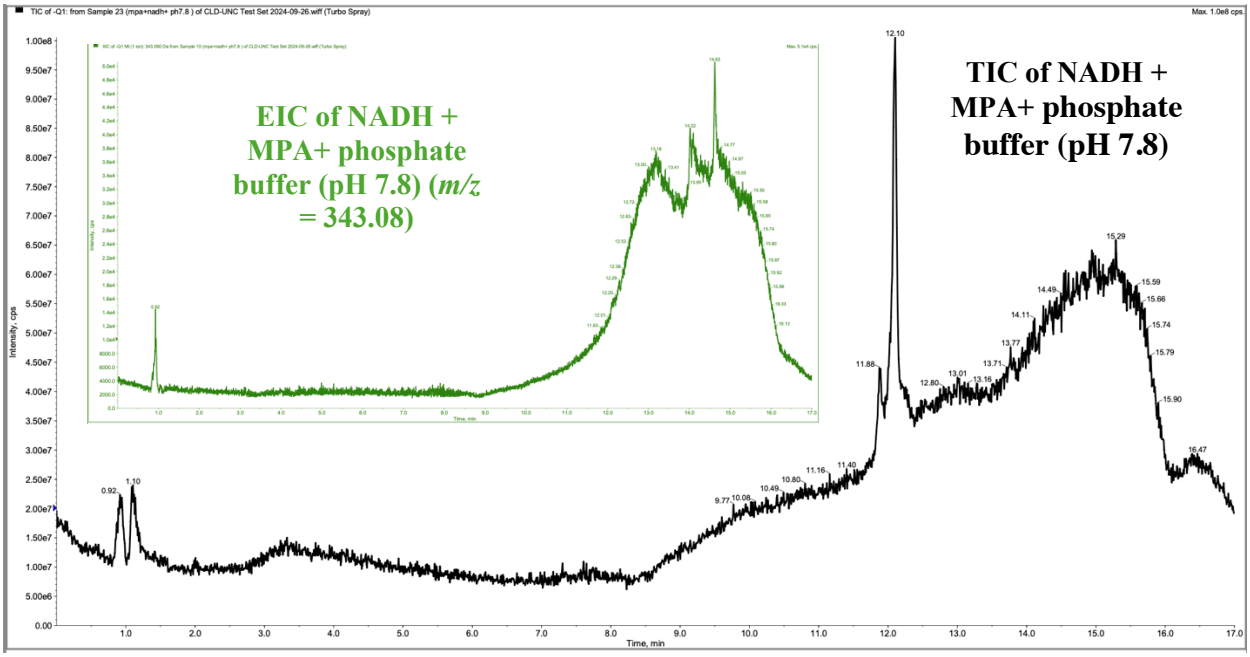

(F) TIC and EIC of bioconversion condition No. 1

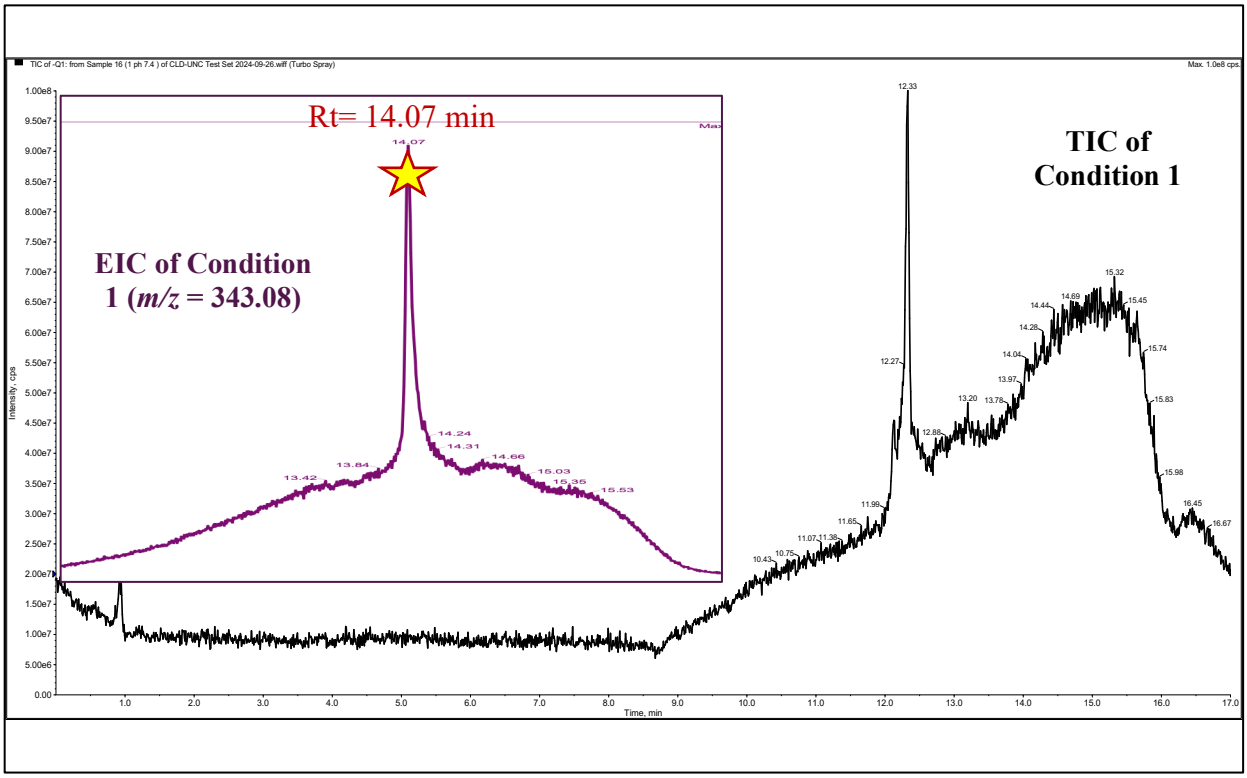

(H)TIC and EIC of bioconversion condition No. 2

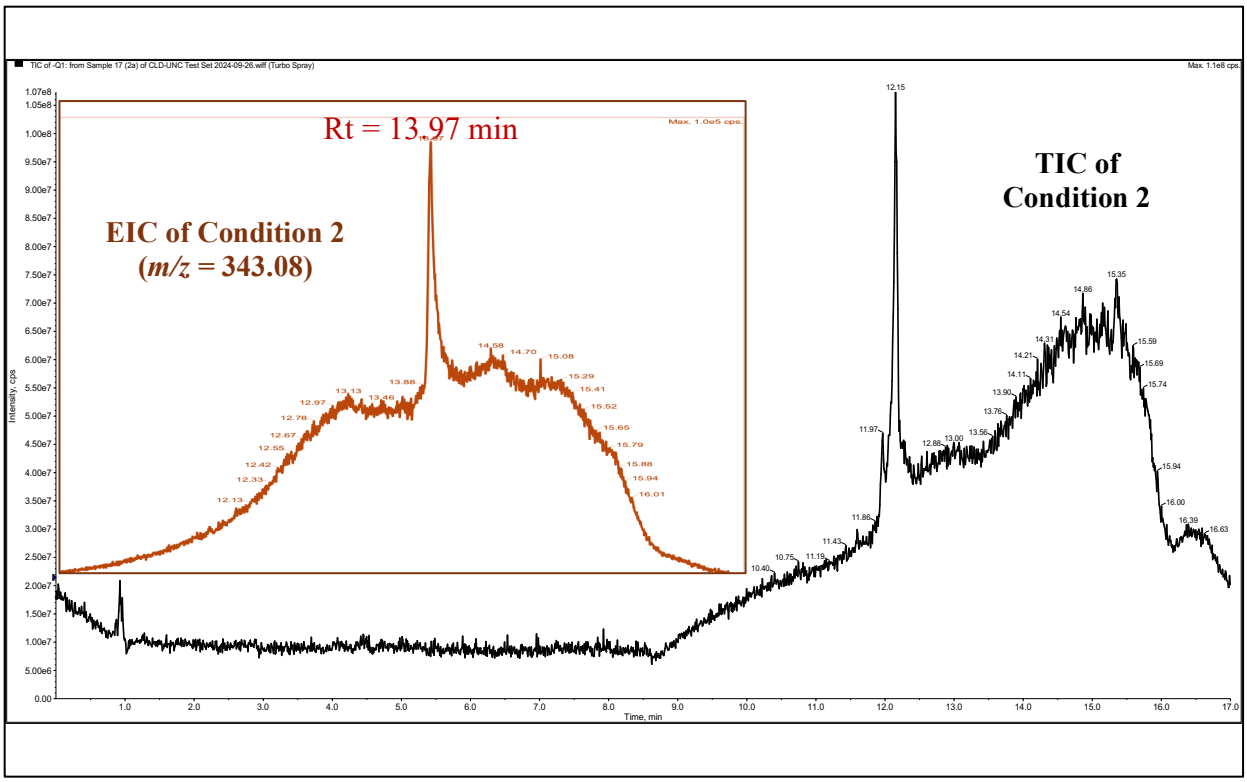

(G)TIC and EIC of bioconversion condition No. 3

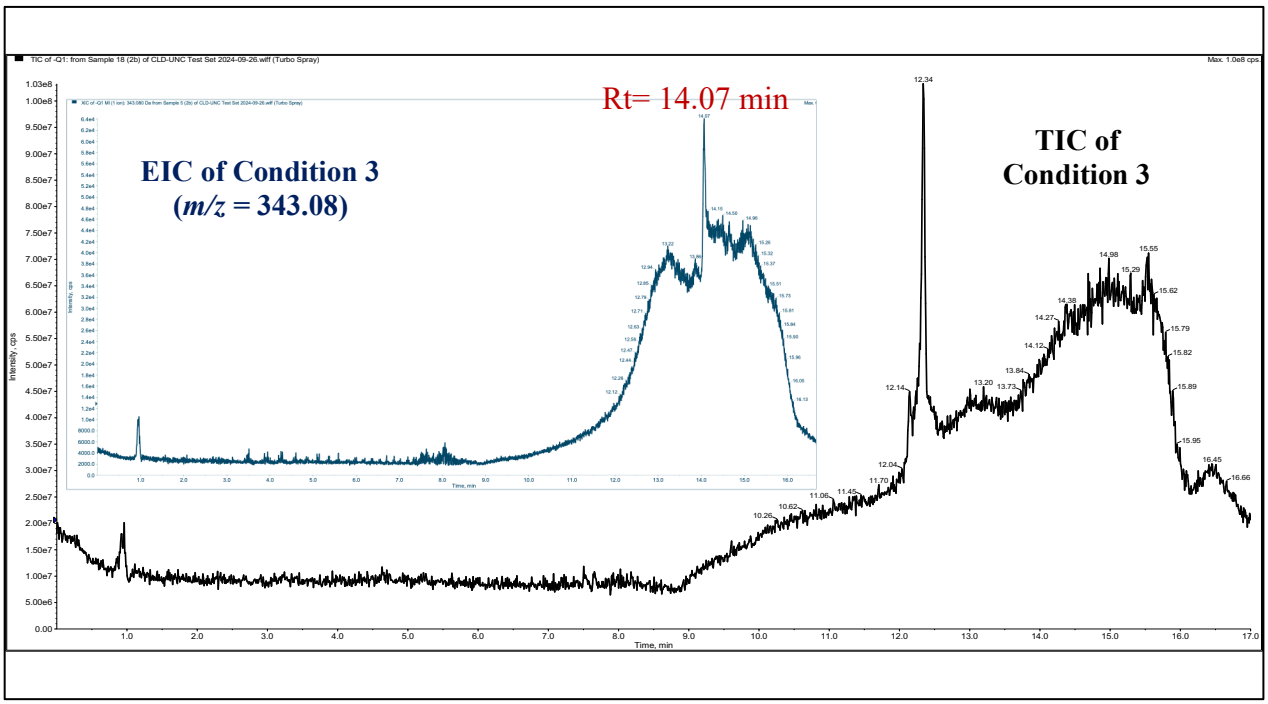

(I) TIC and EIC of bioconversion condition No. 4

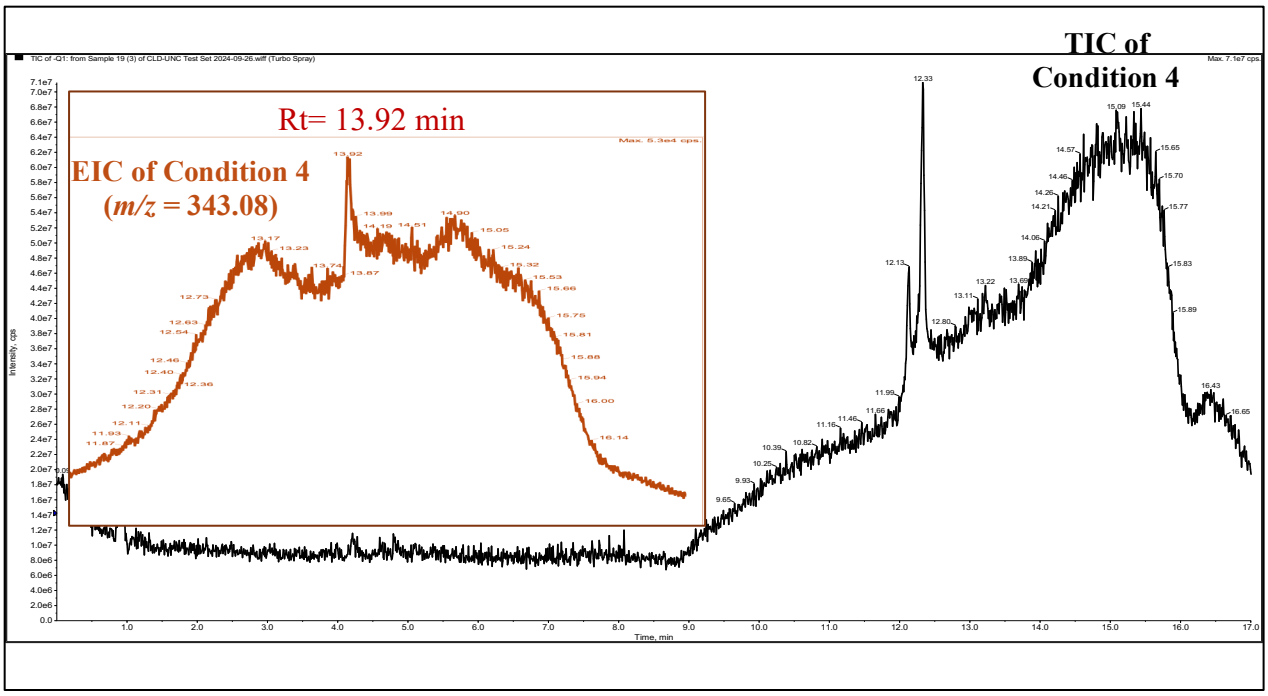

Figure 31. LC-MS results using triple quadrupole mass spectrometer of MPA to UA bioconversion experiments, liquid chromatogram (on the top of each chromatogram) with a retention time on the x-axis and intensity on the y-axis. Mass spectra (on the bottom of each chromatogram) with a base peak and (MS/MS). All spectra were acquired in the negative ion mode. **A**. Usnic acid standard in acetonitrile**; B**.MPA in acetonitrile; C. NADH in acetonitrile; **D**. MPA + NADH in acetonitrile; **E**. Bioconversion condition No.1 **F**. Bioconversion condition No.2; **G.** Bioconversion condition No.3; **H**. Bioconversion condition No.4.

3.9 HPLC and LC-MS/MS qTOF results for second trial

In **Section 3.9**, the bioconversion assay performed under condition **No.1** showed the most intense peak at m/z= 343.08 and Rt=14.07 minutes which matched with UA standard (**Figure 31A).** To validate this observation, the bioconversion assay was repeated. Both the original No.1 condition bioconversion assay (Bioconversion 1), as described in **Section 3.9** and replicate bioconversion (Bioconversion 2) were analyzed using LC-MS/MS qTOF **(Figure 32).** The EIC

and MS/MS spectra of Bioconversion 1 (**Figure 32B)** and bioconversion 2 (**Figure 32C)** consistently revealed the characteristic fragmentation pattern of UA standard (**Figure 32A)**. Specifically, the parent ion m/z 343.08 and daughter ions at m/z 328.06, 313.03, 259.08 and 231.06 were observed, consistent with previously reported UA fragmentation profiles (Sveshnikova et al., 2019). These ions were detected at Rt approximately 8.5 min.

A set of control reactions were analyzed under identical LC-MS/MS conditions. The negative controls were MPAO only, CPR357 only, MPA (substrate) only, NADH cofactor only, MPA+ NADH in the absence of enzymes (**Figure 32D, E, F, G).** None of these control reactions produced a detectable peak at m/z 343.08, nor did they yield the diagnostic daughter ions at m/z 328.06, 313.03, 259.08 and 231.06. The absence of these signals in the controls indicates that the observed UA production was dependent on the complete bioconversion system with both MPAO and CPR357, substrate MPA, co-factor NADH. Therefore, these results confirmed that the enzymatic system catalyzed the formation of UA, and the identity of the product was conclusive established by both retention time alignment and the fragmentation pattern, with daughter ions precisely matching those of the UA standard.

(A) TIC and EIC of UA standard with MS/MS fragmentation

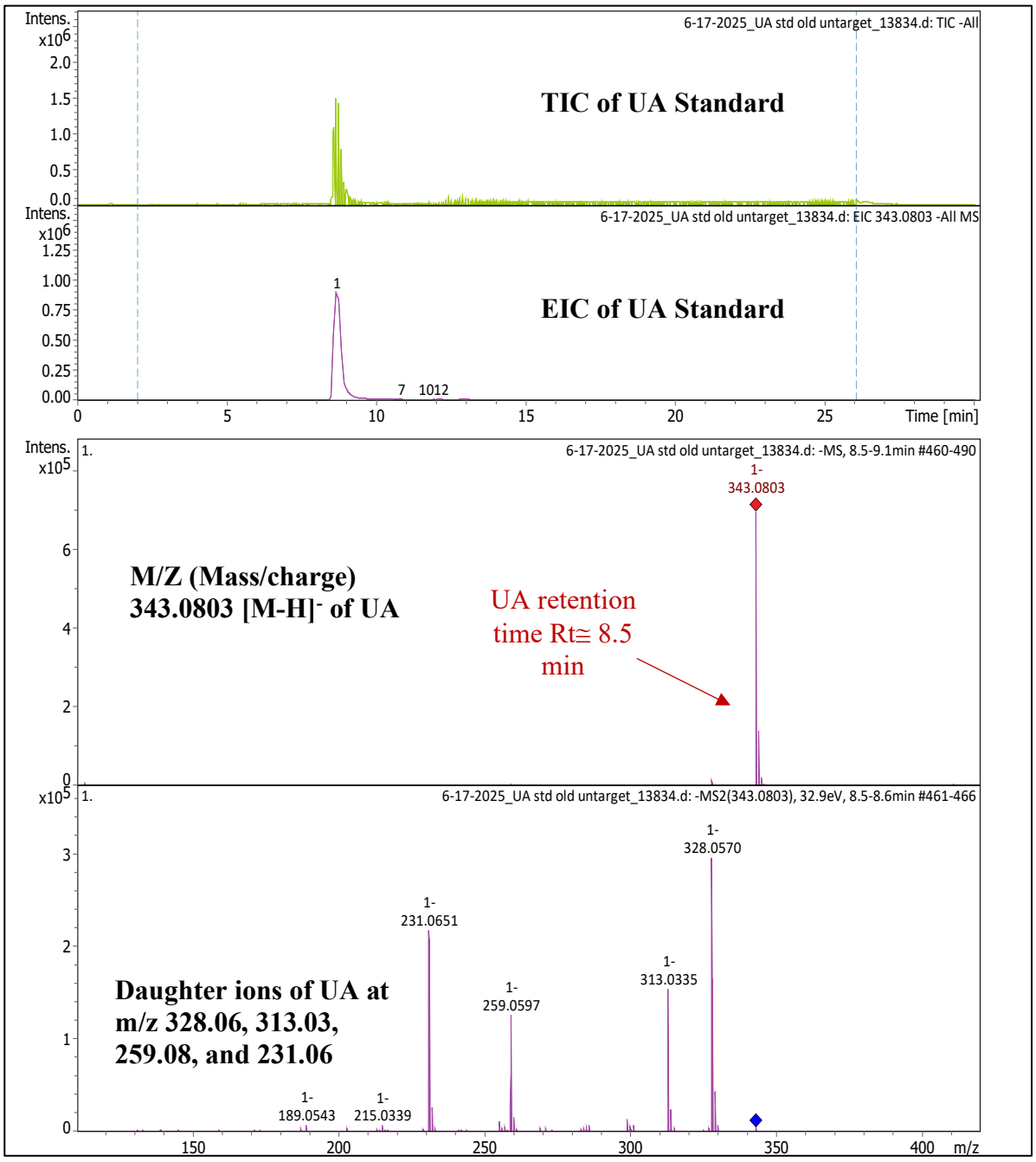

(B) TIC and EIC of bioconversion (1) with MS/MS fragmentation

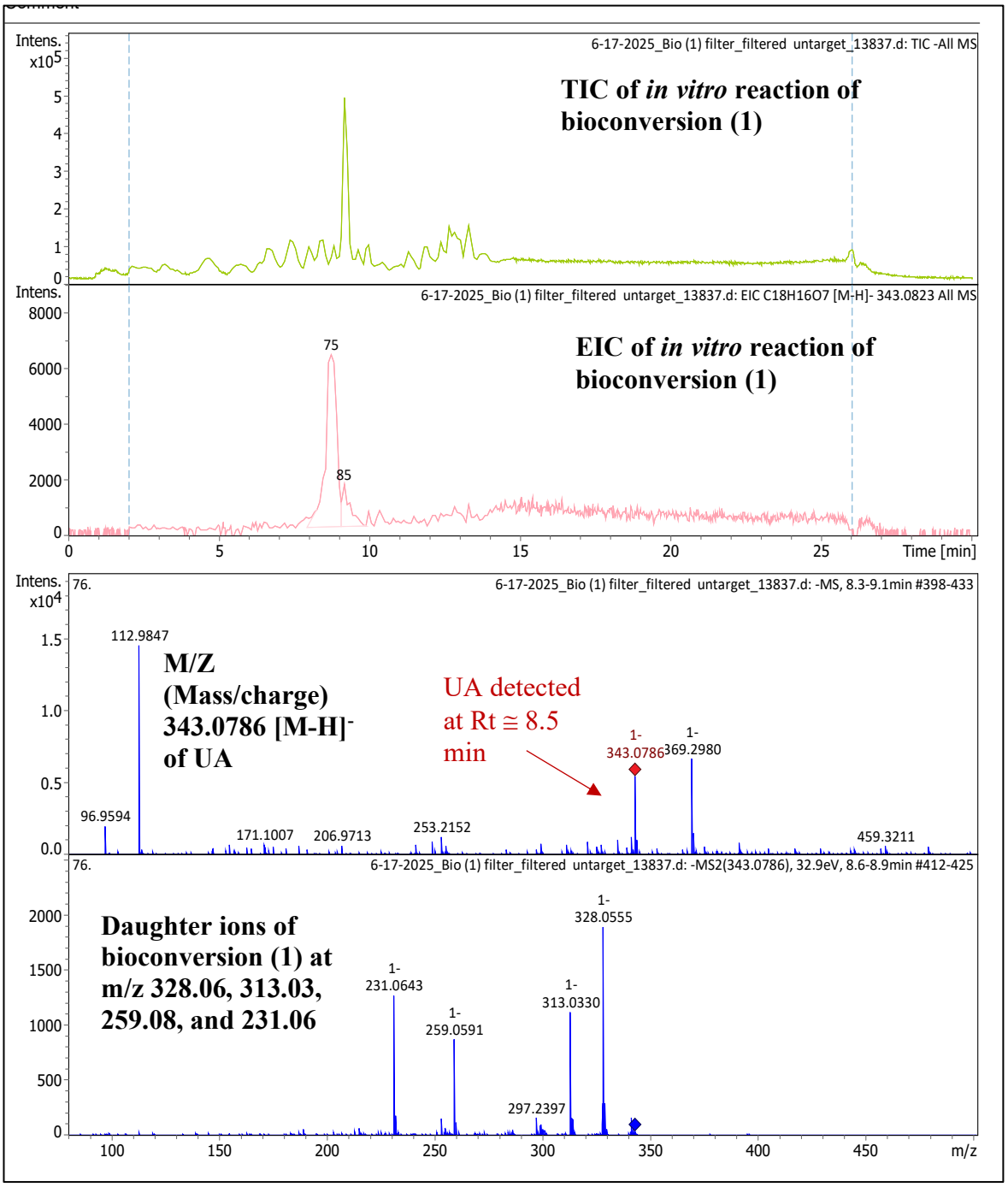

(C) TIC and EIC of bioconversion (2) with MS/MS fragmentation

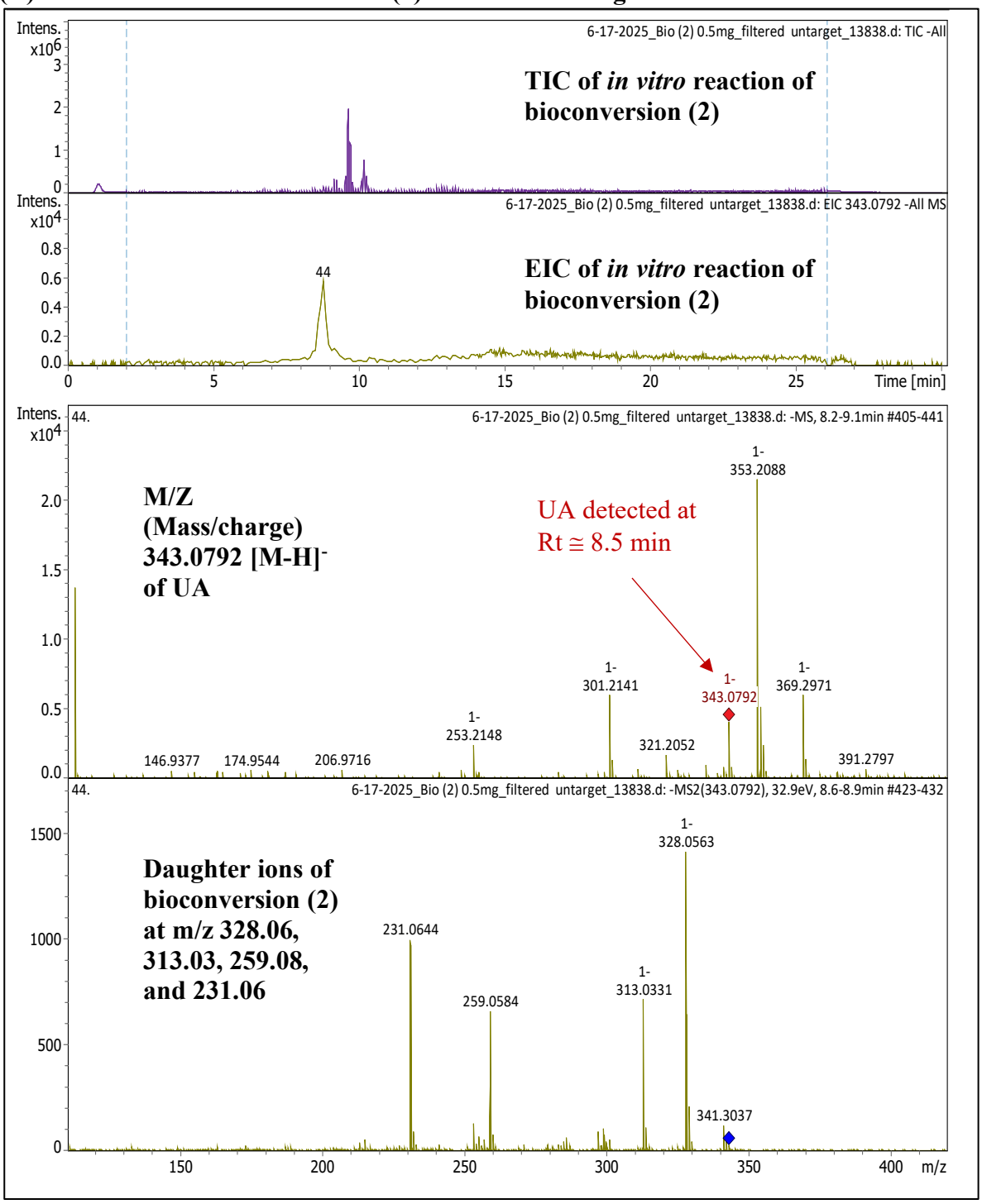

(D) TIC and EIC of MPAO only + MPA+NADH (-ve control) with MS/MS fragmentation

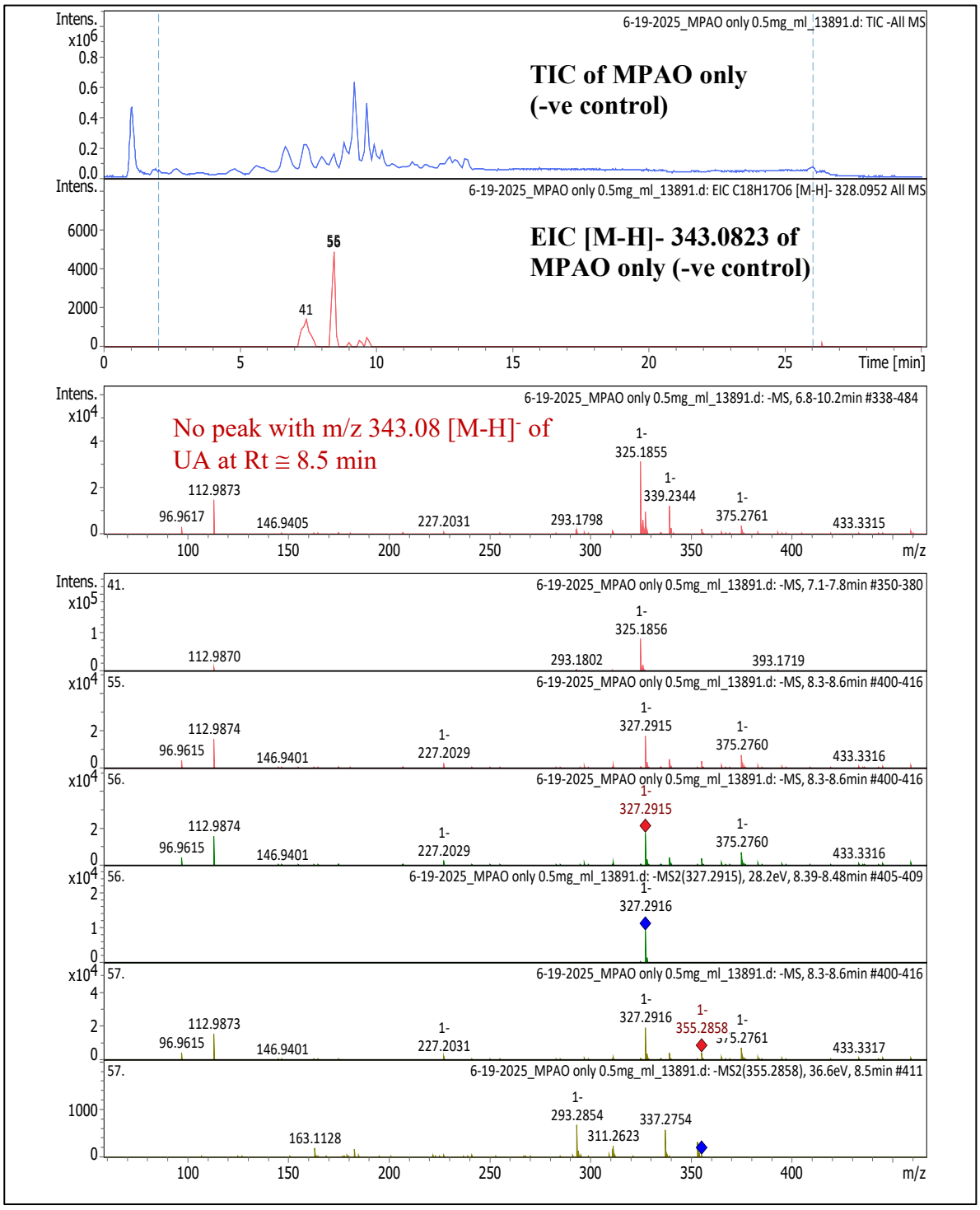

(E) TIC and EIC of CPR357 only + MPA+NADH (-ve control) with MS/MS fragmentation

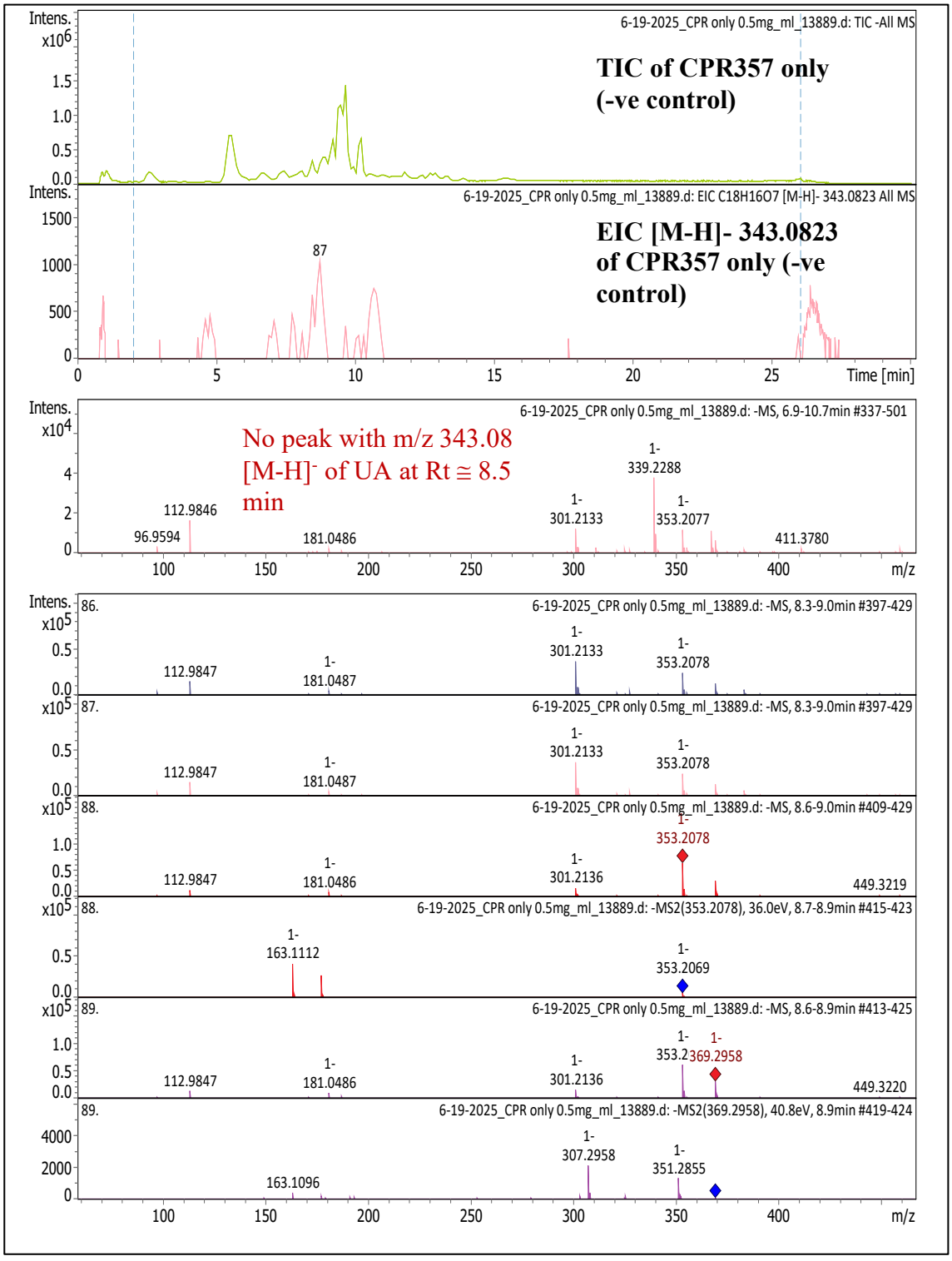

(F) TIC and EIC of MPA (precursor) with MS/MS fragmentation

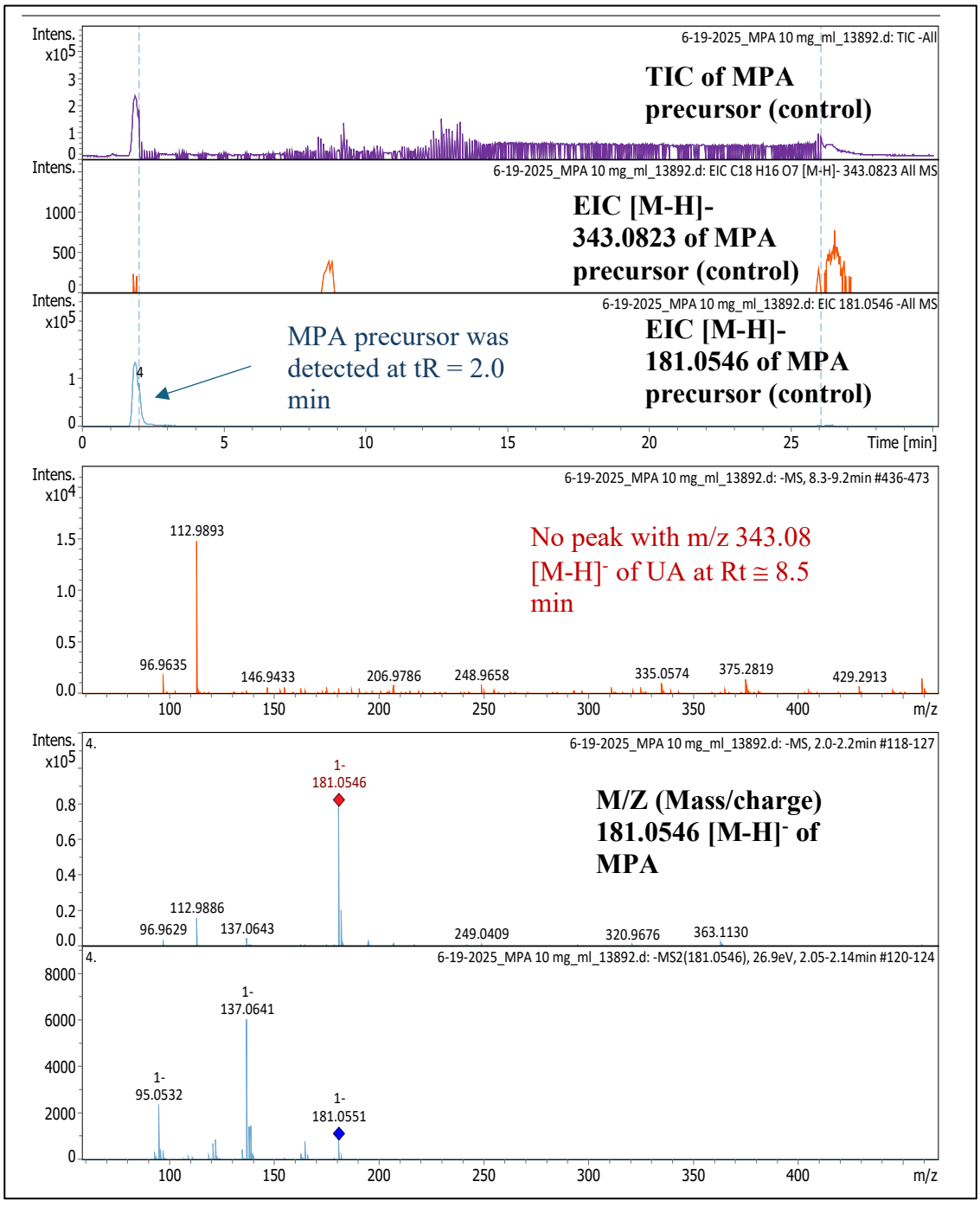

(G) TIC and EIC of MPA + NADH (w/o enzymes) with MS/MS fragmentation

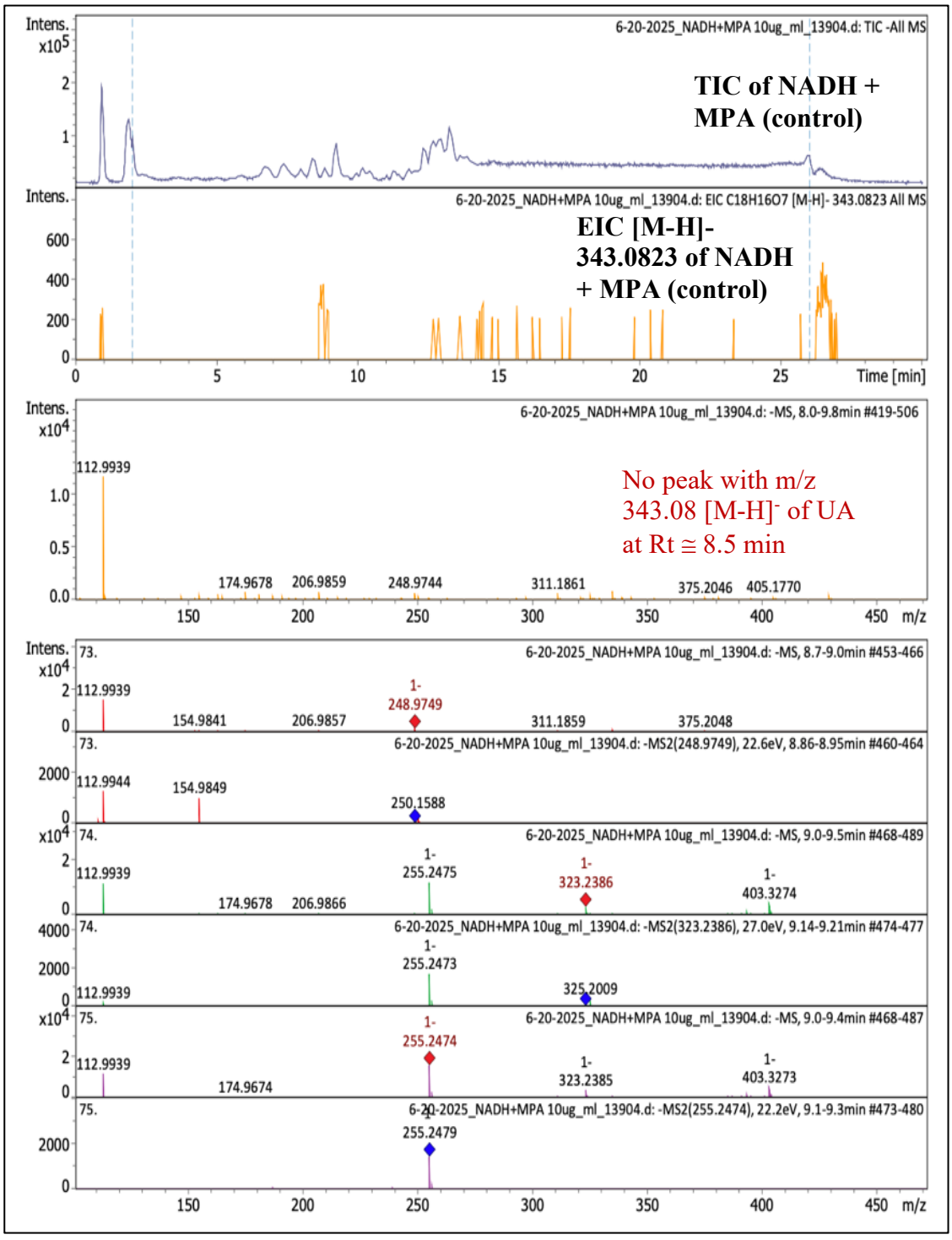

Figure 32. LC-MS/MS results of bioconversion assays from MPA to UA using qTOF LC-MS/MS, liquid chromatogram (on the top of each chromatogram) with a retention time on the x-axis and

intensity on the y-axis. Mass spectra (on the bottom of each chromatogram) with a base peak and (MS/MS) & the fragmentation pattern/ product ion (MS2). All spectra were acquired in the negative ion mode. **A**. Usnic acid standard in acetonitrile**; B.** Bioconversion 1 (bioconversion using purified enzyme under condition No.1 in **Section 3.13**); Bioconversion 2 (replicate reaction under condition No.1); **D**. Negative control MPAO only+ MPA+NADH; **E**. -ve control CPR357 only + MPA+ NADH (w/o enzymes); **F**. MPA in acetonitrile; **G**.MPA+NADH in acetonitrile.

3.10 Summary

This study demonstrated the successful heterologous expression of a lichen-derived cytochrome P450 enzyme, MPAO, and its redox partner, CPR357, in a bacterial host. For the first time, *in vitro* biosynthesis of lichen secondary metabolite usnic acid was achieved using purified MPAO and CPR357 enzymes. Furthermore, this work established a reproducible framework for the heterologous and functional reconstitution of *C. uncialis* cytochrome P450 systems in bacteria, and conclusively confirms UA formation through enzymatic bioconversion.

Chapter 4

Phylogenetic analysis of depsidone formation in *Cladonia uncialis*

4.1 Depsidone in lichen

Lichens produce a remarkable diversity of secondary metabolites (SMs), as outlined in **Section 1.2)**. These compounds arise from multiple biosynthesis pathways, including polyketide-, shikimate-, and terpene-derived routes **(Section 1.5)**, and encompass structurally diverse classes such as depsides, depsidones, dibenzofurans, pulvinic acid derivatives, terpenes, and steroids. Lichen SMs play important ecological roles, contributing to protection against pathogens, herbivores, and protection from ultraviolet (UV) radiation (Furmanek et al., 2019; Molnár & Farkas, 2010). Furthermore, the broad spectrum of biological activities displayed by lichen SMs has attracted significant interest in various application **(Section 1.4)**.

Among lichen SMs, depsidones represent one of the most chemically significant classes, with approximately 100 structures reported to date (Podterob, 2008; Ureña-Vacas et al., 2022). Structurally, depsidones generally arise from two 2,4-dihydroxybenzoic acid derived aromatic rings connected by both an ether and an ester linkage **(Figure 33)** (Estrella et al., 2011; Shukla et al., 2010). They are widespread across various taxa, including free-living fungi (e.g., mollicellin F, emeguisin C, spiromastixones), lichen-forming fungi (e.g., lobarientalone A, lobaric acid), and plants (e.g., garcinisidone B) (Khayat et al., 2023). Although semi-synthetic approaches have been explored for depsidone production, these methods are very tedious, expensive and inappropriate for large-scale or industrial applications (Elix et al., 1987). Alternatively, direct extraction from naturally-growing lichen thalli leads to significant biomass destruction which is a major limitation given the extremely slow growth rates of lichens. Therefore, integrated strategies combining

genomic analysis with heterologous expression, which requires only small amounts of lichen biomass, would represent a practical and sustainable approach for producing depsidones.

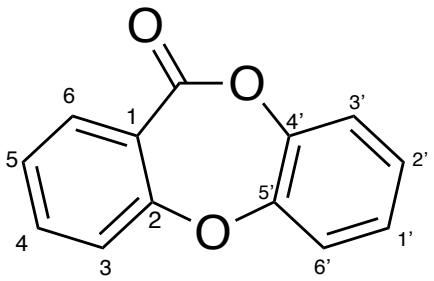

Figure 33. General structure of depsidone.

4.2 Structure and proposed biosynthetic routes for depsides and depsidones

Hundreds of depsides and depsidones have been characterized, and their core structure farwork is highly conserved (Huneck & Yoshimura, 1996). Depsides are considered the biosynthetic precursors of depsidones, which consist of two aromatic rings joined by an ester linkage, whereas depsidones are distinguished by the presence of an additional ether linkage connecting the rings **(Figure 34)**. The aromatic ring that contributes the esterified carbonyl is designated as ring **A**, and other as ring **B (Figure 34)**. Lichen depside and depsidones are grouped into β-orcinol or orcinol series, depending on the presence of a CH_3 on the C3' carbon of their ring **(Figure 34)**. In lichen, these compounds accumulate as semi-crystalline deposits within and above the extracellular matrix coating the fungal hyphae (Culberson & Elix, 1989; Honegger, 2009). Under appropriate culture conditions, depsides and depsidones can also can be produced by mycobionts grown in the absence of the algae (Culberson & Armaleo, 1992).

Depsides and depsidones are acetyl-polymalonyl derived polyketides, with each aromatic ring being synthesized by a PKS **(Figure 34)**. As first suggested by Mosbach (1964), the ester linkage joining individual rings in depside could be formed either directly by the PKS or by

separate enzymes. However, direct experimental evidence for either route remained unavailable for many years, although depside specific esterase found in lichens (Garcia-Junceda & Vicente, 1986; Mosbach & Ehrensvärd, 1966; Schultz & Mosbach, 1971) have been hypothesized to work in reverse as depside synthases (Mateos et al., 1991). The roles of depsidones as biosynthetic precursors of depsidones were demonstrated in lichen by Culberson (1964), nearly two decades after Sheshadri first proposed that depsidones arise via phenyl ether-bond formation from depsides (Seshadri, 1944). Seshadri suggested a direct oxidative coupling between the 2-hydroxyl group of the **A** ring and the 5'-carbon on the **B** ring of a depside. Chemical confirmation of this hypothesis came several year later, although the yield was low (Brown CJ et al., 1960). Consequently, alternative multistep synthesis strategies were developed (Elix et al., 1987; Hendrickson et al., 1972; Sala & Sargent, 1981). Among these, the synthetic process developed by Elix et al.(1987) has been used for the chemical synthesis of numerous depsidones and also offers a plausible model for the *in vivo* biosynthetic sequence. It proposed that (i) two individual polyketides are synthesized from acetate/ malonate and cyclized to orcinol/ β-orcinol, (ii) these units linked by esterification to form a depside which may be (iii) processed to a depsidone in four steps hydroxylation, acyl migration, Smiles rearrangement, and esterification. However, biological verification of the chemistry was lacking. In recent studies, the genomic analyses and functional enzyme studies suggest that the depsidone pathway is catalyzed by type I iterative PKSs, followed by P450-mediated oxidative cyclization that generate the ether bridges characteristic of these compounds (Armaleo et al., 2011a; G. Singh et al., 2021).

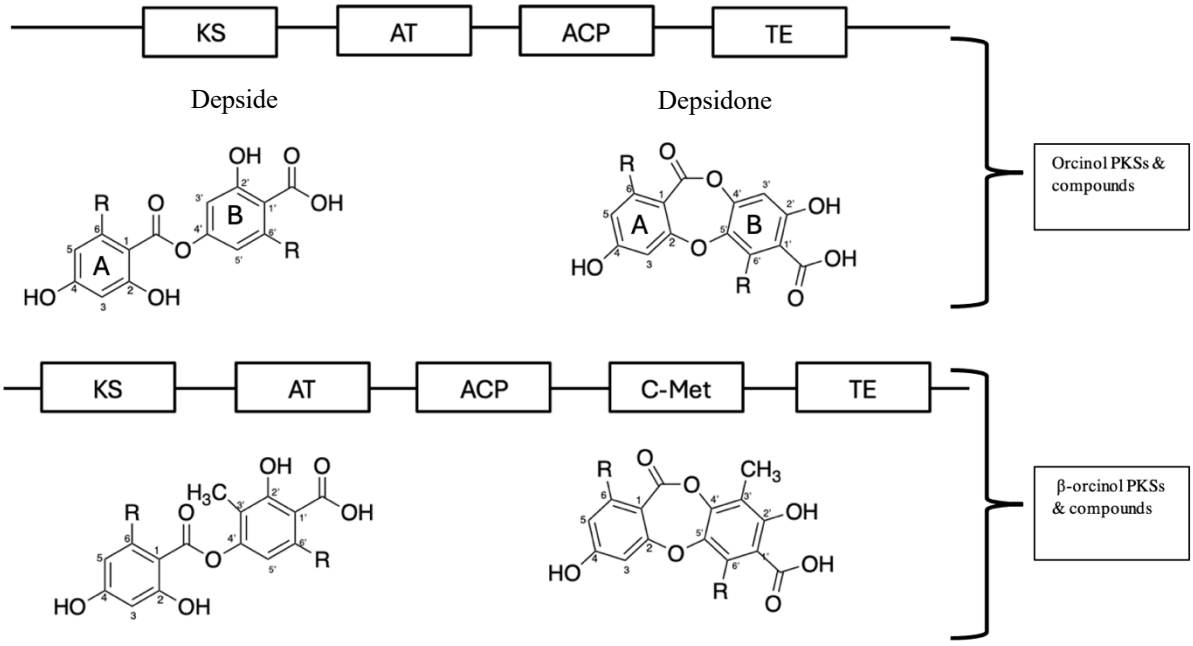

Figure 34. Schematic representation of domain organization in lichen PKSs specific for orcinol and β-orcinol metabolites. PKS domains are drawn as boxes on a line representing the primary sequence from N-terminus (left) to C-terminus (right). Ring designations and numbering (Huneck and Yoshiruma, 1996) are indicated only for orcinol compound and are the same for β-orcinol compound (Armaleo et al., 2011b).

4.3 Depsidone bioactivities

Depsidones secondary metabolite display a broad spectrum of biological activities and pharmacological properties such as antimicrobial, antimalarial, cytotoxic, anti-inflammatory, anti-*Helicobacter pylori*, anti-diarrheal, antidiabetic, herbicidal, and phytotoxic (Addo et al., 2021; Ibrahim et al., 2018) (**Figure 35**). These compounds have attracted considerable scientific interest due to their therapeutic potential.

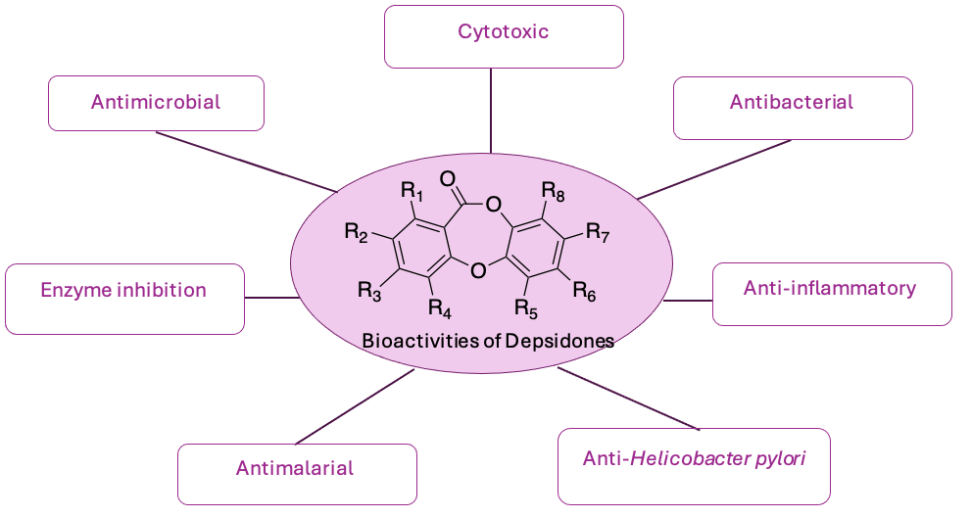

Figure 35. Reported bioactive of depsidones.

Depsidones exhibit remarkable antimicrobial effects on various pathogens including antitubercular, anti-phytopathogenic, antimalarial, and antibacterial activities (Khayat et al., 2023). For examples, himantormiones A and B (**Figure 36**), isolated from an Antarctic lichen *Himantormia lugubris*, showed inhibitory activity against *Staphylococcus aureus* (Hyung Koo et al., 2022)**.** In addition, lobaric acid (**Figure 36**), isolated from the lichen *Candelaria fibrosa*, demonstrated antibacterial efficacy against *Bacillus cereus and S. aureus* (Khayat et al., 2023). Depsidones also display cytotoxic effects against cancer cell lines. For instance, physodic acid (**Figure 36**), isolated from *Hypogymnia physodes* a European lichen, showed cytotoxic effects against several brain cancer cell lines (Studzińska-Sroka et al., 2021). Moreover, himantormiones B was more potent than 5-fluorouracil (a commonly used chemotherapy drug) against colon cancer cells (Hyung Koo et al., 2022). Furthermore, depsidones also inhibit *Helicobacter pylori* urease activity, suggesting an an effective therapeutic approach for managing this infectious disease (Lage et al., 2018). Fumaprotocetraric acid **(Figure 36)**, isolated from *Cladonia rappii* was identified as a competitive inhibitor of jack bean urease and exhibited strong

inhibitory effects against six clinical isolates of *H. pylori* (Lage et al., 2018). These findings underscore depsidones as promising potential in various applications.

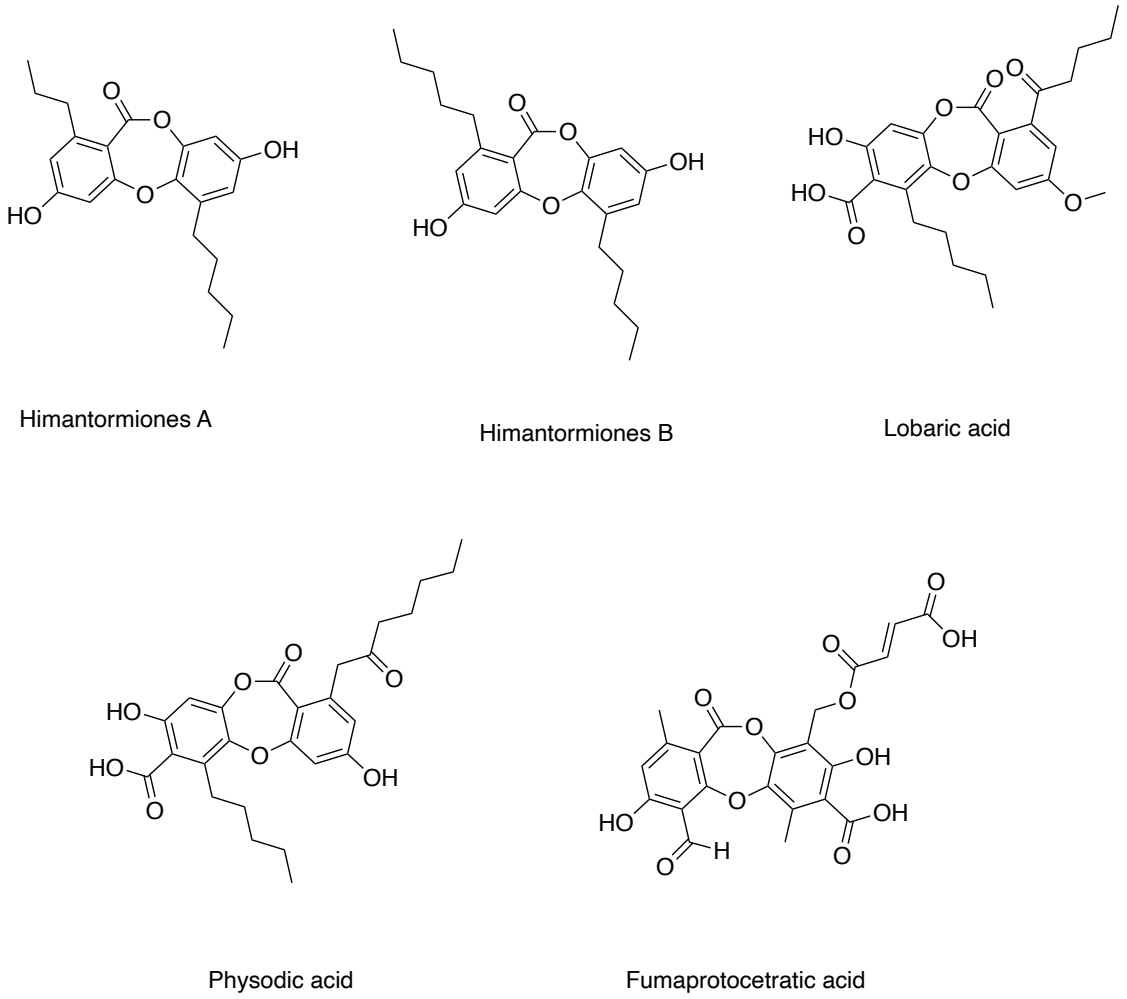

Figure 36. Chemical structures of representative depsidones isolated from lichen species.

4.4 Rationale for Phylogenetic Analysis of *Cladonia uncialis* P450 Enzymes in Lichen-Depsidone Biosynthesis

To date, no depsidone forming pathways have been experimentally characterized in *Cladonia uncialis*. Consequently, comparative phylogenetic analysis of cytochrome P450 enzymes in *C. uncialis* provides a useful strategy for predicting candidate enzymes involved in depsidone formation. The rationale for this analysis was to identify potential functional equivalents

of previously characterized depsidone formation CYPs from other fungal and lichenized fungi systems. Specially, this study focusses on evolutionary relationships among: (**1)** multiple putative cytochrome P450 protein sequences from *C. uncialis* retrieved from GenBank, **(2)** functionally characterized CYPs involved in depsidone biosynthesis from lichen-forming *Lecanoromycetes* species (*Cladonia grayi, Pseudevernia furfuracea*), and **(3)** cytochrome P450 enzyme MollD from a distantly-related ascomycotan fungus *Ovatospora brasiliensis*, which participates in mollicellin depsidone biosynthesis. Protein sequences were retrieved, annotated for cytochrome P450 domains, and aligned for maximum likelihood phylogenetic analysis. Bootstrap values were mapped to identify statistically well supported clades containing known depsidone forming enzymes.

A key reference enzyme in this study in this analysis is MollD, a cytochrome P450 characterized from mollicellin biosynthesis pathway of the free-living ascomycete *Ovatospora* sp. SCSIO SY280D (Zhao et al., 2023). Moll D is a bifunctional enzyme that catalyzes both oxidative ether bond formation and hydroxylation reactions in depsidone biosynthesis (**Figure 37**). The heterologous reconstitution of the mollicellins gene cluster in *Aspergillus nidulans* A1145 revealed that mollD catalyzes critical oxidative steps including the formation of biphenyl ether bonds and subsequent hydroxylation reactions, transformations that are characteristic of depsidone biosynthesis.

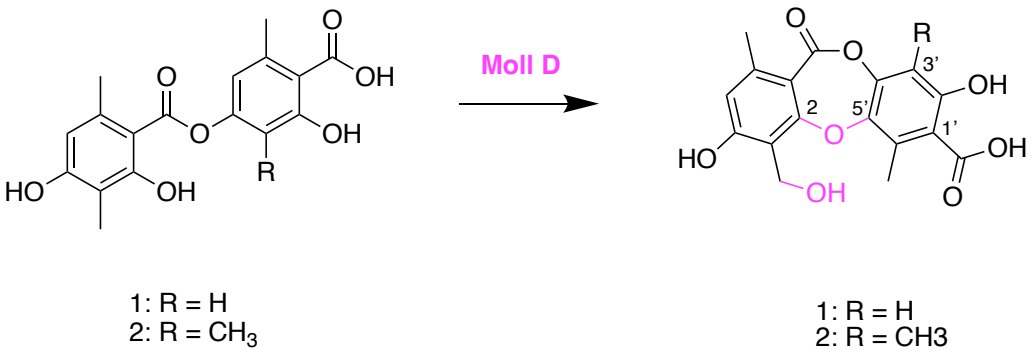

Figure 37. Cytochrome P450 MollD from the *Ovatospora sp. SCSIO SY280D* exhibits dual catalytic functions, mediating both oxidative coupling and ether bond formation during depsidone biosynthesis (Zhao et al., 2023).

The current study was also informed by a comprehensive analysis of lichen cytochrome P450 enzymes from the monooxygenase family in the lichenized fungi in Class *Lecanoromycestes*, with 434 CYP enzymes distributed across 178 families and 345 subfamilies (Mlambo et al., 2023). Notably, the study identified that 73 CYPs were found to be part of secondary metabolite gene clusters, indicating their potential involvement in the biosynthesis of secondary metabolites. The annotation of P450s revealed that ADM79460.1 from *Cladonia grayi* and CYP682BG2 from *Pseudevernia furfuracea* have been functionally linked to the biosynthesis of the depsidone grayanic acid and physodic acid, respectively **(Figure 38)**.

The ADM79460.1 from *C.grayi* has been functionally characterized as catalyzing oxidative coupling reactions in grayanic acid biosynthesis (Zhao et al., 2023). Specifically, ADM79460.1 from *C. grayi* performs the oxidative coupling of 4-O-demethyl sphaerophorin (depside) to 4-O-demethyl grayanic acid (depsidone) via ether bond formation, representing a critical tailoring step in orcinol depsidone biosynthesis (Armaleo et al., 2011b; Zhao et al., 2023). CYP682BG2 from *Pseudevernia furfuracea* represents a functionally characterized CYP involved in physodic

acid biosynthesis, catalyzing the oxidative coupling of olivetoric acid (depside) to physodic acid (depsidone) via ether bond formation (**Figure 39**).

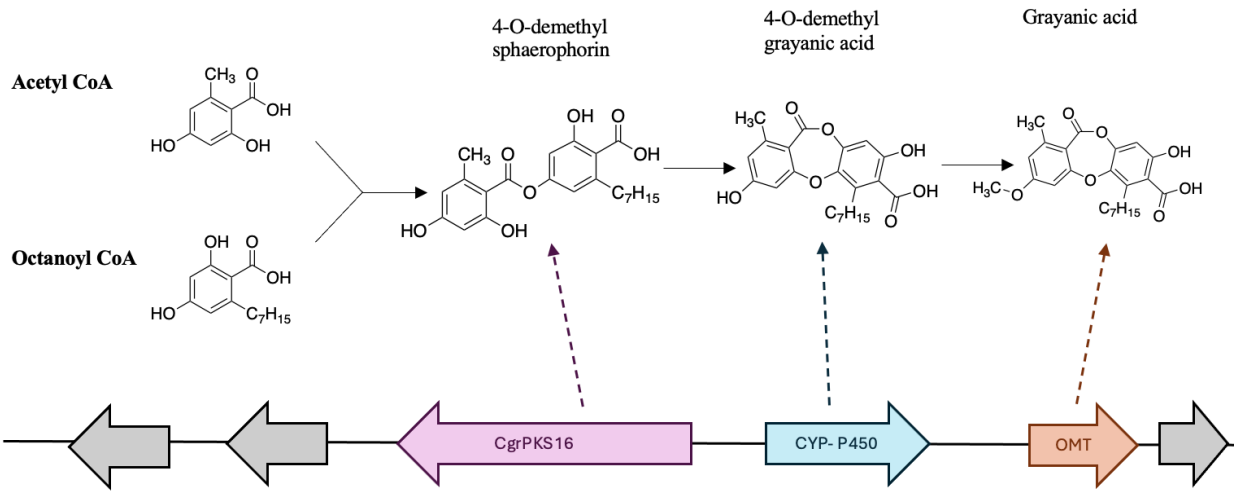

Figure 38. Grayanic acid Biosynthesis within the associated gene cluster (Armaleo et al., 2011b).

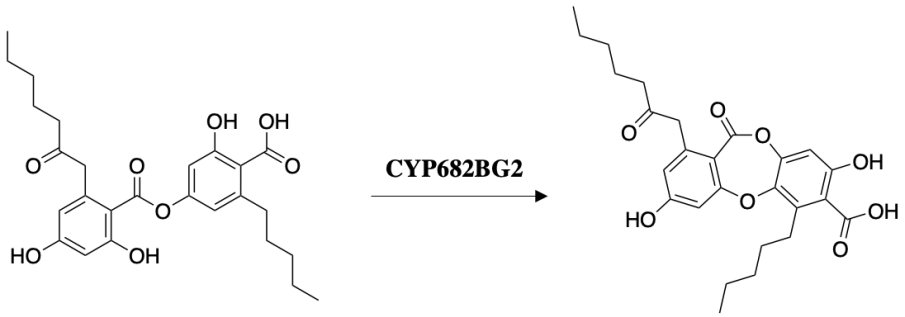

Figure 39. Physodic acid (depsidone) formation via CYP682BG2 from *Pseudevernia furfuracea* from olivetoric acid (depside).

Based on these studies, we hypothesized that *C. uncialis* CYP enzymes will phylogenetically cluster with MollD, ADM79460.1, and CYP682BG2 that may represent functional equivalents capable of catalyzing key steps in depsidone formation. Therefore, the phylogenetic analyses in this study focuses on *C. uncialis* CYP candidates for future functional validation in depsidone biosynthesis. Accordingly, this study encompassed 29 cytochrome P450 protein sequences (**Table 4**). The full amino sequences were listed in **Table S 3**.

Table 4. Cytochrome P450 sequences from GenBank

No.	Species name	GenBank accession No.	Function
1	*Cladonia uncialis*	**Table S3**	Annotated Cytochrome P450
2	*Cladonia grayi*	ADM79460.1	Representative of grayanic acid biosynthesis
3	*Pseudevernia furfuracea*	CYP682BG2	Representative of physodic acid biosynthesis
4	*Ovatospora* sp.	QPI71217.1	Representative mollicellin biosynthesis, known as mollD

4.5 Phylogenetic analysis of Cytochrome P450 Monooxygenases in Lichen Forming Fungi

4.5.1 General features of phylogenetic tree

With the rapid growth of genome sequencing, novel phylogenetic methods allow scientists to understand how genes are related and to predict the functions of both known and unknown genes in lichen gene clusters. Phylogenetic trees illustrate evolutionary relationships among genes or proteins by comparing sequence similarities, which may include amino acid sequences, non-

coding regions, or whole-genome data depending on the analysis approach. These trees are built using multiple sequence alignments (MSA) to compare similarities and differences between proteins. Bootstrap values provide a measure of support for each node under the specified model and analytical parameters, reflecting the consistency with which that branching pattern is recovered across resampled datasets and replicate trees, rather than serving as a direct indicator of true evolutionary history. The horizontal lines (scale bars) show the number of sequence changes, helping to measure how different the sequences are. If two sequences have no horizontal line between them, it means they are identical and are called haplotypes**.** Genes or proteins that come from the same node share a common ancestor, and all such related sequences form a clade. An outgroup is a sequence that is more distantly related and helps to root or orient the tree.

4.5.2 Maximum-Likelihood phylogenetic tree

The phylogenetic tree presented represents a maximum-likelihood (ML) reconstruction of *C. uncialis* cytochrome P450s evolutionary relationship among free-living fungi and lichenized fungi. The analysis included CYP sequences from *Cladonia unciaslis*, ADM79460.1 from *Cladonia grayi*, CYP682BG2 from *Pseudevernia furfuracea*, and QPI71217.1 (MollD) from *Ovatospora* sp. (**Figure 40**).

Maximum-likelihood phylogenetic reconstruction operates on fundamental statistical principles that identify the tree topology, branch lengths, and evolutionary model parameters that maximize the probability of observing the empirical sequence data under specified substitution model. For any given alignment position, the likelihood of observing the nucleotide or amino acid states across taxa is calculated given a particular tree topology and substitution model; the overall likelihood is then computed as the product of individual site likelihoods. This probabilistic

framework renders ML methods statistically rigorous and particularly well-suited for molecular evolutionary analysis of functionally constrained protein families such as cytochrome P450s.

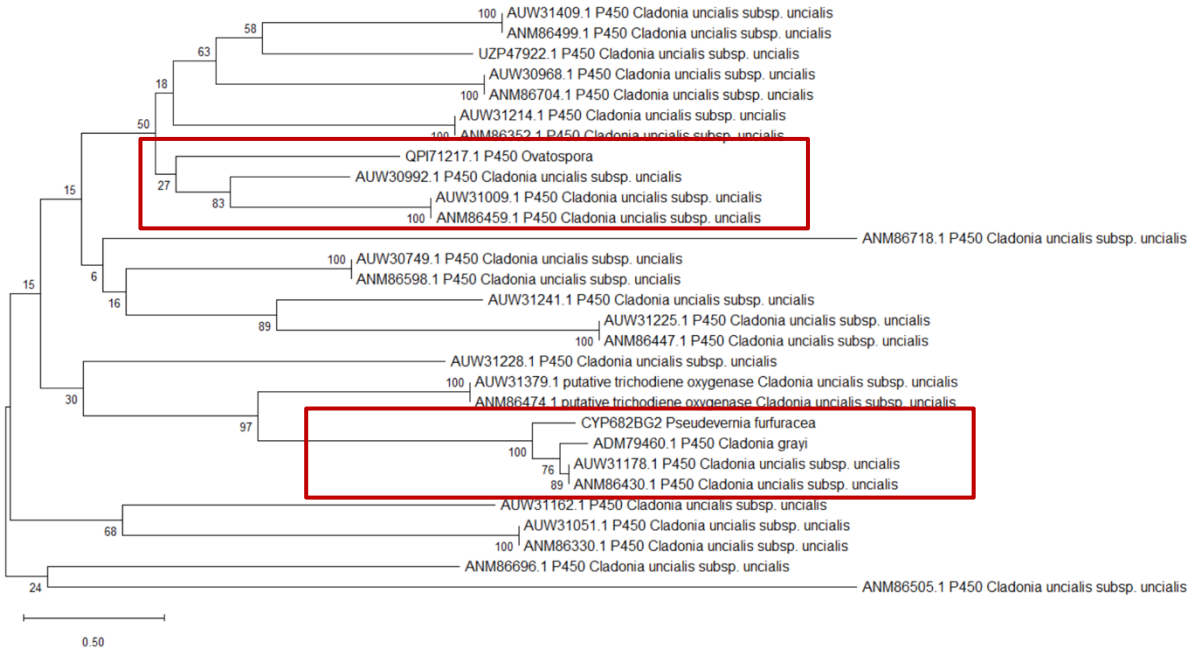

Figure 40. Evolutionary analysis by the maximum likelihood method. The phylogeny was inferred using the Maximum Likelihood method and Jones-Taylor-Thornton (1992) model of amino acid substitutions and the tree with the highest log likelihood is shown. The percentage of replicate trees in which the associated taxa clustered together (1000 replicates) is showed nest to the branches.

4.5.3 *Cladonia uncialis* CYPs within class *Lecanoromycetes* lichens clade

The phylogenetic reconstruction demonstrates strong bootstrap support (76%-100%) for the clade containing *C. uncialis* CYP sequences AUW31178.1 and ANM86430.1, indicating high confidence in their evolutionary relationship with CYP682BG2 from *Pseudevernia furfuracea* and ADM79460.1 from *Cladonia grayi* (**Figure 41**). The truncated phylogenetic tree (**Figure 41**) showed CYP. ADM79460.1 (*C. grayi*), CYP682BG2 (*P. furfuracea*), and the two *C. uncialis* P450

sequences formed a monophyletic clade, consistent with descent from a single common ancestral CYP. Bootstrap support values are high throughout this clade, with 100% support at the basal node containing all four sequences, 76% support for the node group *C. grayi* as sister to the *C. uncialis*, and 89% support at the terminal split between the two *C. uncialis* CYPs. The short branch length (0.0-0.1) connecting ADM79460.1, CYP682BG2 to *C. uncialis* CYPs, together with their high amino acid sequence identities (83.0% for ADM79460.1 and 71.9% for CYP682BG2 based on pBLAST analysis against *C. uncialis* CYPs (**Figure S 12**) and 100% query cover, support the hypothesis that these CYPs enzymes may share functionally related cytochrome P450 enzymes for depsidone biosynthesis. The phylogenetic proximity of ADM79460.1 to *C. uncialis* P450s within this functionally characterized clade suggests that these enzymes may share similar catalytic mechanisms, potentially involved in oxidative coupling reactions that convert depside precursors into depsidone products through C-O-C ether bond formation.

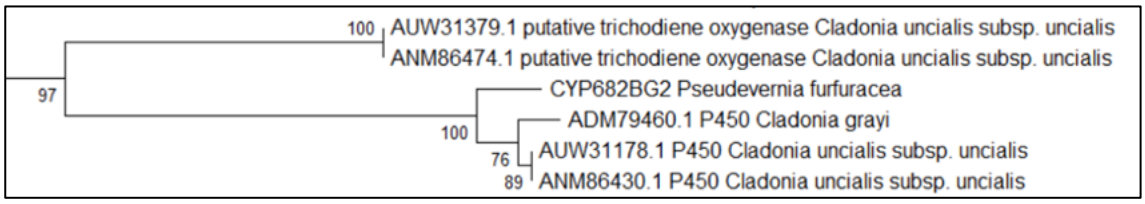

Figure 41. Truncated phylogenetic trees of *Cladonia uncialis subsp. uncialis* CYP sequences (ANM86430.1 and AUW31178.1), ADM79460.1 from *Cladonia grayi*, CYP682BG2 from *Pseudevernia furfuracea*.

4.5.4 *Cladonia uncialis* CYPs with *Ovatospora sp.* clade

The CYP sequence QPI71217.1 from the free-living ascomycete fungi *Ovatospora* showed a phylogenetically distinct position in the tree. This sequence is recovered as basal to one a

C.uncialis subclade, with low bootstrap support (27%), indicating that *C.uncilais* CYP sequence in this analysis do not form a single monophyletic group (**Figure 42**). This long-branch separation likely reflects the deeper taxonomic distance between *Ovatospora* and the *Cladonia uncialis* clade. The low support of amino acid identity <31% based on pBLAST against closest *C. uncialis* CYP sequences (AUW30992.1, AUW31009.1, ANM86459.1) (**Figure S 12**), indicates that QPI71217.1 represents a highly divergent cytochrome P450 lineage. Taken together, the phylogenetic placement of QPI71217.1 suggested that, although MollD is functionally involved in depsidone biosynthesis in *Ovatospora*, it likely possesses catalytic properties that are distinct from those of the CYPs in Class *Lecanoromycetes*, which are better candidates for depsidone formation in *C. uncialis*.

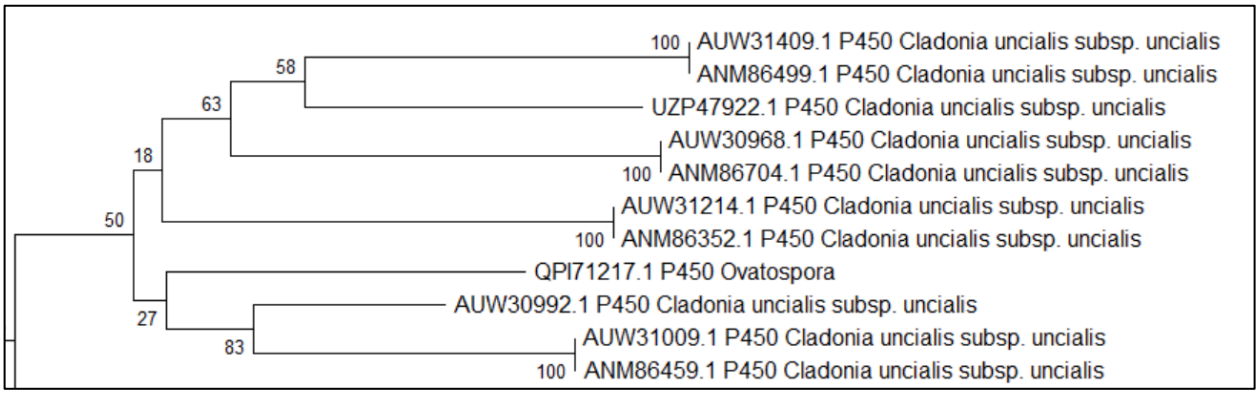

Figure 42. Truncated phylogenetic trees of *Cladonia uncialis* subsp. *uncialis* CYPP450 sequences (AUW30992.1, AUW31009.1 and ANM86459.1), CYPP450 from free-living ascomycetes *Ovatosopora* sp.

4.6 Summary: Phylogenetic analysis of cytochrome P450 Enzymes in Lichen Depsidone biosynthesis

This chapter analyzed the phylogenetic relationship of cytochrome P450 enzymes potentially involved in depsidone biosynthesis in *C. uncialis*. The study is motivated by the

practical problem that direct extraction and chemical synthesis of depsidones are unsuitable for large-scale production, and heterologous expression offers a sustainable alternative, which requires the identification of the correct biosynthetic enzymes. Since *C. uncialis* has not been experimentally studied for depsidone biosynthesis, phylogenetic comparison with functionally characterized P450s from related lichen species (*Cladonia grayi, Pseudevernia furfuracea*) and ascomycetes fungi system *(Ovatosopora brasiliensis)* provided a rational predictive strategy.

Two *C. uncialis* CYP (ANM86430.1 and AUW31178.1) genes showed a well-supported phylogenetic clade with ADM79460.1 (from *Cladonia grayi)*, CYP682BG2 (from *Pseudevernia furfuracea)*, both of which are characterized as depsidone forming CYP enzymes. The high bootstrap support (75–100%), short evolutionary distances (0.0–0.1), and approximately 83% sequence similarity suggest that the *C. uncialis* candidates likely possess similar catalytic functions. In contrast, MollD from *Ovatospora sp.*, although experimentally implicated in structural depsidone biosynthesis pathway, falls within a separate, weakly supported clade (27% bootstrap). This low support indicates that its inferred position is recovered in only a minority of bootstrap replicates, so its placement relative to the lichen-derived P450s is uncertain and it cannot be regarded as a close functional proxy for the *C. uncialis* CYPs.

Chapter 5

Conclusion and Future Prospectives

5.1 Review of previous studies and finding before this study began in 2023

At the start of my master's program, our group had demonstrated functional *in vivo* expression through co-expression of a truncated version of MPAO (lacking the transmembrane domain, TMD) that was codon optimized for *E. coli* using a pETite N-His-SUMO expression vector, alongside a truncated CPR357 (without transmembrane domain) expressed from a non-codon-optimized *E. coli* pET21a N-His_6 plasmid, enabling conversion of methylphloroacetophenone (MPA) to usnic acid (UA) within the cell. These critical biosynthetic enzymes represent the tailoring or accessory enzymes that perform essential post-PKS modifications, including the cytochrome P450 monooxygenase designated MPAO and its redox partner CPR357. However, attempts to achieve *in vitro* bioconversion using purified enzymes were unsuccessful. Obtaining these enzymes as soluble, active proteins was challenging even after optimizing expression conditions. The yield of soluble protein was low, preventing successful *in vitro* bioconversion of MPA to UA using the purified enzymes. In summary, by 2023 it was established that lichen cytochrome P450 tailoring enzymes could be functionally co-expressed in bacterial systems to catalyze *in vivo* usnic acid biosynthesis; however, *in vitro* bioconversion using purified enzymes remained unachieved to solubility and activity limitations.

5.2 Rationale behind the objectives of my thesis

The main goal of this research is to achieve the first functional *in vitro* bioconversion of MPA to usnic acid using a purified cytochrome P450 MPAO and CPR357 enzyme system. To overcome expression challenges, I customized the expression system by ordering two separate constructs from Twist Bioscience: the codon-optimized MPAO gene cloned into the pET28a(+) vector with a His_6-tag, and the non-codon optimized CPR357 gene cloned independently into another pET28a(+) vector with a His_6-tag for heterologous expression in *E. coli*. In addition, 5-aminolevulinic acid (5-ALA), a heme precursor, was supplemented in induction media to enhance heme synthesis and increase the yield of CYP proteins.

Usnic acid naturally exists as a pair of enantiomers, (+) UA and (-)-UA, which exhibit distinct bioactivities dependent on the stereochemistry. However, the basis for the stereospecificity of the enzyme involved in UA biosynthesis has not yet been elucidated. Therefore, our future goal is to elucidate the biosynthesis of (+) and (-) usnic acid by determining which CYP produces each enantiomer and understanding the mechanism of stereospecificity. In the future, this research program aims to elucidate the molecular mechanisms by which lichens achieve stereospecificity in usnic acid production across different lichen species. Understanding these mechanisms could enable the development of engineered cytochrome P450 systems capable of producing specific usnic acid enantiomers for pharmaceutical applications. Usnic acid has demonstrated significant therapeutic potential, including antibacterial, antiviral, anticancer, and anti-inflammatory activities, making it a valuable target for biotechnological production

5.3 Functional expression of cytochrome P450 enzymes in E.coli and in vitro enzyme assays

Building upon previous work in the Sorensen lab, we aimed to achieve heterologous expression and purification of the cytochrome P450 monooxygenase MPAO and its redox partner in CPR357 in *E.coli*, then perform the bioconversion of MPA to UA *in vitro* enzyme assays. In

Chapter 3, I reported that both MPAO and CPR357 were successfully produced as soluble proteins, respectively. Using these purified enzymes, we carried out enzyme assays with co-factor NADH. The MPAO and its redox partner CPR357 catalyzed the oxidative dimerization of MPA to form usnic acid. The reaction products were analyzed by LC-MS/MS, and the chromatography revealed the peaks with fragmentation pattern matching UA standard.

Key results from Chapter 3:

1. Successful independent transformation and expression of cytochrome P450 MPAO and its redox partner CPR357 in *E. coli* BL21(DE3)pLysS cells.

2. Heterologous expression: The genes for MPAO and CPR357 were transformed and expressed in *E. coli*. The SDS-PAGE analysis confirmed production of the recombinant proteins as expected molecular weight.

3. Purification: Both MPAO and CPR357 were purified to near homogeneity via affinity chromatography. SDS-PAGE analysis confirmed production of the recombinant proteins as expected molecular weight.

4. Enzymatic activity: In enzyme assays containing NADPH and both purified MPAO and CPR357, the UA product was formed. LC-MS/MS analysis (qTOF LC-MS/MS) of the reaction mixture identified a molecular ion and fragmentation peaks consistent with usnic acid, matching the retention time and MS/MS spectrum of a UA standard.

These findings demonstrate for the first time that a lichen cytochrome P450 with its reductase CPR357 can convert MPA to UA *in vitro*. These findings hold significant promise for enhancing reaction efficiency and facilitating industrial scale synthesis of UA and related dibenzofuran

compounds. Future optimization of reaction conditions, particularly for usnic acid production from MPA, may provide viable routes for biotechnological production of bioactive compounds.

Furthermore, understanding the enzymatic mechanisms underlying stereoselectivity could enable the development of engineered cytochrome P450 systems capable of producing specific usnic acid enantiomers with tailored bioactivities. This capability would address current limitations in usnic acid research, where the slow growth rates of lichens in nature severely restrict the availability of these compounds for pharmaceutical applications.

5.4 Limitations

5.4.1 Substrate Availability and Synthetic Chemistry Limitations

Low yields from chemical synthesis of the substrate MPA represent a significant limitation constraining enzymatic activity investigations. The complex aromatic structures characteristic of lichen metabolite precursors MPA, present synthetic challenges that result in limited substrate availability and elevated costs. In 2025, there are companies that sell MPA however the price is expensive which is approximate $1000 USD per gram. Consequently, large-scale usnic acid production cannot be achieved without substantial improvements in substrate synthesis yield. This limitation affects both research applications and potential industrial biotechnology implementations of lichen secondary metabolite production systems

5.4.2 Technical Limitations in Heterologous Expression

Several fundamental limitations constrain current approaches to lichen secondary metabolite biosynthesis research. Expressing eukaryotic membrane bound proteins in bacterial systems remains a technically challenge that requires extensive genetic manipulation and optimization. The challenges include removal or modification of N-terminal hydrophobic domains, systematic codon

optimization for *E. coli* expression, and ongoing difficulties achieving high levels of soluble expression of lichen proteins. The membrane topology of cytochrome P450 enzymes involves N-terminal transmembrane domains that anchor these enzymes to endoplasmic reticulum membranes in their native environment. Successful bacterial expression typically requires deletion or modification of these transmembrane regions, potentially affecting protein folding, stability, and catalytic activity.

5.5 Unveiling the biosynthetic potential of depsidone formation in *C. uncialis*

Lichen depsidones have gained attention due to their diverse biological activities in various application, but the enzymes for depsidone formation remain largely unknown in lichen *C. uncialis*. To address this, comparative phylogenetic analysis of cytochrome P450 enzymes in *C. uncialis* provides a critical strategy for predicting candidate enzymes involved in depsidone formation. The rationale for this analysis was to identify potential functional equivalents of previously characterized depsidone formation CYPs from other fungal and lichenized fungi systems.

In Chapter 4, the ML phylogenetic analysis of cytochrome P450 monooxygenases from lichen *C.uncialis* offers key insights into the biosynthesis lichen depsidone metabolites. Two *C. uncialis* CYP (ANM86430.1 and AUW31178.1) formed a well-supported clade with known depsidone-forming CYPs from *Cladonia grayi*, *Pseudevernia furfuracea,* showing high bootstrap support (76-100%), short evolutionary distances, and ~83% sequence similarity, suggesting similar catalytic function. In contrast, MollD from *Ovatospora sp*. clusters separately with low bootstrap support, indicating it has diverged substantially from the lichen-derived P450s and is less suitable as a functional model.

5.6 Future perspective

5.6.1 Substrate analog bioconversion with purified protein.

In the future, the same heterologous expression approach could also be used to biosynthesize the analogs of UA from MPA analogs. The chemical synthesis of MPA analogs is discussed in **Chapter 2.3.1**. Substrate scope of MPAO and CPR357 enzymes can be examined by catalyzing the bioconversion of MPA analogs to UA analogs. If these enzymes demonstrate a broad substrate spectrum, more studies could be initiated for making artificial SMs or analogs of natural products with new or improved biological activities. In addition, more accessory enzymes from different biosynthetic gene clusters could be expressed in bacteria and tested for their substrate scope.

5.6.2 NADPH Cofactor in bioconversion enzyme assays

Cytochrome P450 enzymes require complex electron transfer systems involving NAD(P)H-dependent cytochrome P450 reductases. The efficiency of these electron transfer processes significantly influences overall enzymatic activity and can represent bottlenecks in heterologous expression systems. NADPH is the preferred reducing cofactor, as cytochrome P450 reductases exhibit significantly higher specificity and electron transfer efficiency with NADPH compared to NADH, a preference that has been well documented in previous studies (Backes, 2007; Bapiro et al., 2025).

In this study, a trial bioconversion assay was performed using purified MPAO and its redox partner CPR357 in the presence of NADPH as the cofactor. LC-MS analysis of the reaction mixture revealed the presence of an extracted ion chromatogram corresponding to m/z 343, consistent with the expected mass of the target product **(Figure S 14)**. However, MS/MS fragmentation patterns differed from that of the usnic acid standard, suggesting the formation of a structurally related or modified product rather than the usnic acid. Consequently, further investigation is required to optimize the electron transfer system and to elucidate the structural

identity of the observed product. The corresponding LC-MS/MS data were provided in **Figure S 11-S15**.

5.6.3 Stereochemical Characterization of in vitro Usnic Acid Products

A critical objective is to validate cytochrome P450 function by determining the enantiomeric composition of usnic acid. Most studies to date have focused on (+)-usnic acid, with relatively few reports on the (–)-usnic acid. This work is of particular significance because *Cladonia uncialis* predominantly produces (-)-usnic acid, providing a unique opportunity to investigate the stereoselectivity of its CYP enzyme. Assessing the enantiomeric outcome of *in vitro* enzymatic bioconversion is a critical step in confirming the P450's biosynthetic role and establishing the stereochemistry of its product. This also highlights a distinguishing feature of *C. uncialis* among lichens, its ability to predominantly synthesize (-)-usnic acid.

The comprehensive study by Xu et al., (2022), conducted by our collaborator from Iceland, provided the definitive analytical foundation for usnic acid enantiomer determination. Their research established validated chiral chromatographic methods for separation and quantification of usnic acid enantiomers in four common Icelandic lichens (*Cladonia arbuscula*, *Alectoria ochroleuca*, *Flavocetraria nivalis*, and *Ramalina siliquosa*). This validated approach can be directly applied to characterize the usnic acid produced through bioconversion in our study.

5.6.4 Heterologous expression of Cladonia uncialis depsidone formation protein.

Future studies will test the hypothesis that the candidate depsidone-forming cytochrome P450 from *Cladonia uncialis* catalyzes depsidone formation and can be functionally expressed in a heterologous host system. These enzymes candidates were selected based on their strong sequence homology with strong bootstrap support to the characterized lichen-derived CYPs from *Cladonia grayi, Pseudervenia furfuracea*, and fungal CYP mollD from *Ovatospora*, all of them

are implicated in ether bond formation steps of depsidone biosynthesis. These homologous relationships suggest that the *C. uncialis* enzyme may responsible for a comparable catalytic role.

At present, the gene sequence for Moll D and the *Cladonia uncialis* candidate proteins have been ordered as synthetic construct form Twist Bioscience. These constructs will serve as templates for cloning into appropriate expression vectors. The next steps will involve cloning each gene, verifying the recombinant plasmids, and performing heterologous expression in a bacterial host. This will provide the initial platform for preliminary functional assays. Successful expression will enable downstream characterization, ultimately determining whether the *C. uncialis* enzyme contributes to depsidone formation in a manner comparable to its homologs.

Appendix

Chapter 1: Not applicable

Chapter 2:

Table S 1. List of buffer components

Buffer	**Components**
SDS-PAGE 4X loading buffer	2 mL of 1 M Tris-HCl (pH 6.8), 0.8 g of sodium dodecyl sulfate (SDS), 4 mL glycerol, 0.4 mL of 14.7 M β-mercaptoethanol, 1 mL of 0.5 M EDTA, 0.008 g bromophenol blue, distilled water to final volume 10 mL)
Lysis buffer P1	50mM NaH_2PO_4 or 20 mM 20 mM Tris HCl, 300 mM NaCl or 150 mM NaCl, pH 7.4)

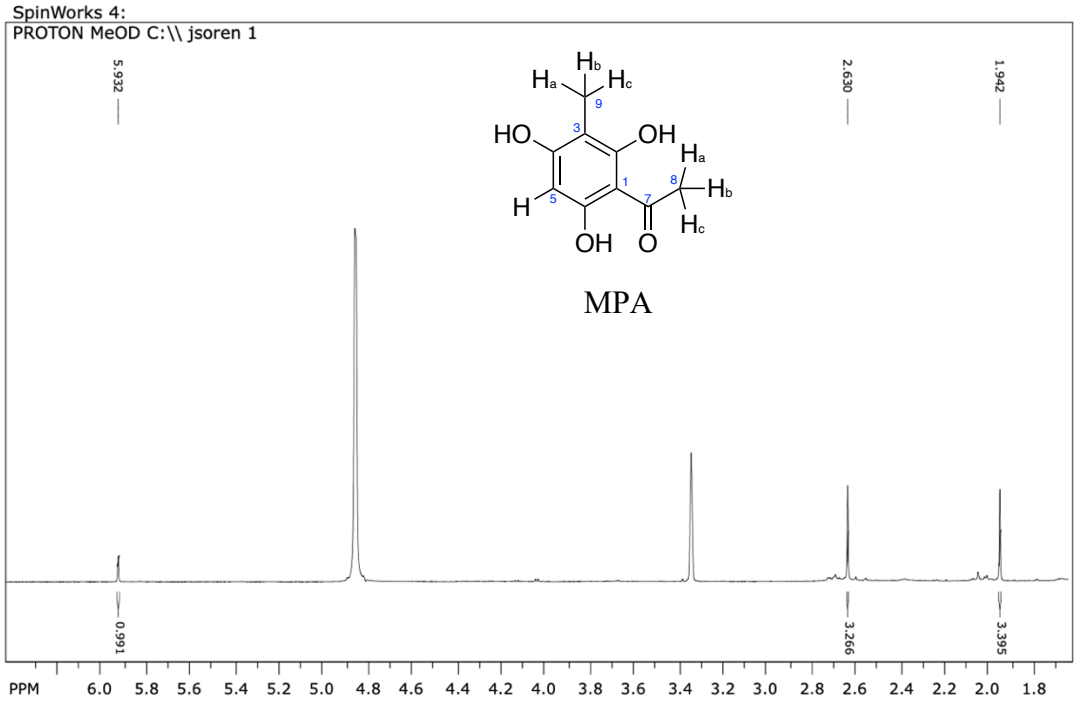

Figure S1. [1]HNMR spectrum of methyl-phloroacetophenol (MPA) (CD_3OD, 500 MHz)

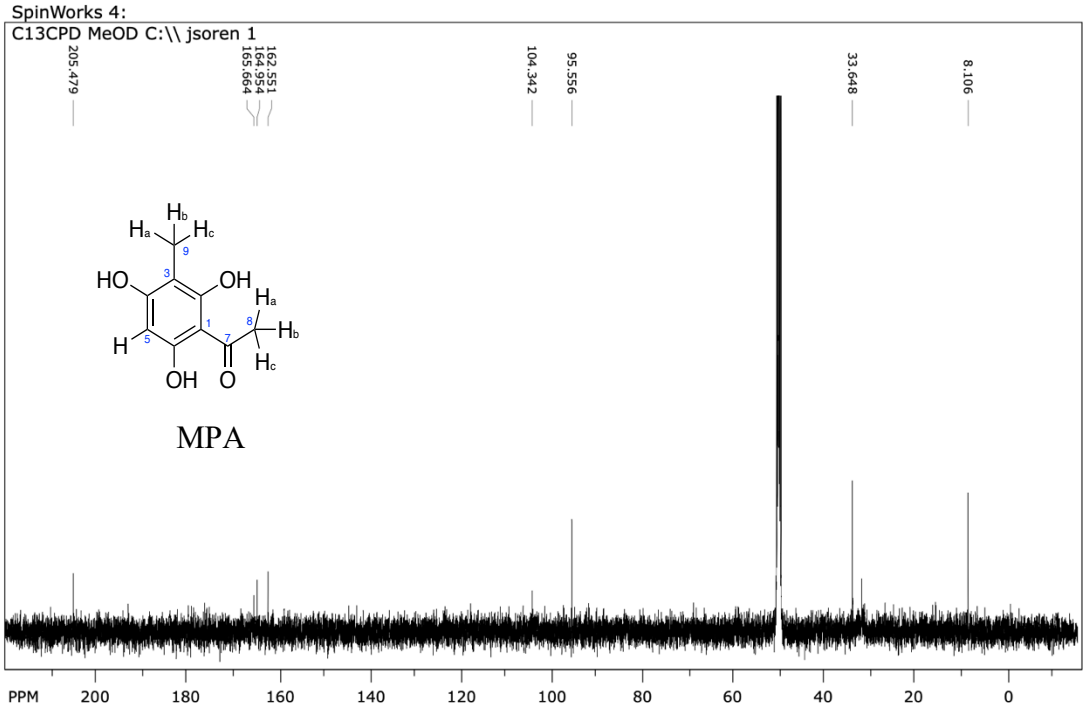

Figure S2. [13]C NMR spectrum of methyl-phloroacetophenol (MPA) (CD3OD, 500 MHz)

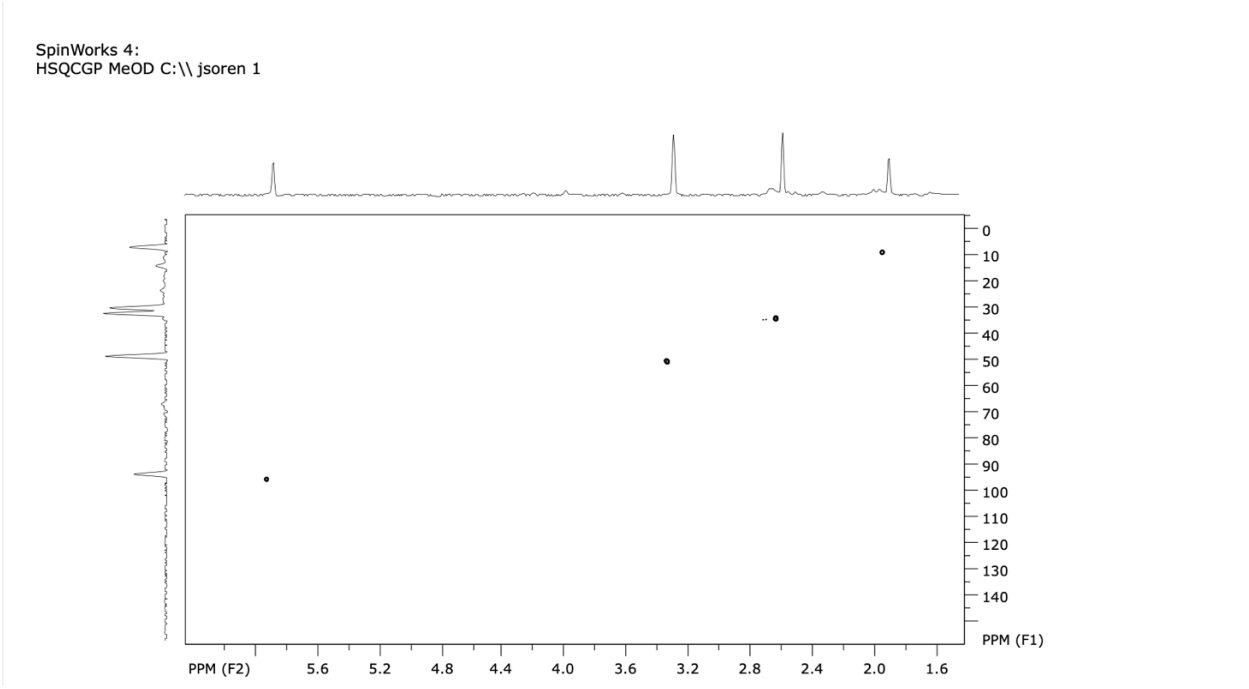

Figure S 3. HSQC spectrum of methyl-phloroacetophenol (MPA) (CD3OD, 500 MHz)

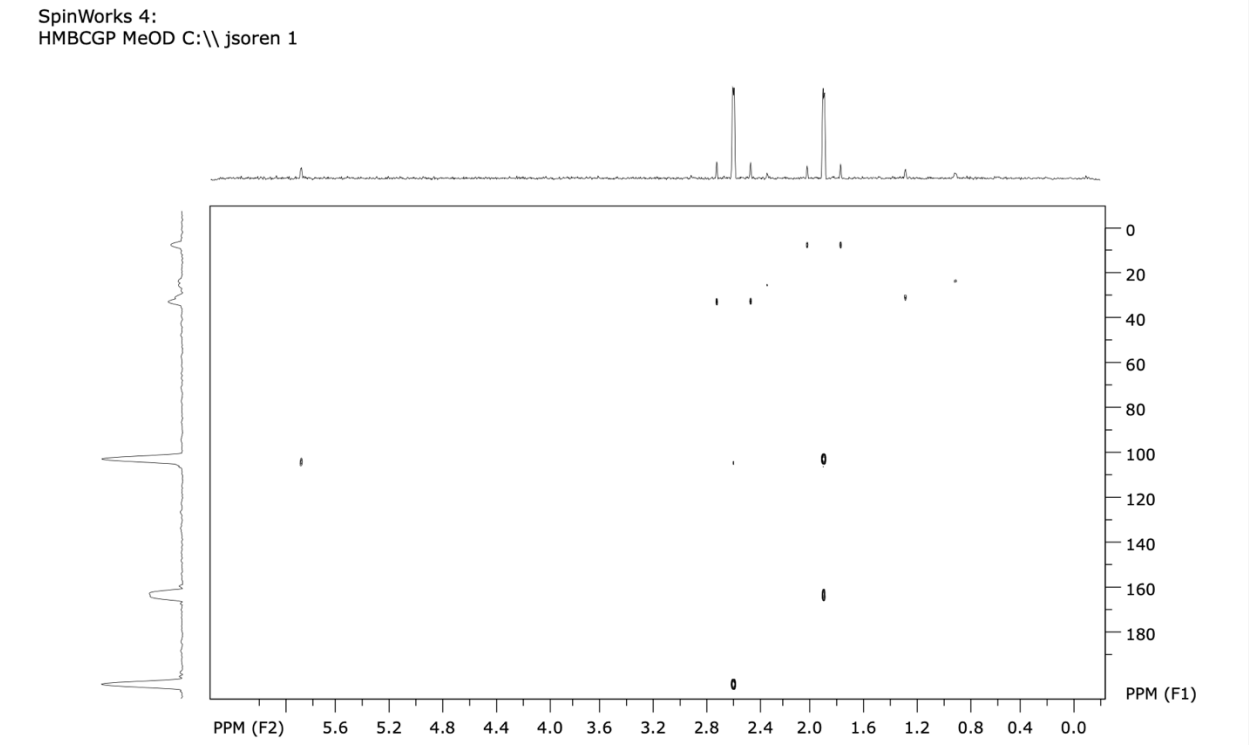

Figure S 4. HMBC spectrum of methyl-phloroacetophenol (MPA) (CD3OD, 500 MHz)

No	δ_H (mult, J in Hz)	δ_c (type)	HSQC	HMBC
1		95.58 (C-C=O)		
2		162.56 (C=C)		
3		104.34 (C=C-CH3)		
4		164.96(C=C)		
5	5.93	(95.58)	95.23	104.14, 162.93
6		165.66 (C=C)		
7		205.48 (C=O)		
8	2.63	33.6 (CH3 – C=O)	33.47	104.5, 204.41
9	1.94	8.11 (-CH3)	8.01	104.14, 162.57

Table S 2. HMBC and HSQC spectrum of MPA

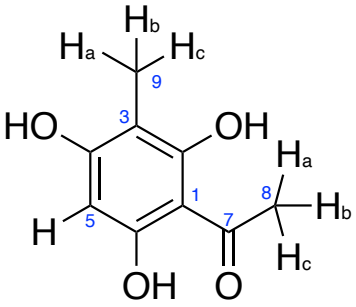

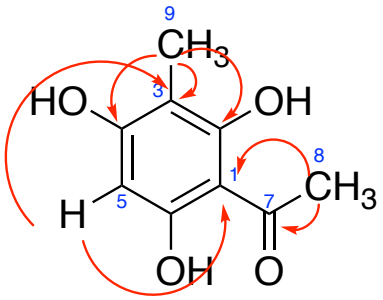

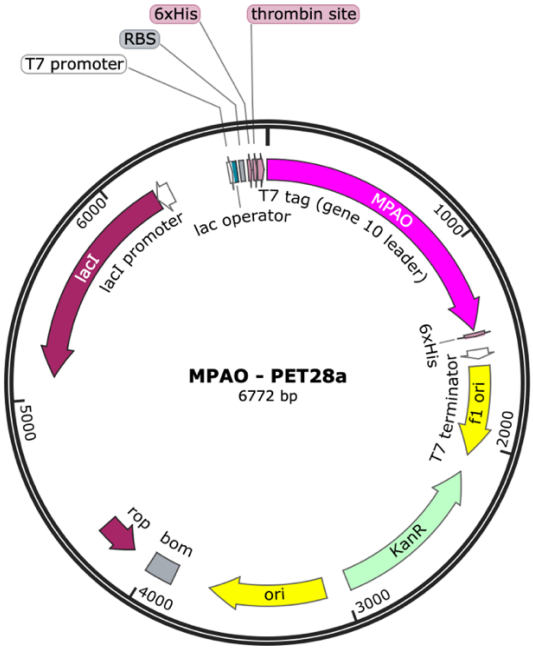

Figure S 5. Map of the Cytochrome P450-MPAO gene in pET28a (+) vector plasmid visualized using SnapGene software.

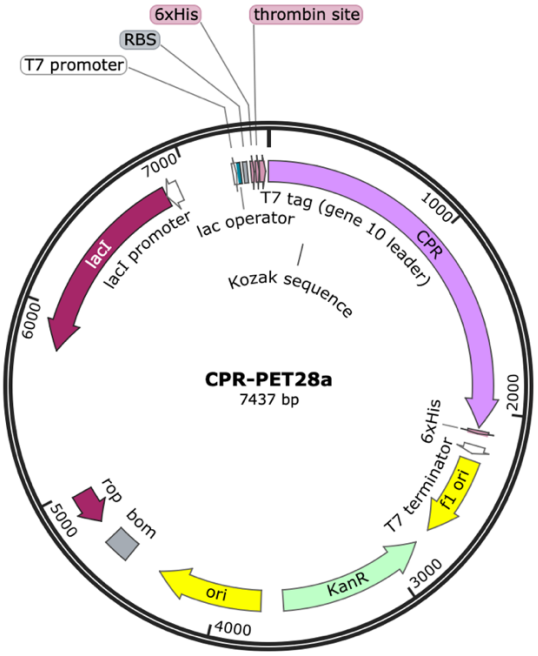

Figure S 6. Map of the Cytochrome P450-CPR357 gene in pET28a (+) vector plasmid visualized using SnapGene software.

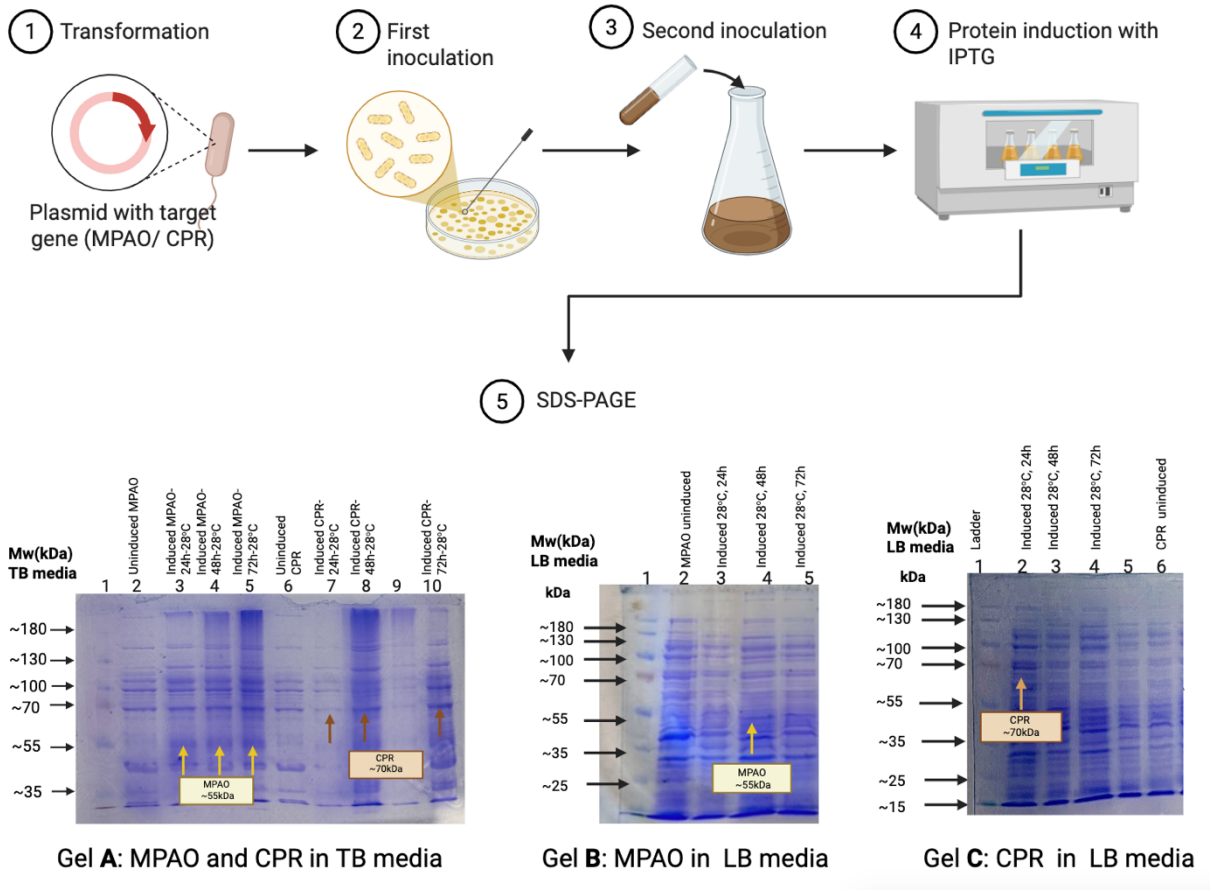

Figure S 7. Illustration of work-flow heterologous expression of CYP-MPAO and CPR357 in TB media compared with heterologous expression of CYP-MPAO and CPR357 in LB media.

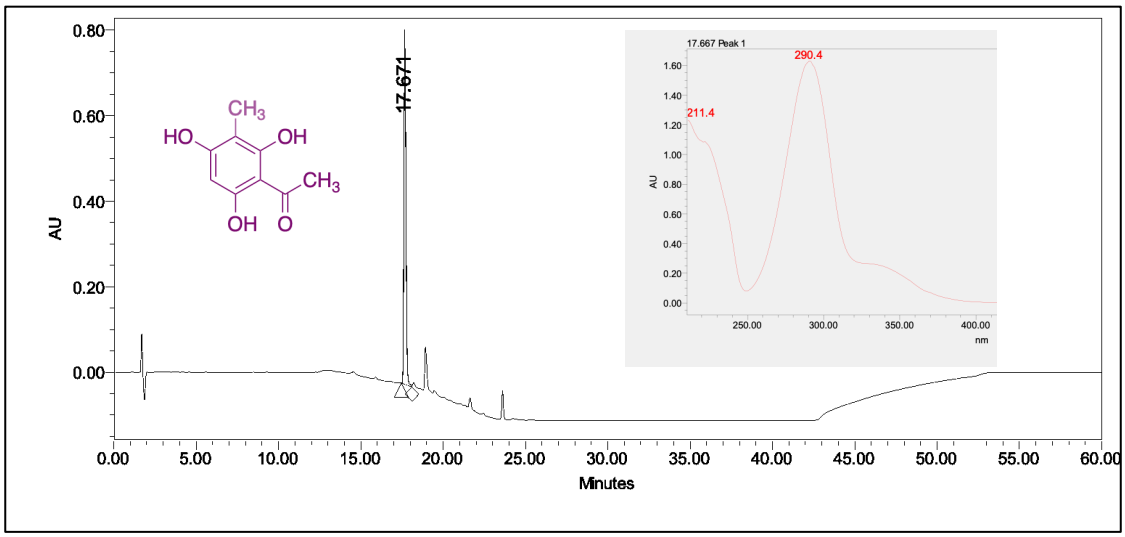

Figure S 8. HPLC chromatogram of MPA showing the UV trace (211.4 and 290.4 nm) and retention time of the major substrate peak.

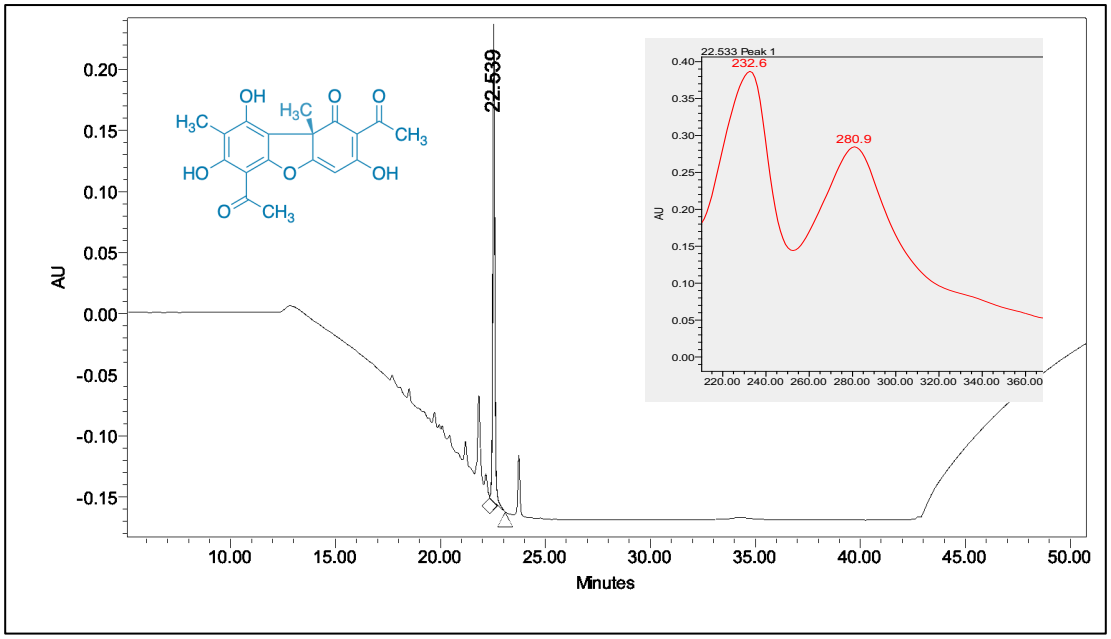

Figure S 9. HPLC chromatogram of usnic acid showing the UV trace (232.6 and 280.9 nm) and retention time of the major substrate peak.

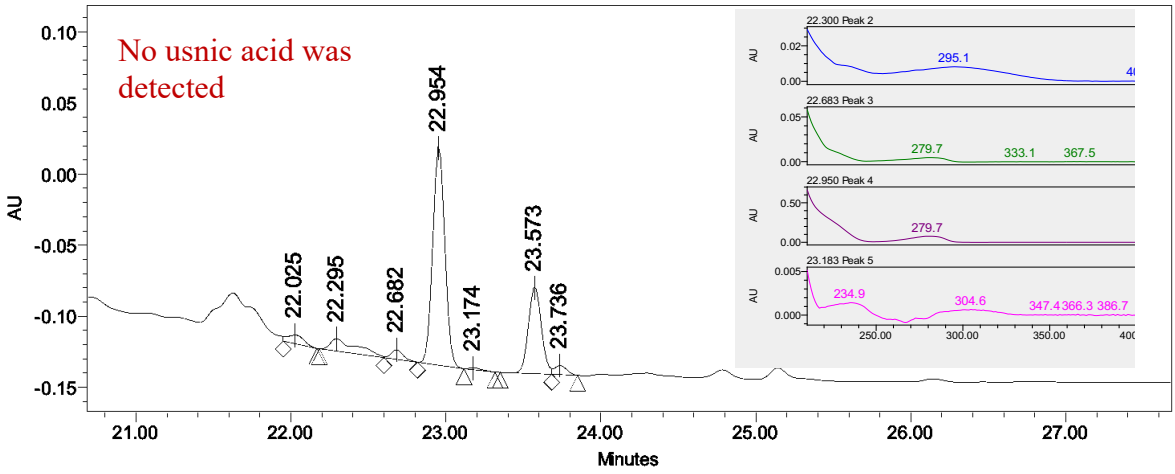

Figure S 10. HPLC chromatogram of bioconversion (1)

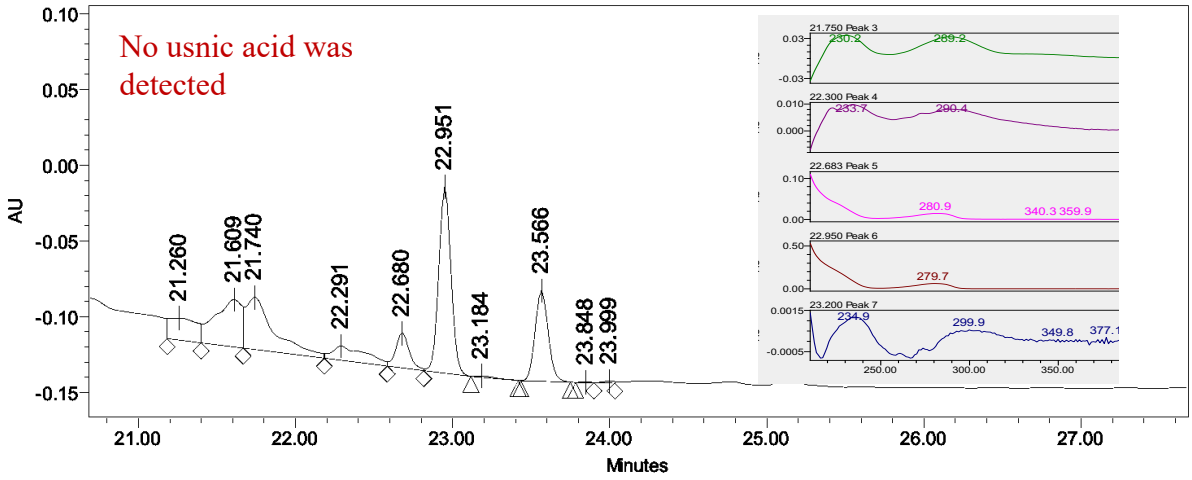

Figure S 11. HPLC chromatogram of bioconversion (2)

Chapter 4

(A) pBLAST ADM79460.1 from *C.grayi*

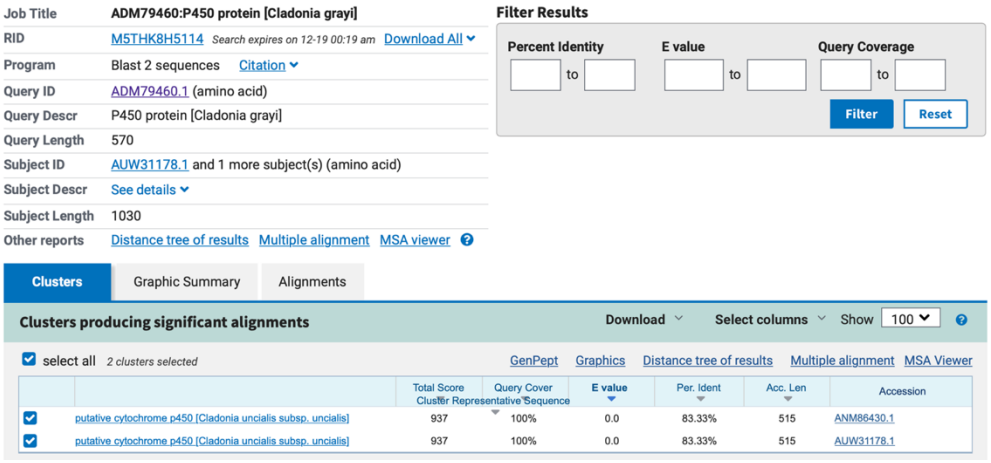

(B) pBLAST CYP682BG2 from *Pseudevernia furfuracea*

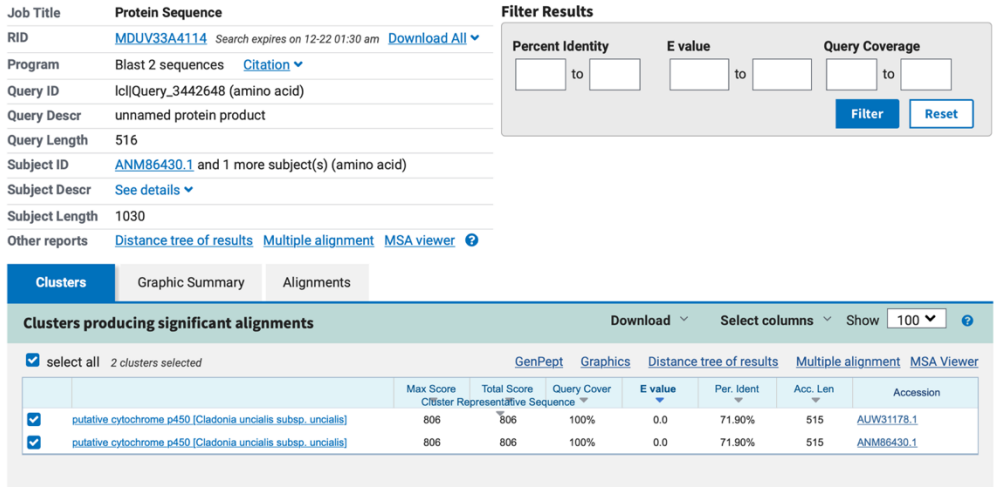

(C) pBLAST QPI71217.1 from *Ovatospora brasiliensis*

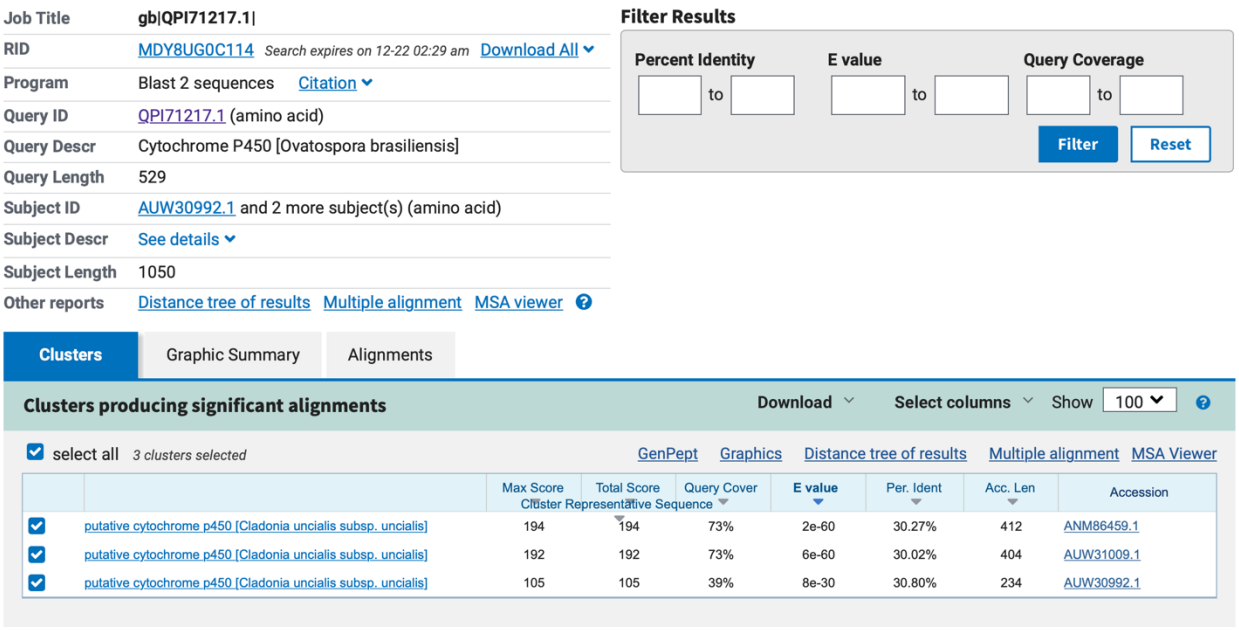

Figure S 12. BLASTp amino acid sequence alignment and similarity analysis of (A) *C. uncialis* CYP amino acid sequences with *C. grayi* CYP; (B) *C. uncialis* CYP amino acid sequences with CYP682BG2 from *P. furfuracea;* (C) *C. uncialis* CYP amino acid sequences with QPI71217.1 *from Ovatospora brasiliensis*

Table S 3. Name, accession numbers, and amino acid sequences used in phylogenetic analysis

Name & Accession number	**Sequence**
CYP682BG2_*Pseudevernia_furfuracea*	MLGLLKIGIFTILWLPLVAVGFYALALAVYRLFLSPLAKFP GPKLAALTRKYEFYYEAIENYEYLWKIKQMHEKYGPIIRI SPHELHVGDVEFFDRLNSFQGKWNKDPYTAHQFANPGSI VGTLDHDIHRKRRAAILPFFSKQKIYALEPVITSMVDKFCD RVEEYRKSGEVMPLRNGFHCFAADVIADYCFAESGGLLD KPGFALSNMQQHKHGLKSGLRARYFPSWYMPVVRGAPE WITQSVDPAAKHFEVWHREVDGPVRRMEERKNDDFFKK AGHRTIFHEVINSPHLPPEEKQTIRVIQEAGAMVGAGGEST TQALITMAYCLIASPEKLARLRDELRTIMPNAKSPLPSLRQ LEQLPYLTGCVKEGLRRLRTGKIARHQRLPRDRPLYYKE WEIPAGTIISMTPIFHQVDPDVFPSPHAFLPERWIDIEEEQR FRMEHHFMPYSKGSRQCAGLSLANAELYMCIPALMTRFD FDLFETDEWDVDMAVDSHHHSPRADTQGVRVFAKASTF
ADM79460.1_P450_[*Cladonia_grayi*]	MLGVIQYSILTIFWLPIAAALYGAGLAIYRLFLSPLAKFPGP KLAALTRKYESYYEAYQNYEYYWKIKELHKQYGELFTPL TASFRGPIVRVNPHELHIDDKDFYYKLNSFQGAWNKDPY TAHQFANPGSIVGTIDHDIHRKRRAAIMPFFSKQKIYALES VIQGMVDKLCYRIEEYGKTGQPVNLRNASKCFAADVVGE YCFAESGGLDKPDFAIEEMNQQQQGLKAGLRARYLPSW WMPVVRGAPAWIRASIDPAAKHFEVWHRVSDSLFVRLY DARKGPVGRMEKRKNDEFYEKAGHRTIFHELINSPHLPPE EKGTGRIIQEAGAMVGAGGESTSQVITAFVYCLLANPQVL SRLREELRSVIPNADSPAPTLRQLEALPYLVGPLLSTYKYV GYLLTLVARLRTGKIARHQRVPRDRPLYFNEWEIPAGVSH EDNIPMASTBTAQTICSMTPIFLQIDPEVYPNPHAFMPERW LNLDEQRQRLEHNLVPYSKGTRGCAGLTLANAELYMLIP ALVTRFDLELFDSDAWDTEMAVDSHHHSPRPDSKGVKVF VKKSTF
QPI71217.1_P450_[*Ovatospora_brasiliensis]*	MGDNTNHHHTIFVNGTEKPGFEPLETLLPTSIWSTAAWAS LLPFLYYGLYAIYSLYFHPLAKFPGPKLASVSRLPFAISAV RGRTYEWLDDLHTRYGPVVRIAPGELTTISPKAWEDVYL RRPQMPKDPHSQTPPLNGADSLFTAEGHTHARMRRTFAN GFSERALREQVEVIESYGELYLQRVRRERAKAPNGELDM RKYYGYASLDVIADLTYGESFHGLENDNEHDWVMGFFL GAKFGAIRNSLSYFYPMDRLFGLLFLRLTAKNRIRNWKHT AERIDKRLTMAAGGIERSDFMTPVIGNVNEGRERGITRNE LNTNSLAMVIAGCQLTTVALSTATYLLLKNPETYRRLREE IRSGFSEEKAIGVDSTQALPYLSAVVKEALRIHHPTPIHLPR IVAPEGQMIDGQWVPGNTIIGMALQTAQTSPVYWVDPLG FHPERFLPQGHKYYDPQFEADNKEAFHPFSVGSRNCLGK

	KVFQAEAALILAKTIYAFDLELSDKTDKDWMNQSAYLVF EPKPIYVNLTERSI
ANM86499.1_P450 *_[Cladonia_uncialis _subsp._uncialis]*	MISLLSERLTWPLVAALALFAGGLTASYFLFLKPVYNIFFH PLKIYPGPKLWAASELPWGFAWMSGKLHLRLMELHDKY GAVVRVGPNELSYGVPEAWEDIFGRYKPGVRQENPKPSW YCSPDHHDIVGAALGDHGRMRRLLHQGFTNSAMLEQEPL IRGHVDLFIQRLHERSDDGKAVIDMFQWFVYCTFDIIGDL SFGEPFGCLRESAMHPWITWVFANIHLTHVFLLCKRNPFF YIFMPVMATVELFKEYEEHQKTLKAVCDKRMALETGRPD FMQVMMSKKGSLYLTPEEIYSNATLLTMGGSETTSNTLS GLAYILAINSVVKKKITDELRATFTREDEINMRSTAKLPYL VAVIEELMRYFPPGPNSMPRITPPEGNSILGKWVPGNTVL GIPHRVMYRSERNFKRANEFIPERWLNEGEDSEFASDRRD GFHPFSYGPRECLAQNLAYAEMRFILSRLVWNFDIEIDEQS REWIDHQRAYLIWEKPALFVHLKAKEKV
ANM86352.1_P450 *_[Cladonia_uncialis _subsp._uncialis]*	MVGGSITRQTASVALASPLLIVAVCFVLVLLVLLGRAFYN VYLHPLRAYPGPKLWAATSFFWIYYRVTGQLVWKSVEL HRNYGNVVRVAPDHLSYTTETAWKTIYGHRSVELQKNV LAGFSRPGLKDVHGILSADRANHTRLRRVLAPAFSEKAV KEQDNCVMKYVNLLIQKLATRSVEGPVDMNQYFTWTTI DLIGDMMFGQPEGALEREYEGSWVNYLIGAIQSQVWLQA LDSYGLGQWQKYFLPKAKANAVLDNFRITSTKIDRRLAN STNDHNDVFSYILPPDDEKGMSVMEMKLNSAIIIGAGTGT TTTWLSTIVHNLTCNPDAYQKLASEIRHAFANGDEITSESV TQLSYLAAVLQESLRMHSPSPSSLGRFVPDGGDVIDGRFV PAGITVGVHQHAAYHLASNFHRPDDFCPERWLPSARDEN SPFAGDRLGVVQPFSYGPRTCLGIKLTHAETRIIVAKLFWH FDLELLPEFKDWQTSQKGTVAWHRTPLKCRLTLIRRD
AUW31009.1_P450 *_[Cladonia_uncialis _subsp._uncialis]*	MDNSSQNQDRTATLWATSAYSSRGAFALLFIGAIVLRFTF YVVYNLFFHPLAKFPGPLLARASLSGRFHRVIEQQHSRYG PVFRVSPNELSFASATSWKSIYGHPPKGKSTLIKSEFYDMY GSGYDSLCIGSERDPQNHARMKKSLSPAFSTKALMEQEEII QRCVDGFVEKIGHESKRETGINVSDWYEMIAFDILGEMAF GETFHCVENEEPHFWIELLTKHLFFITLIDNLRRVSLLFSIG RFLLPRFTVGVRDKHSGYSRAKVDRRLQSVSPRKDILTNV VDKVKGGEVSQEELTAHASTLVIAGGETISTFLAATTFYL CKTPSAYHKLQNEIRNRYQSYQDIDAASALQLPYLQAVIQ EGLRIFPPGSQGFPRTSPGVMIDNYWIPAGVSIIDPLISS
KAK0508818.1_hyp othetical_protein*_[C ladonia_borealis]*	MLGIIQYSLLTIFWLPIAAAALYGAGLAIYRLFLSPLAKFP GPKLAALTRKYESYYEAYQNYEYLWKIKELHKQYGPIVR INPHEIHIDDSDFYYKLNNFQGTWNKDPFTAHQFANPGSI VGTIDHDIHRRRRAAIMPFFSKQKIYALESVIQGMVDKLC DRLQEYGKTGQPVNLRNASKCFAADVVGEYCFAESGGLI DKPDFALENWTEHQQGLKAGLRARYLPSWWMPVVRGA PGWIRASIDPAAKHFEVWHRTVEGPVGRMEEKNNEFYEK AGHRTIFHELINSPHIPPEEKGTIRIIQEAGAMVGAGGESTS

	QVITAFVYCLLANPQVLSRLREELRSVIPTADSPAPSLRQL EALPYLTGCVKEALRLRTGKIARHQRVPRDRPLYFKEWEI PAGTICSMTPIFLQIDPEVYPNPFAFMPERWMNLDEPQRQ RLEHNFVPYSKGTRGCAGLTLANAELYMLIPALVTRLDLE LFDSDAWDTEMAVDAHHHSPRPDSKGVKVFVKKSTY
ANM86450.1_putative_demethylase_*[Cladonia_uncialis_subsp._uncialis]*	MPLVQDSVMAASALQENAPTMLSLALVVFLMPILYRLYF HPLSHVPGPLIGRVTSLYIYAICYMGIEGRVLRQHHQKYN TKVLRVAPNSVSISDSTAVRDIYVTGGGFQKDFRYINFNL GDVISIFSALDTEYRDVRAKAVAPLFAPARLRLASERNGVI GACVAEFVKQFQVLRTSALAQSTGAVRADILDLCARLSID VVTGYLLHGSYGGLREHAGLSIEARQRTKLSANPFIFAIV AFSRFSLLPNWLFRLVYAISSHISSNDNVAKAFARLDRFTD QIVKTACTDPSRAEDTFHGRLLNADMSPAEVVAQSKAIIF AGADSTAVMLATTLFHLVQNVDARSRLRHEIRGLDRHGA MDSQALPYLRAVVKEGLRLGMANPTRFTRVVPRNGLCV GTVHIPPGTVVGCAPYLLHHDPEVFPDPFKFRPERWLEDG QDNGLRRSNMESSLIPFGVGPRACIGKNLAQQQMYESITA VVDSGVLEGTRTCQQRIEIIEWFNGEIKGHKLEIEWSAGY
AUW30992.1_P450_*[Cladonia_uncialis_subsp._uncialis]*	MTVAPGPIQKAIADTKINERYAIDLVQKRIGRKTNRKDFM TRILSCRDEDSIPDVQIAAHASDFVLAGSETTATALSCIVY YLCHTPRALERVKKEICNGFAKYQDINAATTSNLEYLNA VILEGLRIYPPLPFALPRIVPDRGDTVDGHWLPAKVRHVIT SHKRAIDLIGSQTVVSTNPYAACLDSKNFERPYQFEPERW LMRNEKDIIDASQPFSLGSRGCLGQRYAYFPLA
KAK0508896.1_hypothetical_protein_[*Cladonia_borealis]*	MILPVSSILTSIWDNSKMLFEHTSVLSIVLIGVACAISIRSIS YRLRLAYSTPLRHVPGPWYAKFTALGLRANDVAGNRWY YVQGLHKKYGSIVRIAPEEVAISDPQVVSKVHALGTEFRK RQQPGTPFNIFSISDPKAHRTRQRFYAKAFSDETLKASTEP AVRQLIKTAVASIKRDATLRKDHVADVYKWCMLFGSDV AFQVIYGNSNTDGLMATQKTTDEVIMGAYLQRMNAWAQ FCFPVFLLGRWLSPLSSSLHNIFRVEEKYGDFWQEGERQR EIAARTVFVQNTKYSKNDGVFSVSDEVKLSDVDIAHDITT FLGAGGEPVGASLVFLIWQVLRMPDLQSELEAEVAGLTEP ITNATTAQLPILNAVIYETLRLYGGGVTQMPRYAPIATDL GGYVIPPGTAVTTHTGALHRNPAAWDDPEKFDYTRWLSP SQNKTLVQDKFQPFSSGARACIAIHLVMIELRVFASVFFRE CAGAKLAPSTTDASMRILDRFHISPNAKRCEVIVPDEKA
AUW31162.1_P450_*[Cladonia_uncialis_subsp._uncialis]*	MASLTIIGFAFLLLLLFYKYVLFPAFLSPLSKIPNAHFTAPF ASLWISSKRRASAGTRAIFSLHQKYGPILRLGPNELSVCTP AALKTIYIGGFEKDGWYQDAFMNYGRPNMVSMLEHKPH SVQKRMISNLYSKSYLQSSEDLQIASTHLMFDRFMPIMQS VADKGVEMDVLDFFQGVGMDLTSAYLFGLSNGTDFMHD VQYRQHWLAQYSVFKDQLPQERAGGEVERWCLAMCEA AEEFLHSGKADNGSPATQPVVYGRLSQSLAVSSTKPDYTS RLMTTASEMLDHLIAGHETSGITLTYFMHELSKRPALQDS LRSELLTLDPPIRFSLNESPSNGKNRCLPTPRSIDSLPILDSM

	LQETLRLYAAAPAIQPRRTPFSPGGTTIEGYSNIPGGVRVS ANAYTLHRNPKVFPEPLKWIPERWMDATKGNREEMKRW FWAFGSGGRMCLGSNFAIQDMKLIIAAIYTNYATEIVDDE GIEQADTYISRPIADKLILRFKHA
KAK0513963.1_hypothetical_protein_*[Cladonia_borealis]*	MDHGPGRAPLLLLMVGIIVYALRSMFTIGKRGRRLPPGPS TIPVLGNEHQIPAADGHFLLTEWSRKYGGIFSLKRFTNTTL VISDRKLIKNLLDKKSNIFSNRPVSIVAELITQGDHLLIMDY GDTWRKIRKVVHQYFMEPMCEKQHIHVQHAEAIQMVHD FLVDPENHMEHPKRYSNSITNALVFGIRTKTTDSDYMSRL FALMDKWSLVMELGATPPVDSFPLLKWVPQRLLGNWRT RAKEVGVMMKSLYSEVLHQVEERRERGINRDSFMDRVL DQQEKNQLSRNELYFLGGVLMEGGSDTSSSLILAIILAMIA YPQVQDRAQAEIDAVIGDNRSPEWSDFSKLPYINMIIKESH RWRPVSPLGVAHALAEDYEVDGMLLPKGSTVVLNVWA MHHDERTWKDPQHFIPERFESYPGLASSYAASGEWDKRD HFGYGAGRRICPGIHLAERNLFIGVAKLLWAFRFGAKEGA DINTSAETGLSQGFLHCVKEYGSSITLRSEAKRETIFREFEE ARTIFARYE
ANM86505.1_P450_[*Cladonia_uncialis_subsp._uncialis]*	MMSISPHQVISAFDEVPTVGHCLVACITITSVLYGLYQWL LPNPVPGIAFNLEATKSLFGDAPGMIKEVSVTGEFRVWCA KQVKKMDSPICQVFIRPFSKPWILLADFRESKDVLMRRKE FDKSSFLSDGMECMGSFHGIYPTGDKFKWNRQLIQDLMT TSFLNNHVGPAVYSKGLDVMKLFEMKMNLAKGRPFSVK KDFEYASLDVMIEFAFGKNWVHTATGPQVELLSKLGASE VKFDALDQPVSFPIAPIMDFLESVYEAPEIVEKTINAIMPKL QTWWWSKQSWYKKIFDEKERIMKEQVAIAVNNYRSGHV KTGIEHMLMREGARAEKEGREPDFGSEVFRDEMFGDIVG GHHTTSGAMMWLAKYLTDWPQIQSKLRLVLYETLSTAK EENRLFTFEEIRRAKLPYLDAVIEEMLRINAVTVTREALCD TTILGCPIKKGTQIFFVSNGPGFLSPSIPTDDSKRSETSRAA KLNDKWDETHDLTLFDPERWLVRKNNGEGLLEDDVDFD GAAGPQLAFGLGPRACWGRRLAHMETKTLIAMLVWNFR LLETPPALSSHAGFEGIARVPQQCYLRLSKI
ANM86718.1_P450_*[Cladonia_uncialis_subsp._uncialis]*	MSQSQVRNERNAIAYLSLSVDYKPTMALIDKIINPCLQRK LNLVQANVFDEIRASVDDTFGLDENSWHELRLHGSLQTII NRAGTRAFFGLPLSRNHEYLYSLKRFILAMGAGTLIVGQL PLWLVRPLAASVINIPLRYYKAKLLKTLLPIFAERIQYIQR HEAGYTLEDESGDFATQILKVVSNTKDGTYNRGPDYLAE QNLLLSFAALSSTAAAATNLLLDILSSAPEINAYDTLRSEA ASTFTAEQAWGDAASLQNLTCTDSAIREGLRRNSLQIRGL LREVMSQNGITLPDGTHIARGTWVGIPFQAVHTDERFYAK PEMFDPFRFARMRTDPALEGERFDATQTSDKFLAFSYGRH ACPGRWLVAQILKLLIAYITLHYDIQPLEQRPLNTIFGDTNI PSMSATIRVRRRKCA

ANM86696.1_P450_[*Cladonia_uncialis_subsp._uncialis]*	MTHVTEFVLRICLFGAVLLVLRSIYQYITIALPRNKLIQQY GCKDAPRYPQKDPFFGLDTIRDGIRAVKTNCYLAQVEHQ YKEYGNTFSFRFGTSAIINTNEPENIKTVLVTKSKDYGIGW RRKYAFSPLLGSSIILTDGAQWEHSRALLRPSFTRDQINDL STFEVHVARLIQAIPRDRSTVDLAGLFYRLTADVTTDVFF GESIQSLIEPKEEVMKALHDSLEGGELRYLFGGIYSVIPQR RFYAAIKEVHDWIDGYVDRAMSKHASLAKKNVEKPSIEV PAKDSERHVFLRELCKTTDDRDLIRDEILSAFVGGRDTTA GLLGNLFFMLARKPDLWKRLRSEVEYLGGKAPTVGQLRS LSLVRSCVKECKYSIFPTATRGHMSLPFQFEPRSHHCASPA LRLHPASPTNARTAYQDTILPLGGGLDGNSPIFVPAGTSIS WHVSALHRRKDLWGEDADEFRTERWEHEREGWVSLSLA RAS
ANM86704.1_P450_*[Cladonia_uncialis_subsp._uncialis]*	MNIAALVGSFHDATLAQLLRPALGFVLLTWLAVATYYLH FHPLARIPGPKIWILSRLPYILVLRKGRLAVRLKELHDAYG SVVRVAANEVSFIDEKAWTDIYAYHQHYPLPKNPYWYR MRPNKAYGIMASPNADHGRFRRTYAPVFTEKAVREQEPL ILRHIETLIDQLKIEASKKAPTNIVNWFEYIAFDIVGDLSYS HSFDCLRKNDNRYQITIVQGSMKGFTLDASLRLLGVEKV KQLYIPMISPKKQEKYYKTLNYWTQQRLAEGERQQGNDL MKYANLRTNKGLTLPETENSIGDMMIAGSETVASTLAAV FYHLTRSPSTYQDLAKDLRGKFNRQTEINITAVSDLPFLNA VINEAMRLCPSLPMVMPRIVPEPGAHICGYWFPAGTQVSF CQLAAYSSPKNFSFPERFIPSRWLPTSTMKLHNAGVFHPFS VGQRNCIGKEFGLAEVRLILAKLLWSFDITAGEKDWDWN SQKTYHVWEKRPLFVNISPRGL
UZP47922.1_P450_[*Cladonia_uncialis_subsp._uncialis]*	MPLSNIFVEAIQHNIGLQITVTLCVLLAYPTVQVIYNLYFH PLSKFPGPKLWAASRLPFVFNLLTGKLVKRERQFHEKYGE IIRLAPDEVSFASEQAWNDIYAFRRGHKRAGRDKAYYIAP NDMADNLITTNDVKFHARVRKLLSNSFTEQSLHTQHPLIE GHADLLVAKLHALATKSENMNSGALVNMTDWLNFFTM DVIGDLAFGESFGCLRTGEYHTWVRTLFSYSKGMSLAAA PRYYPSVEFLFQKLIPKSVIEGQRQHTQYANKMINRRLEL KTDRPDFMTPFMKNNLNFENMSRDEILSTFNFIIVGGSETT ATTLTGIFNHLSRNERLLQRLCTEIRTKFKKETDITIDKIDH LPYLEAVLNEGLRMCNPIPGGLPRVVPEGGDTYAGVYLP GVDHPQGRSNLMALTDKFVPERWLPQGERPSIYDHDQLS ASKPFSVGFHSCLGRPLAWVELRLVLTRLLWAFDFIEEPA ERVDFDDFPVIMLIQKEAVKMRVKVRNGIEYKSVLKHAG LGGQGQYN
ANM86459.1_P450_*[Cladonia_uncialis_subsp._uncialis]*	MDNSSQNQDRTATLWATSAYSSRGAFALLFIGAIVLRFTF YVVYNLFFHPLAKFPGPLLARASLLWRFWFSQSGRFHRVI EQQHSRYGPVFRVSPNELSFASATSWKSIYGHPPKGKSTLI KSEFYDMYGSGYDSLCIGSERDPQNHARMKKSLSPAFST KALMEQEEIIQRCVDGFVEKIGHESKRETGINVSDWYEMI AFDILGEMAFGETFHCVENEEPHFWIELLTKHLFFITLIDN

	LRRVSLLFSIGRFLLPRFTVGVRDKHSGYSRAKVDRRLQS VSPRKDILTNVVDKVKGGEVSQEELTAHASTLVIAGGETI STFLAATTFYLCKTPSAYHKLQNEIRNRYQSYQDIDAASA LQLPYLQAVIQEGLRIFPPGSQGFPRTSPGVMIDNYWIPAG VSIIDPLISS
ANM86598.1_P450 *_[Cladonia_uncialis _subsp._uncialis]*	MVHQALNTLTISDPKEHGRRRRVVSQGFSDSAMWNYEPS MVALVHRFCDRLLQPVEEEPASNSDLWGPARNMSQWCN YLAFDIMADLIFGGKYNLLERETYRYVPSVIEASNVRVSAI LQAPGLKFGRLDKILFPKAVVARDVFIRFVGKLLRDTLKV DRSNKRDFFAVLSTAKDPQTGSGFTEEEIIAESTTLIVAGA DTVATATTALFFYLSRNPAAYERAANEIRNTFQTVNEIHM GPKLNSCKYLRACVDETMRMSPSVGSSLAREVQQGGAIV DGEYIPAGCDVGVPIYSIQHSAEYFSTPFSFSPERWLLGEG DTTQESLSLASSAYVPFSSGPRGCIGKGMALTEMMLTMA MVLWRLDFKIAEGDSAGGSPDAEWGRHRPDEFQLKDHV TAARNGPLLHFQERKISRRL
ANM86447.1_P450 *_[Cladonia_uncialis _subsp._uncialis]*	MPYTKQGALPAVFNTRDEKLHKQLKSPIAPLFSLSNAVTF ESFIDEVLEVLCRQIDQRYIESQELVDLGNWLQYFAFDVM GTMTFSNRYGFLEQGQDVGGMLETIWQYMRTTAPVTQIP WYDEWWNKNPWIAMWRQPFGFSILKIVGDNIRRRVTEK DSRGAESTNQLNDKDMLSRFMEIQSTNESVPPWSVTAWT FSNVIAGSDSTAVILRCVWYNLLAHPATLDRLHAELLAAE QSHAITRPFPKWSEVRELPYLDACINEAVRLHPPFCLPFER VVPEGGVEICGRFFKGGTIVGMNPYVANRHRRTWGEDA NEWRPERWLGLGEEEHRTLEQSVLTFGAGRRVCLGKNIA MLEMKKLVPALVLAYKIELVDPAAFTVENSWFFRQKGLG VRIRRHTEAE
ANM86430.1_P450 *_[Cladonia_uncialis _subsp._uncialis]*	MLGVLQYSILTIFWLPIAAAALYGAGLAIYRLYLSPLAKFP GPKLAALTRKYESYYEVYQNYEYLWKIKELHKQYGPIIRI SPHEIHIDDKDFYYKLNSFQGTWNKDPFTAHQFANPGSIV GTIDNDIHRKRRAAIMPFFSKQKIYALESVIQGMVDKLCY RLEEYGKTGQPVNLRNASKCFAADVVGEYCFAESGGLID KPDFAIENWTQHNQGLKAGLRARYLPSWWMPVVQGAPG WIRASIDPAAKHFEVWHREVEGPVGRMEKRKNDEFYEK AGHRTIFHELINSPQLPSEEKGTIRIIQEAGAMVGAGGESTS QVITAFVYCLLANPQVLSRLREELRSVIPTADSPAPTLRQL EALPYLTGCVKEALRLRTGKIARHQRVPRDRPLYFKEWEI PAGTICSMTPIFLQIDPEVYPNPHAFMPERWLNLDEPQRQR LEHNLVPYSKGTRGCAGLTLANAELYMLIPALVTRLDLEL FDSDAWDTEMAVDAHRHSPRPDSKGVKVFVKKSTF
AUW30968.1_P450 *_[Cladonia_uncialis _subsp._uncialis]*	MNIAALVGSFHDATLAQLLRPALGFVLLTWLAVATYYLH FHPLARIPGPKIWILSRLPYILVLRKGRLAVRLKELHDAYG SVVRVAANEVSFIDEKAWTDIYAYHQHYPLPKNPYWYR MRPNKAYGIMASPNADHGRFRRTYAPVFTEKAVREQEPL ILRHIETLIDQLKIEASKKAPTNIVNWFEYIAFDIVGDLSYS HSFDCLRKNDNRYQITIVQGSMKGFTLDASLRLLGVEKV

	KQLYIPMISPKKQEKYYKTLNYWTQQRLAEGERQQGNDL MKYANLRTNKGLTLPETENSIGDMMIAGSETVASTLAAV FYHLTRSPSTYQDLAKDLRGKFNRQTEINITAVSDLPFLNA VINEAMRLCPSLPMVMPRIVPEPGAHICGYWFPAGTQVSF CQLAAYSSPKNFSFPERFIPSRWLPTSTMKLHNAGVFHPFS VGQRNCIGKEFGLAEVRLILAKLLWSFDITAGEKDWDWN SQKTYHVWEKRPLFVNISPRGL
AUW31214.1_P450 *_[Cladonia_uncialis _subsp._uncialis]*	MVGGSITRQTASVALASPLLIVAVCFVLVLLVLLGRAFYN VYLHPLRAYPGPKLWAATSFFWIYYRVTGQLVWKSVEL HRNYGNVVRVAPDHLSYTTETAWKTIYGHRSVELQKNV LAGFSRPGLKDVHGILSADRANHTRLRRVLAPAFSEKAV KEQDNCVMKYVNLLIQKLATRSVEGPVDMNQYFTWTTI DLIGDMMFGQPEGALEREYEGSWVNYLIGAIQSQVWLQA LDSYGLGQWQKYFLPKAKANAVLDNFRITSTKIDRRLAN STNDHNDVFSYILPPDDEKGMSVMEMKLNSAIIIGAGTGT TTTWLSTIVHNLTCNPDAYQKLASEIRHAFANGDEITSESV TQLSYLAAVLQESLRMHSPSPSSLGRFVPDGGDVIDGRFV PAGITVGVHQHAAYHLASNFHRPDDFCPERWLPSARDEN SPFAGDRLGVVQPFSYGPRTCLGIKLTHAETRIIVAKLFWH FDLELLPEFKDWQTSQKGTVAWHRTPLKCRLTLIRRD
AUW31409.1_P450 *_[Cladonia_uncialis _subsp._uncialis]*	MISLLSERLTWPLVAALALFAGGLTASYFLFLKPVYNIFFH PLKIYPGPKLWAASELPWGFAWMSGKLHLRLMELHDKY GAVVRVGPNELSYGVPEAWEDIFGRYKPGVRQENPKPSW YCSPDHHDIVGAALGDHGRMRRLLHQGFTNSAMLEQEPL IRGHVDLFIQRLHERSDDGKAVIDMFQWFVYCTFDIIGDL SFGEPFGCLRESAMHPWITWVFANIHLTHVFLLCKRNPFF YIFMPVMATVELFKEYEEHQKTLKAVCDKRMALETGRPD FMQVMMSKKGSLYLTPEEIYSNATLLTMGGSETTSNTLS GLAYILAINSVVKKKITDELRATFTREDEINMRSTAKLPYL VAVIEELMRYFPPGPNSMPRITPPEGNSILGKWVPGNTVL GIPHRVMYRSERNFKRANEFIPERWLNEGEDSEFASDRRD GFHPFSYGPRECLAQNLAYAEMRFILSRLVWNFDIEIDEQS REWIDHQRAYLIWEKPALFVHLKAKEKV
AUW31228.1_P450 _[*Cladonia_uncialis _subsp._uncialis]*	MPLVQDSVMAASALQENAPTMLSLALVVFLMPILYRLYF HPLSHVPGPLIGRVTSLYIYAICYMGIEGRVLRQHHQKYN TKVLRVAPNSVSISDSTAVRDIYVTGGGFQKDFRYINFNL GDVISIFSALDTEYRDVRAKAVAPLFAPARLRLASERNGVI GACVAEFVKQFQVLRTSALAQSTGAVRADILDLCARLSID VVTGYLLHGSYGGLREHAGLSIEARQRTKLSANPFIFAIV AFSRFSLLPNWLFRLVYAISSHISSNDNVAKAFARLDRFTD QIVKTACTDPSRAEDTFHGRLLNADMSPAEVVAQSKAIIF AGADSTAVMLATTLFHLVQNVDARSRLRHEIRGLDRHGA MDSQALPYLRAVVKEGLRLGMANPTRFTRVVPRNGLCV GTVHIPPGTVVGCAPYLLHHDPEVFPDPFKFRPERWLEDG QDNGLRRSNMESSLIPFGVGPRACIGKNLAQQQMYESITA VVDSGVLEGTRTCQQRIEIIEWFNGEIKGHKLEIEWSAGY

AUW31051.1_P450 *_[Cladonia_uncialis _subsp._uncialis]*	MISPVSSILASIWDNSKLLLDHTSVLSIALIGVACAISIRSIL YRLRLAYSTPLRHVPGPWYAKFTALGLRANDVAGNRWY YVQGLHKKYGSIVRIAPEEVAISDPKVVSKVHALGTEFRK RQQPGTPFNIFSISDPKAHRTRQRFYAKAFSDETLKASTEP AVRQLIKTAVASIKRDAALRKDHTADVYKWCMLFGSDV AFQVIYGNSNTEGLMATQKTTDEVIMGAYLQRMNAWAQ FCFPVFLLGRWLSPLSPTLHNIFRVEEKYGDFWQEGQRQR EIAARTVFVQNTKYSKNDGVFSVSDEVKLSDVDIAHDITT FLGAGGEPVGASLVFLIWQVLRMPDLQRELEAEVAGLTE PITDATTAQLPILNGVIYETLRLYGGGVTQMPRYAPIATEL GGYVIPPGTAVTTHTGALHRNPAAWDDPEKFDHTRWLSP SQSKTLVQDKFQPFSSGARACIAIHLVMIELRVFVSVFFRE CAGVKLAPSTTDASMRVLDRFHISPNAKRCEVIVPDEKA
ANM86330.1_P450 *_[Cladonia_uncialis _subsp._uncialis]*	MISPVSSILASIWDNSKLLLDHTSVLSIALIGVACAISIRSIL YRLRLAYSTPLRHVPGPWYAKFTALGLRANDVAGNRWY YVQGLHKKYGSIVRIAPEEVAISDPKVVSKVHALGTEFRK RQQPGTPFNIFSISDPKAHRTRQRFYAKAFSDETLKASTEP AVRQLIKTAVASIKRDAALRKDHTADVYKWCMLFGSDV AFQVIYGNSNTEGLMATQKTTDEVIMGAYLQRMNAWAQ FCFPVFLLGRWLSPLSPTLHNIFRVEEKYGDFWQEGQRQR EIAARTVFVQNTKYSKNDGVFSVSDEVKLSDVDIAHDITT FLGAGGEPVGASLVFLIWQVLRMPDLQRELEAEVAGLTE PITDATTAQLPILNGVIYETLRLYGGGVTQMPRYAPIATEL GGYVIPPGTAVTTHTGALHRNPAAWDDPEKFDHTRWLSP SQSKTLVQDKFQPFSSGARACIAIHLVMIELRVFVSVFFRE CAGVKLAPSTTDASMRVLDRFHISPNAKRCEVIVPDEKA
ANM86363.1_putative_demethylase *_[Cladonia_uncialis_subsp._uncialis]*	MLYNICWLGFGFMLALVVIRSLATRYLSSLRKFKGPVLAS FTNAWRLNYVYWHRHETPMSKIHEKYGDIVRLGPNVLAF RQHQAMLDIYGPQGRNFKKSEFYPVNSSTTKGRRNYTLF STHDKPYHDNLRRAVGSAFSVTSVLRYEPFVDSTIGLFLK TVNQRYADKTDAEGVFNFAEWLLYFAFDTIEQLTYGARD DGLIESGRDVSGLLGYLQDFLNYGYLAGQMPVLDKILRH NPILSWLNSWGLFLGTTFPGIPFAIKRIQGKLDRQKIIGTQV EDPATQESLLDRFLRAKQEHPETVTDREVFGLTLSMIFAG SDTTAITLTALFYYLLKNPECYSRLQREVDENFPAFGVKA LEDPVDYTKAQKLLYLHACLQETFRIHPATGFNNERVVD PQGAIICGERIPGGTIVSCSSWVLHRNKETFGEDVDSYRPE RWLGDSEDVKEMNRAMFQFAQGNFSCIGKNISMMEMM KVVPAILRAFHISLADPNMKLKVFNGQNVRILNLNSRQGA DNASREKLVSGGDGSLGTADRTTPLLTLKPSYHSRPLIIAN SSPYGKTPQCARRERKQCRTVTIPQLSPPPQNPSKTHVKH NCIQCSSSLPSPSSSVALPESSMHPFHSLSRTYATSSTIRRSL LANKPPLSLDHFLLRQRVLALYRTIIRACDRIPLPIREEMKE YARVEFERQKDVEDLRKIRYLLSTGKAEFDRLMGQISVKS

AUW31241.1_P450_[*Cladonia_uncialis_subsp._uncialis]*	MLYNICWLGFGFMLALVVIRSLATRYLSSLRKFKGPVLAS FTNAWRLNYVYWHRHETPMSKIHEKYGDIVRLGPNVLAF RQHQAMLDIYGPQGRNFKKSEFYPVNSSTTKGRRNYTLF STHDKPYHDNLRRAVGSAFSVTSVLRYEPFVDSTIGLFLK TVNQRYADKTDAEGVFNFAEWLLYFAFDTIEQLTYGARD DGLIESGRDVSGLLGYLQDFLNYGYLAGQMPVLDKILRH NPILSWLNSWGLFLGTTFPGIPFAIKRIQGKLDRQKIIGTQV EDPATQESLLDRFLRAKQEHPETVTDREVFGLTLSMIFAG SDTTAITLTALFYYLLKNPECYSRLQREVDENFPAFGVKA LEDPVDYTKAQKLLYLHACLQETFRIHPATGFNNERVVD PQGAIICGERIPGGTIVSCSSWVLHRNKETFGEDVDSYRPE RWLGDSEDVKEMNRAMFQFAQGNFSCIGKNISMMEMM KVVPAILRAFHISLADPNMKLKVFNGQNVRILNLNSRQGA DNASREKLVSGGDGSLGTADRTTPLLTLKPSYHSRPLIIAN SSPYGKTPQCARRERKQCRTVTIPQLSPPPQNPSKTHVKH NCIQCSSSLPSPSSSVALPESSMHPFHSLSRTYATSSTIRRSL LANKPPLSLDHFLLRQRVLALYRTIIRACDRIPLPIREEMKE YARVEFERQKDVEDLRKIRYLLSTGKAEFDRLMGQISVKS
ANM86474.1_putative_trichodiene_oxygenase_[*Cladonia_uncialis_subsp._uncialis]*	MATNALVMPKYLRSPFSAGLEQVSGRQVIVAAATIFIAFV ISLALYRAFFSPLSSVPGPLLAGITYYYEAYWEVWLGGQY FKKVAQLHEQYGPIVRITPHEIHWNDPEFIDNVYPGPSRKT NKPVWFAERTGTPHSIVSTIDHDLHRQRRNALNSLFSVAS VRRLEPIMKTYLAKMMARMEQSGKSGEVVQIHHVFKAC ASDIITQYAFGECLNFIDEGDYGRWYFQAIDWFFSLTHVF GLAPGLVHLAQNIPKWSLMIFAPFLKPLRDRQDYWTGRV REIRESLNRDAAKSTIFESIFNSSLPPKEKTDKRLASEAQLL VFAGEGTTAHSLTCCVFHLLDNPDDVQKLRLELSQAKIDP ENVSIAQVDSLPFLGAVIQEAVRLHPGVMARQVRMSPKE PIVYKDPHAQKQYIVPPNTVTSMSPLDIHMHPKAFGADAY EFRPQRWIENPNLRRYFIGFSRGTRNCVGMTLARREMAM TLACIFSKYDVYRGQARPSLELYHTDRKRDVDANSDYIIPI PAKGSKGLQIKIRD
AUW31379.1_putative_trichodiene_oxygenase*_[Cladonia_uncialis_subsp._uncialis]*	MATNALVMPKYLRSPFSAGLEQVSGRQVIVAAATIFIAFV ISLALYRAFFSPLSSVPGPLLAGITYYYEAYWEVWLGGQY FKKVAQLHEQYGPIVRITPHEIHWNDPEFIDNVYPGPSRKT NKPVWFAERTGTPHSIVSTIDHDLHRQRRNALNSLFSVAS VRRLEPIMKTYLAKMMARMEQSGKSGEVVQIHHVFKAC ASDIITQYAFGECLNFIDEGDYGRWYFQAIDWFFSLTHVF GLAPGLVHLAQNIPKWSLMIFAPFLKPLRDRQDYWTGRV REIRESLNRDAAKSTIFESIFNSSLPPKEKTDKRLASEAQLL VFAGEGTTAHSLTCCVFHLLDNPDDVQKLRLELSQAKIDP ENVSIAQVDSLPFLGAVIQEAVRLHPGVMARQVRMSPKE PIVYKDPHAQKQYIVPPNTVTSMSPLDIHMHPKAFGADAY EFRPQRWIENPNLRRYFIGFSRGTRNCVGMTLARREMAM TLACIFSKYDVYRGQARPSLELYHTDRKRDVDANSDYIIPI PAKGSKGLQIKIRD

AUW31178.1_P450 *_[Cladonia_uncialis _subsp._uncialis]*	MLGVLQYSILTIFWLPIAAAALYGAGLAIYRLYLSPLAKFP GPKLAALTRKYESYYEVYQNYEYLWKIKELHKQYGPIIRI SPHEIHIDDKDFYYKLNSFQGTWNKDPFTAHQFANPGSIV GTIDNDIHRKRRAAIMPFFSKQKIYALESVIQGMVDKLCY RLEEYGKTGQPVNLRNASKCFAADVVGEYCFAESGGLID KPDFAIENWTQHNQGLKAGLRARYLPSWWMPVVQGAPG WIRASIDPAAKHFEVWHREVEGPVGRMEKRKNDEFYEK AGHRTIFHELINSPQLPSEEKGTIRIIQEAGAMVGAGGESTS QVITAFVYCLLANPQVLSRLREELRSVIPTADSPAPTLRQL EALPYLTGCVKEALRLRTGKIARHQRVPRDRPLYFKEWEI PAGTICSMTPIFLQIDPEVYPNPHAFMPERWLNLDEPQRQR LEHNLVPYSKGTRGCAGLTLANAELYMLIPALVTRLDLEL FDSDAWDTEMAVDAHRHSPRPDSKGVKVFVKKSTF
AUW31225.1_P450 _[*Cladonia_uncialis _subsp._uncialis]*	MPYTKQGALPAVFNTRDEKLHKQLKSPIAPLFSLSNAVTF ESFIDEVLEVLCRQIDQRYIESQELVDLGNWLQYFAFDVM GTMTFSNRYGFLEQGQDVGGMLETIWQYMRTTAPVTQIP WYDEWWNKNPWIAMWRQPFGFSILKIVGDNIRRRVTEK DSRGAESTNQLNDKDMLSRFMEIQSTNESVPPWSVTAWT FSNVIAGSDSTAVILRCVWYNLLAHPATLDRLHAELLAAE QSHAITRPFPKWSEVRELPYLDACINEAVRLHPPFCLPFER VVPEGGVEICGRFFKGGTIVGMNPYVANRHRRTWGEDA NEWRPERWLGLGEEEHRTLEQSVLTFGAGRRVCLGKNIA MLEMKKLVPALVLAYKIELVDPAAFTVENSWFFRQKGLG VRIRRHTEAE
AUW30749.1_P450 _[*Cladonia_uncialis _subsp._uncialis]*	MVHQALNTLTISDPKEHGRRRRVVSQGFSDSAMWNYEPS MVALVHRFCDRLLQPVEEEPASNSDLWGPARNMSQWCN YLAFDIMADLIFGGKYNLLERETYRYVPSVIEASNVRVSAI LQAPGLKFGRLDKILFPKAVVARDVFIRFVGKLLRDTLKV DRSNKRDFFAVLSTAKDPQTGSGFTEEEIIAESTTLIVAGA DTVATATTALFFYLSRNPAAYERAANEIRNTFQTVNEIHM GPKLNSCKYLRACVDETMRMSPSVGSSLAREVQQGGAIV DGEYIPAGCDVGVPIYSIQHSAEYFSTPFSFSPERWLLGEG DTTQESLSLASSAYVPFSSGPRGCIGKGMALTEMMLTMA MVLWRLDFKIAEGDSAGGSPDAEWGRHRPDEFQLKDHV TAARNGPLLHFQERKISRRL

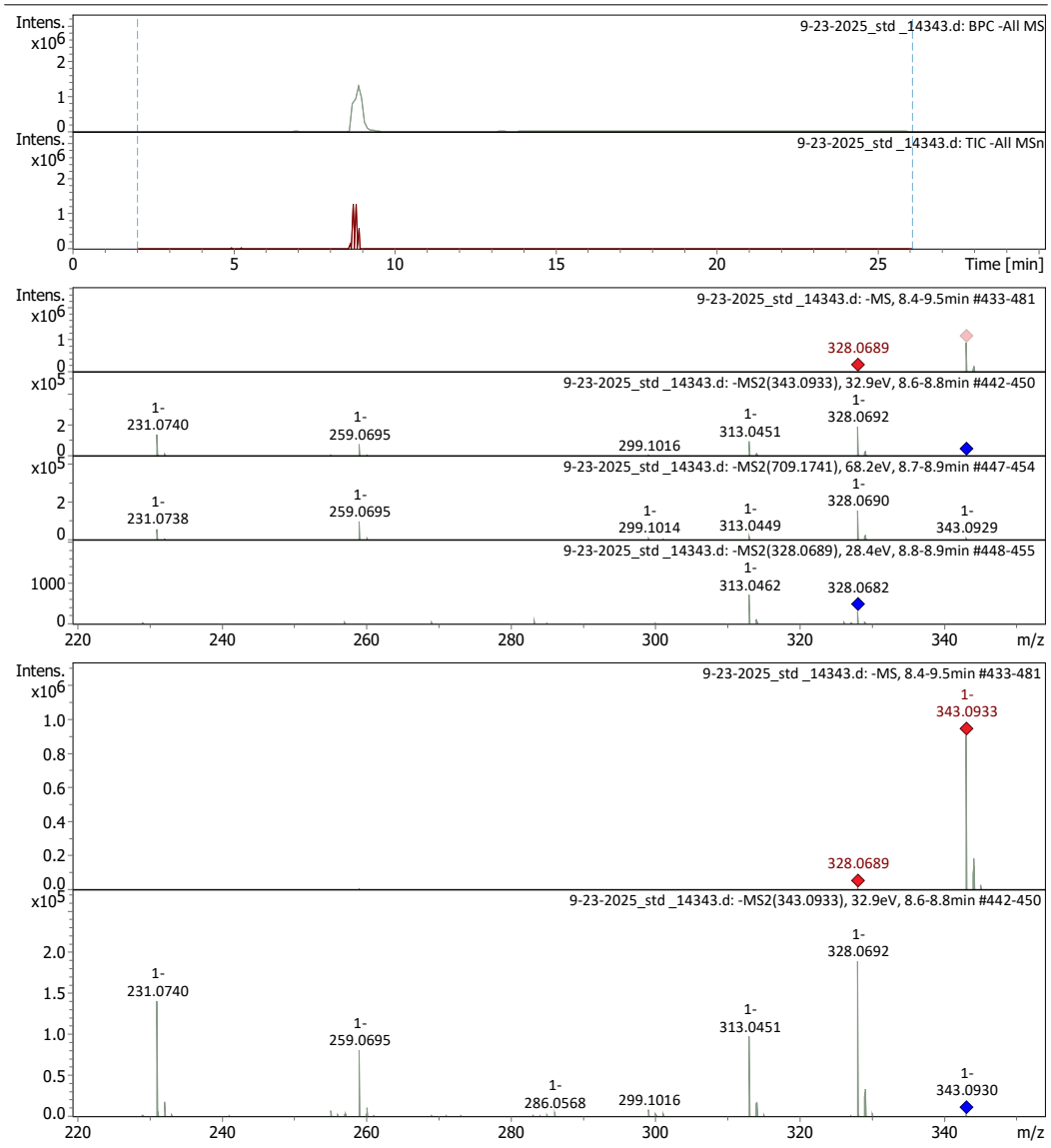

Figure S 13. LC-MS of usnic acid standard

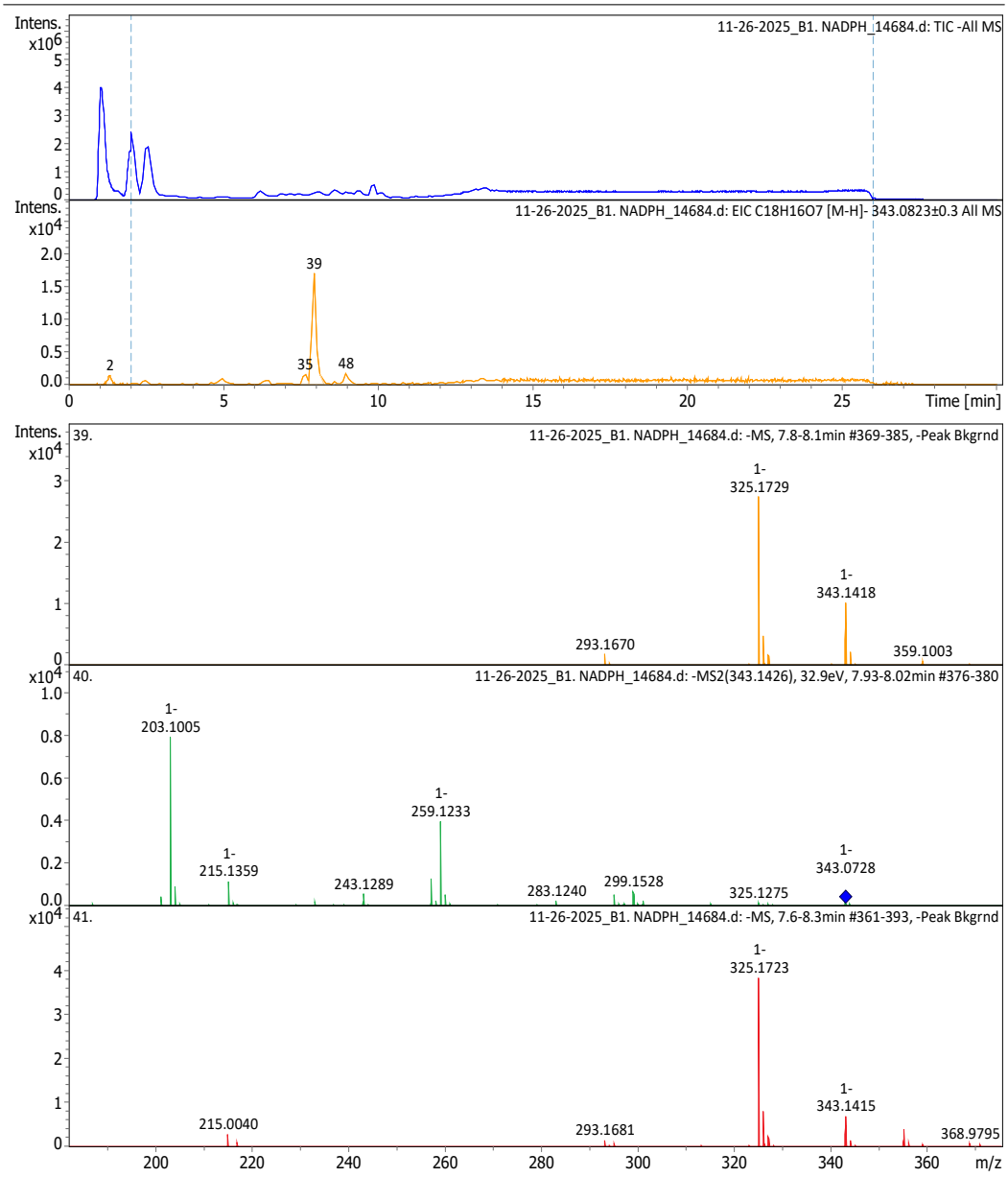

Figure S 14. LC-MS/MS bioconversion assays using NADPH as cofactor

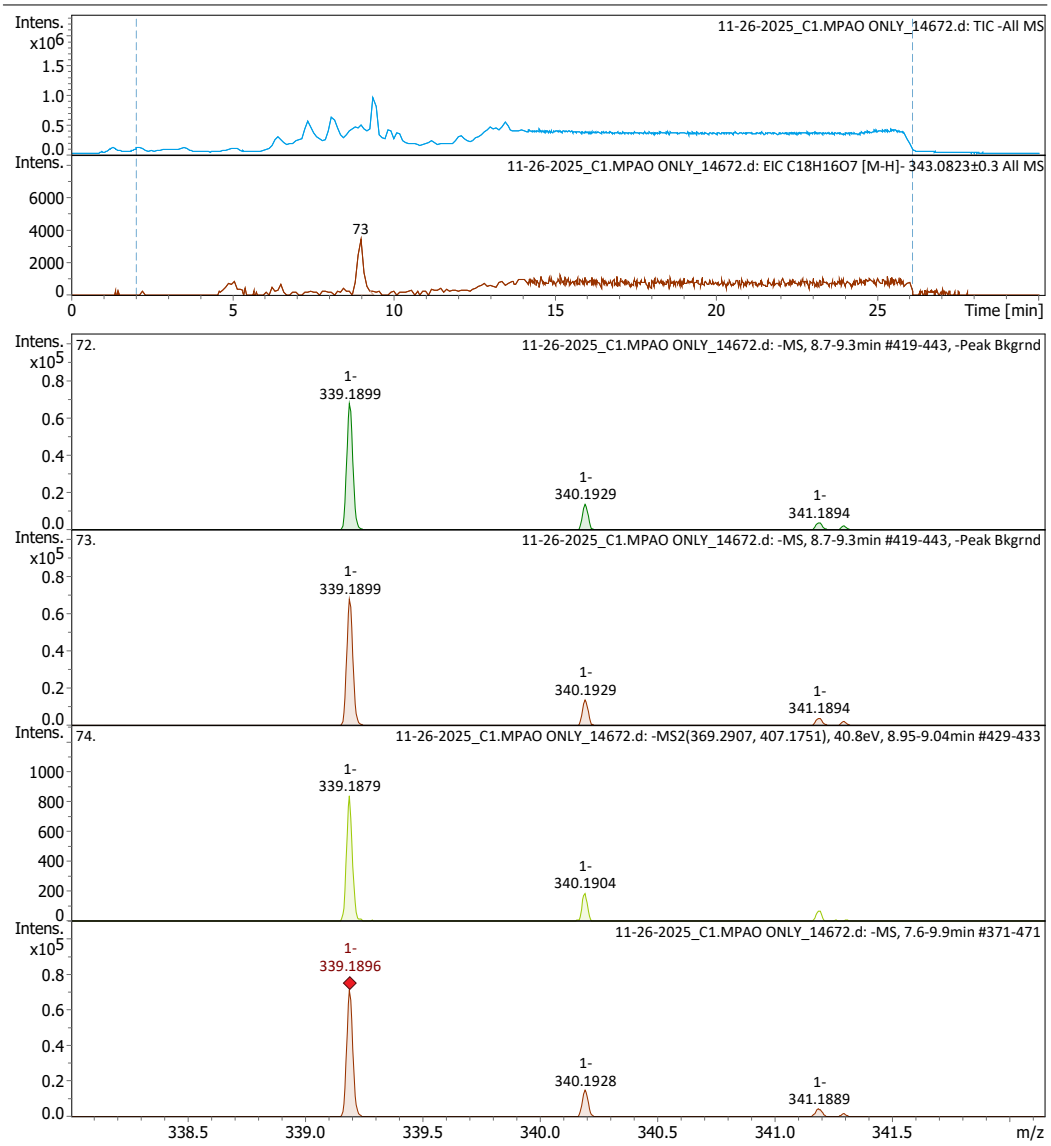

Figure S 15. LC-MS MPAO only in bioconversion using NADPH as cofactor

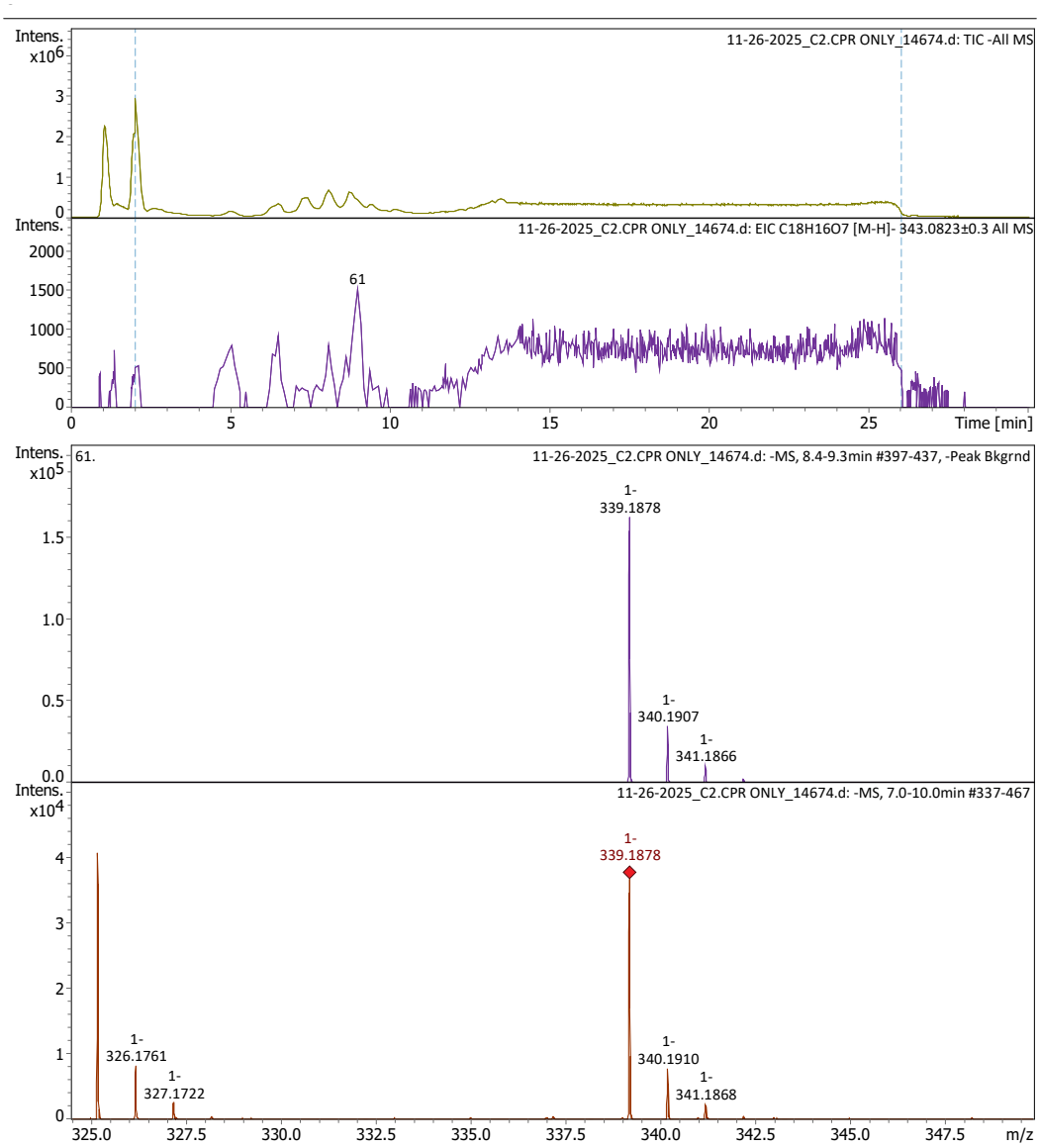

Figure S 16. LC-MS/MS CPR357 only in bioconversion assay using NADPH as cofactor

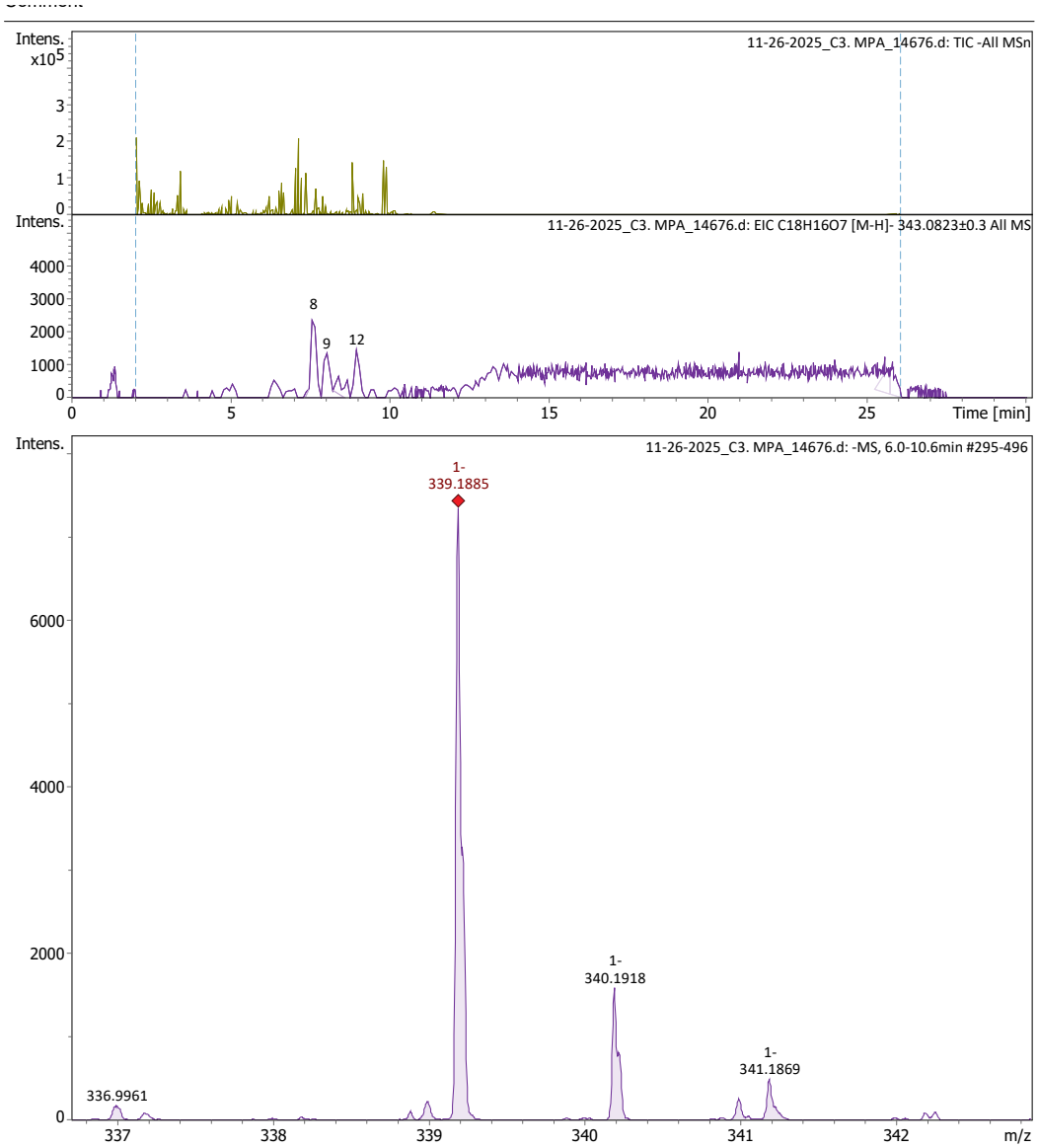

Figure S 17. LC-MS/MS MPA substrate in bioconversion assays using NADPH as cofactor

Reference

Abdel-Hameed, M., Bertrand, R. L., Piercey-Normore, M. D., & Sorensen, J. L. (2016). Putative identification of the usnic acid biosynthetic gene cluster by de novo whole-genome sequencing of a lichen-forming fungus. *Fungal Biology*, *120*(3), 306–316. https://doi.org/10.1016/j.funbio.2015.10.009

Addo, E. M., Ren, Y., Anaya-Eugenio, G. D., Ninh, T. N., Rakotondraibe, H. L., Carcache De Blanco, E. J., Soejarto, D. D., & Kinghorn, A. D. (2021). Spermidine alkaloid and glycosidic constituents of Vietnamese Homalium cochinchinensis. *Phytochemistry Letters*, *43*, 154–162. https://doi.org/10.1016/j.phytol.2021.04.002

Ahad, A. M., Goto, Y., Kiuchi, F., Tsuda, Y., Kondo, K., & Sato, T. (1991). Nematocidal Principles in "Oakmoss Absolute" and Nematocidal Activity of 2, 4-Dihydroxybenzoates. *Chemical and Pharmaceutical Bulletin*, *39*(4), 1043–1046. https://doi.org/10.1248/cpb.39.1043

Altschul, S. F., Gish, W., Miller, W., Myers, E. W., & Lipman, D. J. (1990). Basic local alignment search tool. *Journal of Molecular Biology*, *215*(3), 403–410. https://doi.org/10.1016/S0022-2836(05)80360-2

Armaleo, D., Sun, X., & Culberson, C. (2011a). Insights from the first putative biosynthetic gene cluster for a lichen depside and depsidone. *Mycologia*, *103*(4), 741–754. https://doi.org/10.3852/10-335

Armaleo, D., Sun, X., & Culberson, C. (2011b). Insights from the first putative biosynthetic gene cluster for a lichen depside and depsidone. *Mycologia*, *103*(4), 741–754. https://doi.org/10.3852/10-335

Aslan Engin, T. (2025). Exploring the antioxidant and protective effects of usnic acid: Opportunities and challenges. *Frontiers in Life Sciences and Related Technologies*, *6*(1), 53–59. https://doi.org/10.51753/flsrt.1572004

Austin, M. B., & Noel, J. P. (2003). The chalcone synthase superfamily of type III polyketide synthases. *Natural Product Reports*, *20*(1), 79–110. https://doi.org/10.1039/b100917f

Azhamuthu, T., Kathiresan, S., Senkuttuvan, I., Asath, N. A. A., Ravichandran, P., & Vasu, R. (2024). Usnic acid alleviates inflammatory responses and induces apoptotic signaling through inhibiting NF-κB expressions in human oral carcinoma cells. *Cell Biochemistry and Function*, *42*(4), e4074. https://doi.org/10.1002/cbf.4074

Backes, W. L. (2007). Phase I Biotransformation Reactions-NADPH-Cytochrome P450 Reductase. In *xPharm: The Comprehensive Pharmacology Reference* (pp. 1–8). Elsevier. https://doi.org/10.1016/B978-008055232-3.60276-4

Bapiro, T. E., Martin, S., Blacker, T. S., Wilkinson, S. D., Orton, A. L., Hariparsad, N., Jones, R. D. O., Duchen, M. R., & Harlfinger, S. (2025). A mismatch in enzyme-redox partnerships underlies divergent cytochrome P450 activities between human hepatocytes and microsomes. *Communications Biology*, *8*(1), 1539. https://doi.org/10.1038/s42003-025-08903-1

Bazin, M.-A., Lamer, A.-C. L., Delcros, J.-G., Rouaud, I., Uriac, P., Boustie, J., Corbel, J.-C., & Tomasi, S. (2008). Synthesis and cytotoxic activities of usnic acid derivatives. *Bioorganic & Medicinal Chemistry*, *16*(14), 6860–6866. https://doi.org/10.1016/j.bmc.2008.05.069

Bernhardt, R. (2006). Cytochromes P450 as versatile biocatalysts. *Journal of Biotechnology*, *124*(1), 128–145. https://doi.org/10.1016/j.jbiotec.2006.01.026

Bertrand, R. L. (n.d.). *Characterization of the Secondary Metabolome of a Lichenizing Fungus*.

Blackwell,Meredith. (2011). *The Fungi: 1, 2, 3 … 5.1 million species?†*. https://doi.org/10.3732/ajb.1000298

Blin, K., Medema, M. H., Kazempour, D., Fischbach, M. A., Breitling, R., Takano, E., & Weber, T. (2013). antiSMASH 2.0—A versatile platform for genome mining of secondary metabolite producers. *Nucleic Acids Research*, *41*(W1), W204–W212. https://doi.org/10.1093/nar/gkt449

Blin, K., Shaw, S., Kloosterman, A. M., Charlop-Powers, Z., van Wezel, G. P., Medema, M. H., & Weber, T. (2021). antiSMASH 6.0: Improving cluster detection and comparison capabilities. *Nucleic Acids Research*, *49*(W1), W29–W35. https://doi.org/10.1093/nar/gkab335

Braun, A., Geier, M., Bühler, B., Schmid, A., Mauersberger, S., & Glieder, A. (2012). Steroid biotransformations in biphasic systems with Yarrowia lipolytica expressing human liver cytochrome P450 genes. *Microbial Cell Factories*, *11*(1), 106. https://doi.org/10.1186/1475-2859-11-106

Brown CJ, Clark DE, Ollis WD, & Veal PL. (1960). The synthesis of the depsidone, diploicin. *Proc CHem Soc London*, 383–394.

Campbell, C. D., & Vederas, J. C. (2010). Biosynthesis of lovastatin and related metabolites formed by fungal iterative PKS enzymes. *Biopolymers*, *93*(9), 755–763. https://doi.org/10.1002/bip.21428

Campelo, D., Esteves, F., Brito Palma, B., Costa Gomes, B., Rueff, J., Lautier, T., Urban, P., Truan, G., & Kranendonk, M. (2018). Probing the Role of the Hinge Segment of Cytochrome P450 Oxidoreductase in the Interaction with Cytochrome P450. *International Journal of Molecular Sciences*, *19*(12), 3914. https://doi.org/10.3390/ijms19123914

Cavalloro, V., Malacrida, A., Miloso, M., Ronchi, D., Porta, A., Fossati, A., Gheza, G., De Siervi, S., Mantovani, S., Oliviero, B., Mondelli, M. U., Pugliese, L., Turato, C., Martino, E., & Collina, S. (2025). From lichen to organoids: Usnic acid enantiomers show promise against Cholangiocarcinoma via MNK2 targeting and MAPK pathway modulation. *Biomedicine & Pharmacotherapy*, *188*, 118208. https://doi.org/10.1016/j.biopha.2025.118208

Chan, Y. A., Podevels, A. M., Kevany, B. M., & Thomas, M. G. (2009). Biosynthesis of polyketide synthase extender units. *Nat. Prod. Rep.*, *26*(1), 90–114. https://doi.org/10.1039/B801658P

Chen, S., Dobrovolsky, V. N., Liu, F., Wu, Y., Zhang, Z., Mei, N., & Guo, L. (2014). The role of autophagy in usnic acid-induced toxicity in hepatic cells. *Toxicological Sciences: An Official Journal of the Society of Toxicology*, *142*(1), 33–44. https://doi.org/10.1093/toxsci/kfu154

Chiliza, Z. E., Martínez-Oyanedel, J., & Syed, K. (2020). An overview of the factors playing a role in cytochrome P450 monooxygenase and ferredoxin interactions. *Biophysical Reviews*, *12*(5), 1217–1222. https://doi.org/10.1007/s12551-020-00749-7

Chin, Y.-W., Balunas, M. J., Chai, H. B., & Kinghorn, A. D. (2006). Drug discovery from natural sources. *The AAPS Journal*, *8*(2), E239–E253. https://doi.org/10.1007/BF02854894

Chung, Y.-H., Song, J.-W., Choi, K.-Y., Yoon, J. W., Yang, K.-M., & Park, J.-B. (2012). Cloning, expression, and characterization of P450 monooxygenase CYP102H1 from Nocardia farcinica. *Journal of the Korean Society for Applied Biological Chemistry*, *55*(2), 259–264. https://doi.org/10.1007/s13765-012-1018-8

Cleland, W. W. (1990). Kinetic competence of enzymic intermediates: Fact or fiction? *Biochemistry*, *29*(13), 3194–3197. https://doi.org/10.1021/bi00465a006

Cocchietto, M., Skert, N., Nimis, P., & Sava, G. (2002). A review on usnic acid, an interesting natural compound. *Naturwissenschaften*, *89*(4), 137–146. https://doi.org/10.1007/s00114-002-0305-3

Correche, E., Carrasco, M., Giannini, F., Piovano, M., Garbarino, J., & Enriz, D. (2002). Cytotoxic Screening Activity of Secondary Lichen Metabolites. *Acta Farmaceutica Bonaerense*, *21*.

Crawford, J. M., Korman, T. P., Labonte, J. W., Vagstad, A. L., Hill, E. A., Kamari-Bidkorpeh, O., Tsai, S.-C., & Townsend, C. A. (2009). Structural basis for biosynthetic programming of fungal aromatic polyketide cyclization. *Nature*, *461*(7267), 1139–1143. https://doi.org/10.1038/nature08475

Culberson, C. F. (1964). Joint Occurrence of a Lichen Depsidone and Its Probable Depside Precursor. *Science*, *143*(3603), 255–256. https://doi.org/10.1126/science.143.3603.255

Culberson, C. F., & Armaleo, D. (1992). Induction of a complete secondary-product pathway in a cultured lichen fungus. *Experimental Mycology*, *16*(1), 52–63. https://doi.org/10.1016/0147-5975(92)90041-O

Culberson, C. F., & Elix, J. A. (1989). Lichen Substances. In *Methods in Plant Biochemistry* (Vol. 1, pp. 509–535). Elsevier. https://doi.org/10.1016/B978-0-12-461011-8.50021-4

Curd, F. H., & Robertson, A. (1933). 114. Usnic acid. Part I. Derivatives of methylphloroglucinol. *Journal of the Chemical Society (Resumed)*, 437. https://doi.org/10.1039/jr9330000437

Cvjetan, N., & Walde, P. (2023). Ferric heme *b* in aqueous micellar and vesicular systems: State-of-the-art and challenges. *Quarterly Reviews of Biophysics*, *56*, e1. https://doi.org/10.1017/S0033583522000130

Dadras, A., Rieseberg, T. P., Zegers, J. M. S., Fürst-Jansen, J. M. R., Irisarri, I., De Vries, J., & De Vries, S. (2025). Accessible versatility underpins the deep evolution of plant specialized

metabolism. *Phytochemistry Reviews*, *24*(1), 13–26. https://doi.org/10.1007/s11101-023-09863-2

Degtyarenko, K. N., & Archakov, A. I. (1993). Molecular evolution of P450 superfamily and P450-containing monooxygenase systems. *FEBS Letters*, *332*(1–2), 1–8. https://doi.org/10.1016/0014-5793(93)80470-F

Dewick, P. M. (2009). *Medicinal natural products: A biosynthetic approach* (3rd edition). Wiley, A John Wiley and Sons, Ltd., Publication.

Du, L., & Lou, L. (2010). PKS and NRPS release mechanisms. *Nat. Prod. Rep.*, *27*(2), 255–278. https://doi.org/10.1039/B912037H

Dubey, K. D., & Shaik, S. (2019). Cytochrome P450—The Wonderful Nanomachine Revealed through Dynamic Simulations of the Catalytic Cycle. *Accounts of Chemical Research*, *52*(2), 389–399. https://doi.org/10.1021/acs.accounts.8b00467

Durairaj, P., Hur, J.-S., & Yun, H. (2016). Versatile biocatalysis of fungal cytochrome P450 monooxygenases. *Microbial Cell Factories*, *15*(1), 125. https://doi.org/10.1186/s12934-016-0523-6

Durairaj, P., Jung, E., Park, H. H., Kim, B.-G., & Yun, H. (2015). Comparative functional characterization of a novel benzoate hydroxylase cytochrome P450 of Fusarium oxysporum. *Enzyme and Microbial Technology*, *70*, 58–65. https://doi.org/10.1016/j.enzmictec.2014.12.013

Durairaj, P., & Li, S. (2022). Functional expression and regulation of eukaryotic cytochrome P450 enzymes in surrogate microbial cell factories. *Engineering Microbiology*, *2*(1), 100011. https://doi.org/10.1016/j.engmic.2022.100011

Einarsdóttir, E., Groeneweg, J., Björnsdóttir, G., Harðardottir, G., Omarsdóttir, S., Ingólfsdóttir, K., & Ögmundsdóttir, H. (2010). Cellular Mechanisms of the Anticancer Effects of the Lichen Compound Usnic Acid. *Planta Medica*, *76*(10), 969–974. https://doi.org/10.1055/s-0029-1240851

Elix, J., Jenie, U., & Parker, J. (1987). A Novel Synthesis of the Lichen Depsidones Divaronic Acid and Stenosporonic Acid, and the Biosynthetic Implications. *Australian Journal of Chemistry*, *40*(8), 1451–1464. https://doi.org/10.1071/CH9871451

Ershov, P. V., Yablokov, E. O., Florinskaya, A. V., Mezentsev, Yu. V., Kaluzhskiy, L. A., Tumilovich, A. M., Gilep, A. A., Usanov, S. A., & Ivanov, A. S. (2019). SPR—Based study of affinity of cytochrome P450s / redox partners interactions modulated by steroidal substrates. *The Journal of Steroid Biochemistry and Molecular Biology*, *187*, 124–129. https://doi.org/10.1016/j.jsbmb.2018.11.009

Esteves, F., Campelo, D., Gomes, B. C., Urban, P., Bozonnet, S., Lautier, T., Rueff, J., Truan, G., & Kranendonk, M. (2020). The Role of the FMN-Domain of Human Cytochrome P450 Oxidoreductase in Its Promiscuous Interactions With Structurally Diverse Redox Partners. *Frontiers in Pharmacology*, *11*, 299. https://doi.org/10.3389/fphar.2020.00299

Estrella, M., De, R., & Vicente, C. (2011). Bioproduction of Depsidones for Pharmaceutical Purposes. In C. Rundfeldt (Ed.), *Drug Development—A Case Study Based Insight into Modern Strategies*. InTech. https://doi.org/10.5772/27051

Fang, Y., Tai, Z., Hu, K., Luo, L., Yang, S., Liu, M., & Xie, X. (2024). Comprehensive Review on Plant Cytochrome P450 Evolution: Copy Number, Diversity, and Motif Analysis From Chlorophyta to Dicotyledoneae. *Genome Biology and Evolution*, *16*(11), evae240. https://doi.org/10.1093/gbe/evae240

Funa, N., Ohnishi, Y., Fujii, I., Shibuya, M., Ebizuka, Y., & Horinouchi, S. (1999). A new pathway for polyketide synthesis in microorganisms. *Nature*, *400*(6747), 897–899. https://doi.org/10.1038/23748

Furmanek, Ł., Czarnota, P., & Seaward, M. R. D. (2019). Antifungal activity of lichen compounds against dermatophytes: A review. *Journal of Applied Microbiology*, *127*(2), 308–325. https://doi.org/10.1111/jam.14209

Galanty, A., Paśko, P., & Podolak, I. (2019). Enantioselective activity of usnic acid: A comprehensive review and future perspectives. *Phytochemistry Reviews*, *18*(2), 527–548. https://doi.org/10.1007/s11101-019-09605-3

Garc□a-Junceda, E., & Vicente, C. (1986). The use of immobilized cells to stabilize orsellinate depside hydrolase of Pseudevernia furfuracea. *Plant Cell Reports*, *5*(2), 155–157. https://doi.org/10.1007/BF00269258

Gill, H., Sorensen, J. L., & Collemare, J. (2023). Lichen Fungal Secondary Metabolites: Progress in the Genomic Era Toward Ecological Roles in the Interaction. In B. Scott & C. Mesarich (Eds.), *Plant Relationships* (Vol. 5, pp. 185–208). Springer International Publishing. https://doi.org/10.1007/978-3-031-16503-0_7

Goga, M., Elečko, J., Marcinčinová, M., Ručová, D., Bačkorová, M., & Bačkor, M. (2018). Lichen Metabolites: An Overview of Some Secondary Metabolites and Their Biological Potential. In J.-M. Mérillon & K. G. Ramawat (Eds.), *Bioactive Molecules in Food* (pp. 1–36). Springer International Publishing. https://doi.org/10.1007/978-3-319-76887-8_57-1

Gouterman, M. (1961). Spectra of porphyrins. *Journal of Molecular Spectroscopy*, *6*, 138–163. https://doi.org/10.1016/0022-2852(61)90236-3

Grube, M., Cardinale, M., De Castro, J. V., Müller, H., & Berg, G. (2009). Species-specific structural and functional diversity of bacterial communities in lichen symbioses. *The ISME Journal*, *3*(9), 1105–1115. https://doi.org/10.1038/ismej.2009.63

Grube, M., Cernava, T., Soh, J., Fuchs, S., Aschenbrenner, I., Lassek, C., Wegner, U., Becher, D., Riedel, K., Sensen, C. W., & Berg, G. (2015). Exploring functional contexts of symbiotic sustain within lichen-associated bacteria by comparative omics. *The ISME Journal*, *9*(2), 412–424. https://doi.org/10.1038/ismej.2014.138

Guengerich, F. P., & Munro, A. W. (2013). Unusual cytochrome p450 enzymes and reactions. *The Journal of Biological Chemistry*, *288*(24), 17065–17073. https://doi.org/10.1074/jbc.R113.462275

Guo, L., Shi, Q., Fang, J.-L., Mei, N., Ali, A. A., Lewis, S. M., Leakey, J. E. A., & Frankos, V. H. (2008). Review of Usnic Acid and *Usnea Barbata* Toxicity. *Journal of Environmental Science and Health, Part C*, *26*(4), 317–338. https://doi.org/10.1080/10590500802533392

Hatakeyama, M., Kitaoka, T., & Ichinose, H. (2016). Heterologous expression of fungal cytochromes P450 (CYP5136A1 and CYP5136A3) from the white-rot basidiomycete Phanerochaete chrysosporium: Functionalization with cytochrome b5 in Escherichia coli. *Enzyme and Microbial Technology*, *89*, 7–14. https://doi.org/10.1016/j.enzmictec.2016.03.004

Hausjell, J., Weissensteiner, J., Molitor, C., Halbwirth, H., & Spadiut, O. (2018). E. coli HMS174(DE3) is a sustainable alternative to BL21(DE3). *Microbial Cell Factories*, *17*(1), 169. https://doi.org/10.1186/s12934-018-1016-6

Hawranik, D. J., Anderson, K. S., Simmonds, R., & Sorensen, John. L. (2009). The chemoenzymatic synthesis of usnic acid. *Bioorganic & Medicinal Chemistry Letters*, *19*(9), 2383–2385. https://doi.org/10.1016/j.bmcl.2009.03.087

Hendrickson, J. B., Ramsay, M. V. J., & Kelly, T. R. (1972). New synthesis of depsidones. Diploicin and gangaleoidin. *Journal of the American Chemical Society*, *94*(19), 6834–6843. https://doi.org/10.1021/ja00774a043

Hertweck, C., Luzhetskyy, A., Rebets, Y., & Bechthold, A. (2007). Type II polyketide synthases: Gaining a deeper insight into enzymatic teamwork. *Nat. Prod. Rep.*, *24*(1), 162–190. https://doi.org/10.1039/B507395M

Honegger, R. (1997). Metabolic Interactions at the Mycobiont-Photobiont Interface in Lichens. In G. C. Carroll & P. Tudzynski (Eds.), *Plant Relationships* (pp. 209–221). Springer Berlin Heidelberg. https://doi.org/10.1007/978-3-662-10370-8_12

Honegger, R. (2009). Lichen-Forming Fungi and Their Photobionts. In H. B. Deising (Ed.), *The Mycota* (Vol. 5, pp. 307–333). Springer Berlin Heidelberg. https://doi.org/10.1007/978-3-540-87407-2_16

Huneck, S., Akinniyi, J. A., Cameron, A. F., Connolly, J. D., & Mulholland, A. G. (1981). The absolute configurations of (+)-usnic and (+)-isousnic acid. X-ray analyses of the (–)-α-phenylethylamine derivative of (+)-usnic acid and of (–)-pseudoplacodiolic acid, a new dibenzofuran, from the lichen . *Tetrahedron Letters*, *22*(4), 351–352. https://doi.org/10.1016/0040-4039(81)80095-0

Huneck, S., Yoshimura, I.,. (n.d.). *Identification of Lichen Substances*. Springer Berlin Heidelberg.

Huneck, S., & Yoshimura, I. (1996). *Identification of Lichen Substances*. Springer Berlin Heidelberg. https://doi.org/10.1007/978-3-642-85243-5

Hyung Koo, M., Shin, M., Ju Kim, M., Lee, S., Eun So, J., Hee Kim, J., Hyuck Lee, J., Suh, S., & Joung Youn, U. (2022). Bioactive Secondary Metabolites Isolated from the Antarctic Lichen *Himantormia lugubris*. *Chemistry & Biodiversity*, *19*(10), e202200374. https://doi.org/10.1002/cbdv.202200374

Ibrahim, S. R. M., Mohamed, G. A., Al Haidari, R. A., El-Kholy, A. A., Zayed, M. F., & Khayat, M. T. (2018). Biologically active fungal depsidones: Chemistry, biosynthesis, structural characterization, and bioactivities. *Fitoterapia*, *129*, 317–365. https://doi.org/10.1016/j.fitote.2018.04.012

Ichinose, H., Michizoe, J., Maruyama, T., Kamiya, N., & Goto, M. (2004). Electron-Transfer Reactions and Functionalization of Cytochrome P450cam Monooxygenase System in Reverse Micelles. *Langmuir*, *20*(13), 5564–5568. https://doi.org/10.1021/la049752n

Ingólfsdóttir, K. (2002). Usnic acid. *Phytochemistry*, *61*(7), 729–736. https://doi.org/10.1016/S0031-9422(02)00383-7

Ingólfsdóttir, K., Chung, G. A. C., Skúlason, V. G., Gissurarson, S. R., & Vilhelmsdóttir, M. (1998). Antimycobacterial activity of lichen metabolites in vitro. *European Journal of Pharmaceutical Sciences*, *6*(2), 141–144. https://doi.org/10.1016/S0928-0987(97)00078-X

Jennewein, S., Park, H., DeJong, J. M., Long, R. M., Bollon, A. P., & Croteau, R. B. (2005). Coexpression in yeast of *Taxus* cytochrome P450 reductase with cytochrome P450 oxygenases involved in Taxol biosynthesis. *Biotechnology and Bioengineering*, *89*(5), 588–598. https://doi.org/10.1002/bit.20390

Johnson, M. (2013). Detergents: Triton X-100, Tween-20, and More. *Materials and Methods*, *3*. https://doi.org/10.13070/mm.en.3.163

Joseph, A., Lee, T., Moland, C. L., Branham, W. S., Fuscoe, J. C., Leakey, J. E. A., Allaben, W. T., Lewis, S. M., Ali, A. A., & Desai, V. G. (2009). Effect of (+)-usnic acid on mitochondrial functions as measured by mitochondria-specific oligonucleotide microarray in liver of B6C3F1 mice. *Mitochondrion*, *9*(2), 149–158. https://doi.org/10.1016/j.mito.2009.02.002

Khayat, M. T., Ghazawi, K. F., Samman, W. A., Alhaddad, A. A., Mohamed, G. A., & Ibrahim, S. R. (2023). Recent advances on natural depsidones: Sources, biosynthesis, structure-activity relationship, and bioactivities. *PeerJ*, *11*, e15394. https://doi.org/10.7717/peerj.15394

Klingenberg, M. (1958). Pigments of rat liver microsomes. *Archives of Biochemistry and Biophysics*, *75*(2), 376–386. https://doi.org/10.1016/0003-9861(58)90436-3

Knop, W. (1844). Chemisch-physiologische Untersuchung über die Flechten. *Justus Liebigs Annalen Der Chemie*, *49*(2), 103–124. https://doi.org/10.1002/jlac.18440490202

Kořený, L., Oborník, M., Horáková, E., Waller, R. F., & Lukeš, J. (2022). The convoluted history of haem biosynthesis. *Biological Reviews*, *97*(1), 141–162. https://doi.org/10.1111/brv.12794

Kutney, J. P., Sanchez, I. H., & Yee, T. H. (1974). Mass spectral fragmentation studies in usnic acid and related compounds. *Organic Mass Spectrometry*, *8*(1), 129–146. https://doi.org/10.1002/oms.1210080117

Lage, T. C. A., Maciel, T. M. S., Mota, Y. C. C., Sisto, F., Sabino, J. R., Santos, J. C. C., Figueiredo, I. M., Masia, C., De Fátima, Â., Fernandes, S. A., & Modolo, L. V. (2018). *In vitro* inhibition of *Helicobacter pylori* and interaction studies of lichen natural products with jack bean urease. *New Journal of Chemistry*, *42*(7), 5356–5366. https://doi.org/10.1039/C8NJ00072G

Lamb, D. C., Follmer, A. H., Goldstone, J. V., Nelson, D. R., Warrilow, A. G., Price, C. L., True, M. Y., Kelly, S. L., Poulos, T. L., & Stegeman, J. J. (2019). On the occurrence of cytochrome P450 in viruses. *Proceedings of the National Academy of Sciences of the United States of America*, *116*(25), 12343–12352. https://doi.org/10.1073/pnas.1901080116

Lamb, D. C., & Waterman, M. R. (2013). Unusual properties of the cytochrome P450 superfamily. *Philosophical Transactions of the Royal Society B: Biological Sciences*, *368*(1612), 20120434. https://doi.org/10.1098/rstb.2012.0434

Lauterwein, M., Oethinger, M., Belsner, K., Peters, T., & Marre, R. (1995). In vitro activities of the lichen secondary metabolites vulpinic acid, (+)-usnic acid, and (-)-usnic acid against aerobic and anaerobic microorganisms. *Antimicrobial Agents and Chemotherapy*, *39*(11), 2541–2543. https://doi.org/10.1128/AAC.39.11.2541

Layer, G. (2021). Heme biosynthesis in prokaryotes. *Biochimica et Biophysica Acta (BBA) - Molecular Cell Research*, *1868*(1), 118861. https://doi.org/10.1016/j.bbamcr.2020.118861

Lücking, R., & Spribille, T. (2024). *The lives of lichens: A natural history*. Princeton University Press.

Lutzoni, F. (2009). *Current Biology, Volume 19, Issue 13, R502—R503*.

Lutzoni, F., & Miadlikowska, J. (2009). Lichens. *Current Biology*, *19*(13), R502–R503. https://doi.org/10.1016/j.cub.2009.04.034

Ma, S. M., Zhan, J., Xie, X., Watanabe, K., Tang, Y., & Zhang, W. (2008). Redirecting the cyclization steps of fungal polyketide synthase. *Journal of the American Chemical Society*, *130*(1), 38–39. https://doi.org/10.1021/ja078091o

Macedo, D. C. S., Almeida, F. J. F., Wanderley, M. S. O., Ferraz, M. S., Santos, N. P. S., López, A. M. Q., Santos-Magalhães, N. S., & Lira-Nogueira, M. C. B. (2021). Usnic acid: From an ancient lichen derivative to promising biological and nanotechnology applications. *Phytochemistry Reviews*, *20*(3), 609–630. https://doi.org/10.1007/s11101-020-09717-1

Mateos, J. L., Conde, E., Miranda, T., & Vicente, C. (1991). Regulation mechanisms of phenolic production in the lichen Himantormia lugubris, as deduced from the analysis of metabolite accumulation. *Plant Science*, *77*(1), 1–9. https://doi.org/10.1016/0168-9452(91)90175-8

Medema, M. H., Kottmann, R., Yilmaz, P., Cummings, M., Biggins, J. B., Blin, K., De Bruijn, I., Chooi, Y. H., Claesen, J., Coates, R. C., Cruz-Morales, P., Duddela, S., Düsterhus, S., Edwards, D. J., Fewer, D. P., Garg, N., Geiger, C., Gomez-Escribano, J. P., Greule, A., … Glöckner, F. O. (2015). Minimum Information about a Biosynthetic Gene cluster. *Nature Chemical Biology*, *11*(9), 625–631. https://doi.org/10.1038/nchembio.1890

Mendes Hacke, A. C., Vu, H. N. D., Hardy, B., Kuss, S., & Sorensen, J. L. (2025). Electron Transfer Reaction Studies of Usnic Acid and Its Biosynthetic Precursor Methylphloroacetophenone. *Electrochemical Science Advances*, *5*(1), e202400011. https://doi.org/10.1002/elsa.202400011

Merinero, S., & Gauslaa, Y. (2018). Specialized fungal parasites reduce fitness of their lichen hosts. *Annals of Botany*, *121*(1), 175–182. https://doi.org/10.1093/aob/mcx124

Mittal, N. (n.d.). *Functional Characterization of Lichen Fungal (Cladonia uncialis) Genes and Exploration of Its Secondary Metabolome*.

Mlambo, G., Padayachee, T., Nelson, D. R., & Syed, K. (2023). Genome-Wide Analysis of the Cytochrome P450 Monooxygenases in the Lichenized Fungi of the Class

Lecanoromycetes. *Microorganisms*, *11*(10), 2590. https://doi.org/10.3390/microorganisms11102590

Molnár, K., & Farkas, E. (2010). Current Results on Biological Activities of Lichen Secondary Metabolites: A Review. *Zeitschrift Für Naturforschung C*, *65*(3–4), 157–173. https://doi.org/10.1515/znc-2010-3-401

Morillas, L., Roales, J., Cruz, C., & Munzi, S. (2022). Lichen as Multipartner Symbiotic Relationships. *Encyclopedia*, *2*(3), 1421–1431. https://doi.org/10.3390/encyclopedia2030096

Morrison, J. F. (1969). Kinetics of the reversible inhibition of enzyme-catalysed reactions by tight-binding inhibitors. *Biochimica et Biophysica Acta (BBA) - Enzymology*, *185*(2), 269–286. https://doi.org/10.1016/0005-2744(69)90420-3

Mosbach, K. (1969). Biosynthesis of Lichen Substances, Products of a Symbiotic Association. *Angewandte Chemie International Edition in English*, *8*(4), 240–250. https://doi.org/10.1002/anie.196902401

Mosbach, K., & Ehrensvärd, U. (1966). Studies on lichen enzymes part I. Preparation and properties of a depside hydrolysing esterase and of orsellinic acid decarboxylase. *Biochemical and Biophysical Research Communications*, *22*(2), 145–150. https://doi.org/10.1016/0006-291X(66)90423-2

Mosbach, K., Laurent, T. C., Rodmar, S., Nihlgård, B., & Nilsson, L. (1964). On the Biosynthesis of Lichen Substances. Part 1. The Depside Gyrophoric Acid. *Acta Chemica Scandinavica*, *18*, 329–334. https://doi.org/10.3891/acta.chem.scand.18-0329

Moss, G. P. (1988). Nomenclature of tetrapyrroles: Recommendations 1986. *European Journal of Biochemistry*, *178*(2), 277–328. https://doi.org/10.1111/j.1432-1033.1988.tb14453.x

Moss, G. P., Smith, P. A. S., & Tavernier, D. (1995). *GLOSSARY OF CLASS NAMES OF ORGANIC COMPOUNDS AND REACTIVE INTERMEDIATES BASED ON STRUCTURE*. Pure & Appl. Chem.

Munro, A. W., McLean, K. J., Grant, J. L., & Makris, T. M. (2018). Structure and function of the cytochrome P450 peroxygenase enzymes. *Biochemical Society Transactions*, *46*(1), 183–196. https://doi.org/10.1042/BST20170218

Mushegian, A. A., Peterson, C. N., Baker, C. C. M., & Pringle, A. (2011). Bacterial Diversity across Individual Lichens. *Applied and Environmental Microbiology*, *77*(12), 4249–4252. https://doi.org/10.1128/AEM.02850-10

Neamati, N., Hong, H., Mazumder, A., Wang, S., Sunder, S., Nicklaus, M. C., Milne, G. W. A., Proksa, B., & Pommier, Y. (1997). Depsides and Depsidones as Inhibitors of HIV-1 Integrase: Discovery of Novel Inhibitors through 3D Database Searching. *Journal of Medicinal Chemistry*, *40*(6), 942–951. https://doi.org/10.1021/jm960759e

Nelson, D. R. (2018). Cytochrome P450 diversity in the tree of life. *Biochimica et Biophysica Acta (BBA) - Proteins and Proteomics*, *1866*(1), 141–154. https://doi.org/10.1016/j.bbapap.2017.05.003

Ngcobo, P. E., Nkosi, B. V. Z., Chen, W., Nelson, D. R., & Syed, K. (2023). Evolution of Cytochrome P450 Enzymes and Their Redox Partners in Archaea. *International Journal of Molecular Sciences*, *24*(4), 4161. https://doi.org/10.3390/ijms24044161

Noh, H.-J., Lee, Y. M., Park, C. H., Lee, H. K., Cho, J.-C., & Hong, S. G. (2020). Microbiome in Cladonia squamosa Is Vertically Stratified According to Microclimatic Conditions. *Frontiers in Microbiology*, *11*, 268. https://doi.org/10.3389/fmicb.2020.00268

Omura, T. (1999). Forty Years of Cytochrome P450. *Biochemical and Biophysical Research Communications*, *266*(3), 690–698. https://doi.org/10.1006/bbrc.1999.1887

Omura, T., & Sato, R. (1964). The Carbon Monoxide-binding Pigment of Liver Microsomes. *Journal of Biological Chemistry*, *239*(7), 2370–2378. https://doi.org/10.1016/S0021-9258(20)82244-3

Øvstedal, D. O., & Lewis Smith, R. I. (2001). *Lichens of Antarctica and South Georgia: A Guide to their Identification and Ecology. (Reviews). Arctic, 55(2)* (Vols. 1–14). Antartic Science. https://doi.org/10.1017/S0954102002210639

Park, H., Kevany, B. M., Dyer, D. H., Thomas, M. G., & Forest, K. T. (2014). A Polyketide Synthase Acyltransferase Domain Structure Suggests a Recognition Mechanism for Its Hydroxymalonyl-Acyl Carrier Protein Substrate. *PLoS ONE*, *9*(10), e110965. https://doi.org/10.1371/journal.pone.0110965

Park, J., Lee, S., Choi, J., Park, B., Park, J., & Moktali, V. (2020). *Fungal Cytochrome P450 Database* (Version 0.0.40.26.1) [Computer software]. http://p450.riceblast.snu.ac.kr/intro.php

Podterob, A. P. (2008). Chemical composition of lichens and their medical applications. *Pharmaceutical Chemistry Journal*, *42*(10), 582–588. https://doi.org/10.1007/s11094-009-0183-5

Prokopiev, I. A., Filippov, E. V., Filippova, G. V., & Gladkina, N. P. (2017). Genotoxicity of usnic-acid enantiomers in vitro in human peripheral-blood lymphocytes. *Cell and Tissue Biology*, *11*(2), 141–146. https://doi.org/10.1134/S1990519X17020031

Purvis, O. W., British Lichen Society, & British Museum (Eds.). (1992). *The Lichen flora of Great Britain and Ireland*. Natural History Museum Publications in association with The British Lichen Society.

Qi, F., Lei, C., Li, F., Zhang, X., Wang, J., Zhang, W., Fan, Z., Li, W., Tang, G.-L., Xiao, Y., Zhao, G., & Li, S. (2018). Deciphering the late steps of rifamycin biosynthesis. *Nature Communications*, *9*(1), 2342. https://doi.org/10.1038/s41467-018-04772-x

Ranković, B., & Kosanić, M. (2021). Biotechnological substances in lichens. In *Natural Bioactive Compounds* (pp. 249–265). Elsevier. https://doi.org/10.1016/B978-0-12-820655-3.00012-4

Rubin-Pitel, S. B., Zhang, H., Vu, T., Brunzelle, J. S., Zhao, H., & Nair, S. K. (2008). Distinct Structural Elements Dictate the Specificity of the Type III Pentaketide Synthase from Neurospora crassa. *Chemistry & Biology*, *15*(10), 1079–1090. https://doi.org/10.1016/j.chembiol.2008.08.011

Sala, T., & Sargent, M. V. (1981). Depsidone synthesis. Part 16. Benzophenone–grisa-3′,5′-diene-2′,3-dione–depsidone interconversion: A new theory of depsidone biosynthesis. *J. Chem. Soc., Perkin Trans. 1*, (0), 855–869. https://doi.org/10.1039/P19810000855

Schultz, J., & Mosbach, K. (1971). Studies on Lichen Enzymes: Purification and Properties of an Orsellinate Depside Hydrolase Obtained from *Lasallia pustlata*. *European Journal of Biochemistry*, *22*(2), 153–157. https://doi.org/10.1111/j.1432-1033.1971.tb01526.x

Seneviratne, G., & Indrasena, I. K. (2006). Nitrogen fixation in lichens is important for improved rock weathering. *Journal of Biosciences*, *31*(5), 639–643. https://doi.org/10.1007/BF02708416

Seshadri, T. R. (1944). A theory of biogenesis of lichen depsides and depsidones. *Proceedings of the Indian Academy of Sciences - Section A*, *20*(1), 1–14. https://doi.org/10.1007/BF03048954

Shishido, T. K., Wahlsten, M., Laine, P., Rikkinen, J., Lundell, T., & Auvinen, P. (2021). Microbial Communities of Cladonia Lichens and Their Biosynthetic Gene Clusters Potentially Encoding Natural Products. *Microorganisms*, *9*(7), 1347. https://doi.org/10.3390/microorganisms9071347

Shrestha, G., & St. Clair, L. L. (2013). Lichens: A promising source of antibiotic and anticancer drugs. *Phytochemistry Reviews*, *12*(1), 229–244. https://doi.org/10.1007/s11101-013-9283-7

Shukla, V., Joshi, G. P., & Rawat, M. S. M. (2010). Lichens as a potential natural source of bioactive compounds: A review. *Phytochemistry Reviews*, *9*(2), 303–314. https://doi.org/10.1007/s11101-010-9189-6

Siedlarczyk, G., Paśko, P., & Galanty, A. (2025). An Evaluation of the Cytotoxicity and Safety Profile of Usnic Acid for a Broad Panel of Human Cancers and Normal Cells with Respect to Its Enantiospecificity. *Molecules*, *30*(14), 2964. https://doi.org/10.3390/molecules30142964

Sigurbjörnsdóttir, M. A., & Vilhelmsson, O. (2016). Selective isolation of potentially phosphate-mobilizing, biosurfactant-producing and biodegradative bacteria associated with a sub-Arctic, terricolous lichen, *Peltigera membranacea*. *FEMS Microbiology Ecology*, *92*(6), fiw090. https://doi.org/10.1093/femsec/fiw090

Silverman, R. B. (2002). *The organic chemistry of enzyme-catalyzed reactions* (Revised edition). Academic Press.

Singh, G., Armaleo, D., Dal Grande, F., & Schmitt, I. (2021). Depside and Depsidone Synthesis in Lichenized Fungi Comes into Focus through a Genome-Wide Comparison of the Olivetoric Acid and Physodic Acid Chemotypes of Pseudevernia furfuracea. *Biomolecules*, *11*(10), 1445. https://doi.org/10.3390/biom11101445

Singh, N. K., Baranwal, J., Pati, S., Barse, B., Khan, R. H., & Kumar, A. (2023). Application of plant products in the synthesis and functionalisation of biopolymers. *International Journal of Biological Macromolecules*, *237*, 124174. https://doi.org/10.1016/j.ijbiomac.2023.124174

Skiba, M. A., Sikkema, A. P., Fiers, W. D., Gerwick, W. H., Sherman, D. H., Aldrich, C. C., & Smith, J. L. (2016). Domain Organization and Active Site Architecture of a Polyketide Synthase *C* -methyltransferase. *ACS Chemical Biology*, *11*(12), 3319–3327. https://doi.org/10.1021/acschembio.6b00759

Spribille, T., Resl, P., Stanton, D. E., & Tagirdzhanova, G. (2022). Evolutionary biology of lichen symbioses. *New Phytologist*, *234*(5), 1566–1582. https://doi.org/10.1111/nph.18048

Spribille, T., Tagirdzhanova, G., Goyette, S., Tuovinen, V., Case, R., & Zandberg, W. F. (2020). 3D biofilms: In search of the polysaccharides holding together lichen symbioses. *FEMS Microbiology Letters*, *367*(5), fnaa023. https://doi.org/10.1093/femsle/fnaa023

Spribille, T., Tuovinen, V., Resl, P., Vanderpool, D., Wolinski, H., Aime, M. C., Schneider, K., Stabentheiner, E., Toome-Heller, M., Thor, G., Mayrhofer, H., Johannesson, H., & McCutcheon, J. P. (2016a). Basidiomycete yeasts in the cortex of ascomycete macrolichens. *Science*, *353*(6298), 488–492. https://doi.org/10.1126/science.aaf8287

Spribille, T., Tuovinen, V., Resl, P., Vanderpool, D., Wolinski, H., Aime, M. C., Schneider, K., Stabentheiner, E., Toome-Heller, M., Thor, G., Mayrhofer, H., Johannesson, H., &

McCutcheon, J. P. (2016b). Basidiomycete yeasts in the cortex of ascomycete macrolichens. *Science*, *353*(6298), 488–492. https://doi.org/10.1126/science.aaf8287

Staunton, J., & Weissman, K. J. (2001). Polyketide biosynthesis: A millennium review. *Natural Product Reports*, *18*(4), 380–416. https://doi.org/10.1039/a909079g

Studzińska-Sroka, E., Majchrzak-Celińska, A., Zalewski, P., Szwajgier, D., Baranowska-Wójcik, E., Żarowski, M., Plech, T., & Cielecka-Piontek, J. (2021). Permeability of Hypogymnia physodes Extract Component—Physodic Acid through the Blood–Brain Barrier as an Important Argument for Its Anticancer and Neuroprotective Activity within the Central Nervous System. *Cancers*, *13*(7), 1717. https://doi.org/10.3390/cancers13071717

Sveshnikova, N., Yuan, T., Warren, J. M., & Piercey-Normore, M. D. (2019). Development and validation of a reliable LC-MS/MS method for quantitative analysis of usnic acid in Cladonia uncialis. *BMC Research Notes*, *12*(1), 550. https://doi.org/10.1186/s13104-019-4580-x

Taguchi, H., Sankawa, U., & Shibata, S. (1966). Biosynthesis of usnic acid in lichens. *Tetrahedron Letters*, *7*(42), 5211–5214. https://doi.org/10.1016/S0040-4039(01)89308-4

Taguchi, H., Sankawa, U., & Shibata, S. (1969). Biosynthesis of Natural Products. VI. Biosynthesis of Usnic Acid in Lichens. (1). A General Scheme of Biosynthesis of Usnic Acid. *Chemical and Pharmaceutical Bulletin*, *17*(10), 2054–2060. https://doi.org/10.1248/cpb.17.2054

Teng, L., Fan, X., Nelson, D. R., Han, W., Zhang, X., Xu, D., Renault, H., Markov, G. V., & Ye, N. (2019). Diversity and evolution of cytochromes P450 in stramenopiles. *Planta*, *249*(3), 647–661. https://doi.org/10.1007/s00425-018-3028-1

Udwary, D. W., Merski, M., & Townsend, C. A. (2002). A Method for Prediction of the Locations of Linker Regions within Large Multifunctional Proteins, and Application to a Type I

Polyketide Synthase. *Journal of Molecular Biology*, *323*(3), 585–598. https://doi.org/10.1016/S0022-2836(02)00972-5

Ureña-Vacas, I., González-Burgos, E., Divakar, P. K., & Gómez-Serranillos, M. P. (2022). Lichen Depsidones with Biological Interest. *Planta Medica*, *88*(11), 855–880. https://doi.org/10.1055/a-1482-6381

Wayne, L. L., Wallis, J. G., Kumar, R., Markham, J. E., & Browse, J. (2013). Cytochrome b5 Reductase Encoded by *CBR1* Is Essential for a Functional Male Gametophyte in *Arabidopsis*. *The Plant Cell*, *25*(8), 3052–3066. https://doi.org/10.1105/tpc.113.113324

Weissman, K. J. (2009). Chapter 1 Introduction to Polyketide Biosynthesis. In *Methods in Enzymology* (Vol. 459, pp. 3–16). Elsevier. https://doi.org/10.1016/S0076-6879(09)04601-1

Winker, Dr. M., Geier, Dr. M., Hanlon, Dr. S. P., Nidetzky, Prof. Dr. B., & Glieder, Prof. Dr. A. (2018). *Human Enzymes for Organic Synthesis*. https://doi.org/10.1002/anie.201800678

Xu, M., Heidmarsson, S., Olafsdottir, E. S., Buonfiglio, R., Kogej, T., & Omarsdottir, S. (2016). Secondary metabolites from cetrarioid lichens: Chemotaxonomy, biological activities and pharmaceutical potential. *Phytomedicine*, *23*(5), 441–459. https://doi.org/10.1016/j.phymed.2016.02.012

Xu, M., Oppong-Danquah, E., Wang, X., Oddsson, S., Abdelrahman, A., Pedersen, S. V., Szomek, M., Gylfason, A. E., Snorradottir, B. S., Christensen, E. A., Tasdemir, D., Jameson, C. J., Murad, S., Andresson, O. S., Magnusson, K. P., De Boer, H. J., Thorsteinsdottir, M., Omarsdottir, S., Heidmarsson, S., & Olafsdottir, E. S. (2022). Novel methods to characterise spatial distribution and enantiomeric composition of usnic acids in four

Icelandic lichens. *Phytochemistry*, *200*, 113210. https://doi.org/10.1016/j.phytochem.2022.113210

Yuan, X., Rietzschel, N., Kwon, H., Walter Nuno, A. B., Hanna, D. A., Phillips, J. D., Raven, E. L., Reddi, A. R., & Hamza, I. (2016). Regulation of intracellular heme trafficking revealed by subcellular reporters. *Proceedings of the National Academy of Sciences of the United States of America*, *113*(35), E5144-5152. https://doi.org/10.1073/pnas.1609865113

Zambare, V. P., & Christopher, L. P. (2012). Biopharmaceutical potential of lichens. *Pharmaceutical Biology*, *50*(6), 778–798. https://doi.org/10.3109/13880209.2011.633089

Zhang, H., Wang, Y., Wu, J., Skalina, K., & Pfeifer, B. A. (2010). Complete Biosynthesis of Erythromycin A and Designed Analogs Using E. coli as a Heterologous Host. *Chemistry & Biology*, *17*(11), 1232–1240. https://doi.org/10.1016/j.chembiol.2010.09.013

Zhang, W., Du, L., Li, F., Zhang, X., Qu, Z., Han, L., Li, Z., Sun, J., Qi, F., Yao, Q., Sun, Y., Geng, C., & Li, S. (2018). Mechanistic Insights into Interactions between Bacterial Class I P450 Enzymes and Redox Partners. *ACS Catalysis*, *8*(11), 9992–10003. https://doi.org/10.1021/acscatal.8b02913

Zhao, X., Chen, Y., Long, T., Liu, Z., Zhang, Q., Zhang, H., Yan, Y., Zhang, C., & Zhu, Y. (2023). Genome Mining and Biosynthetic Reconstitution of Fungal Depsidone Mollicellins Reveal a Dual Functional Cytochrome P450 for Ether Formation. *Journal of Natural Products*, *86*(8), 2046–2053. https://doi.org/10.1021/acs.jnatprod.3c00609